Master of Science Thesis

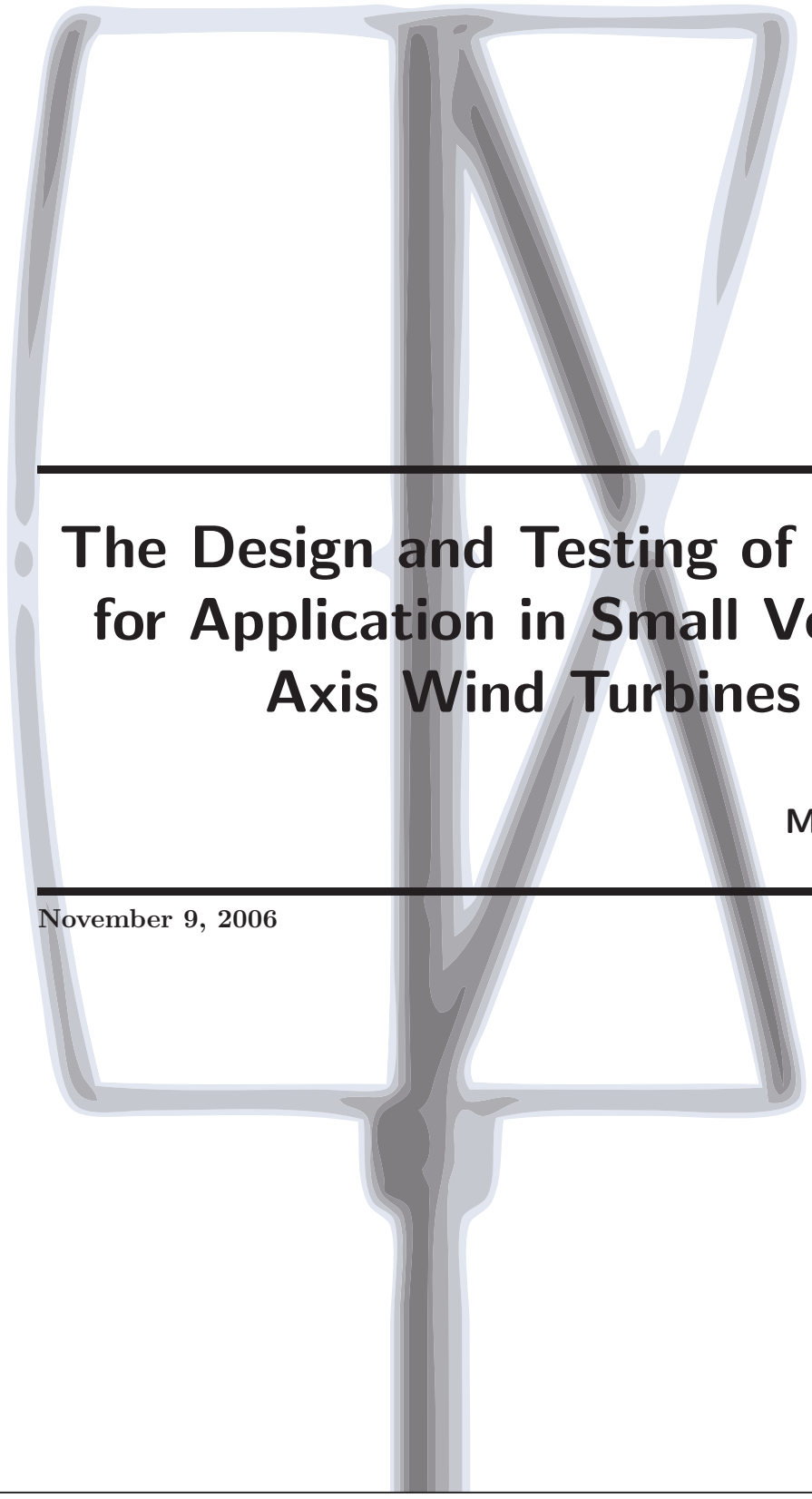

The Design and Testing of Airfoils for Application in Small Vertical Axis Wind Turbines

M.C. Claessens

November 9, 2006

Aerodynamics

TU Delft

Faculty of Aerospace Engineering

Delft University of Technology

The Design and Testing of Airfoils for Application in Small Vertical Axis Wind Turbines

Master of Science Thesis

For obtaining the degree of Master of Science in Aerospace Engineering at Delft University of Technology

M.C. Claessens

November 9, 2006

Faculty of Aerospace Engineering · Delft University of Technology

Delft University of Technology

DELFT UNIVERSITY OF TECHNOLOGY
DEPARTMENT OF
AERODYNAMICS

The undersigned hereby certify that they have read and recommend to the Faculty of Aerospace Engineering for acceptance the thesis entitled **"The Design and Testing of Airfoils for Application in Small Vertical Axis Wind Turbines"** by **M.C. Claessens** in fulfillment of the requirements for the degree of **Master of Science**.

Dated: November 9, 2006

Supervisors:

Prof.Dr.Ir. P.G. Bakker

Ir. W.A. Timmer

Ir. C. Ferreira

Dr.Ir. S. Mertens

Preface

This report is the final work of my Master of Science thesis at Aerospace Engineering, TU Delft. In this report the research that I have did during the 18 months of my studies in the area of VAWT aerodynamics can be found.

I would like to thank my supervisor Nando Timmer for all his time, the people at the LTT wind tunnel, Daniel Twigt for reviewing my report and everybody else who has contributed to my report. Special thanks go out to my girlfriend and my family for all their support.

Maarten Claessens
Delft, the 2^{nd} of October, 2006

Summary

In recent years more focus is put on the applications of wind turbines in the urban environment. One of the ways to do this is using a turbine with a vertical axis (a VAWT). This type of wind turbines is around for many centuries. The modern equivalent which is based on lift producing blades only exists for 30 years. In this period airfoils for this application have been developed, but still much work can be done in this field.

During this project a design process is developed with the purpose of improving the NACA 0018 airfoil, which is commonly used in VAWT turbines. The aerodynamics involved in VAWT are investigated to find the design goals for the airfoil characteristics. Furthermore the currently used NACA 0018, which is used as the design reference, is investigated.

The two main pillars of the design process are the RFOIL program and the VAWT simulation program. RFOIL is a panel method based program with boundary layer equations which can calculate the properties of 2D airfoils. RFOIL gives accurate enough results to be a powerful design tool in the Reynolds number range from 300,000 to 700,000.

The VAWT simulation program, written in MATLAB, calculates the performance of a VAWT using 2D airfoil data. The final Matlab program allows to adjust the turbines geometry, to chose from multiple airfoils and to set a dynamic stall model on or off. As such 2D airfoil characteristic from RFOIL or wind tunnel tests can be inserted to view the turbines performance with this airfoil.

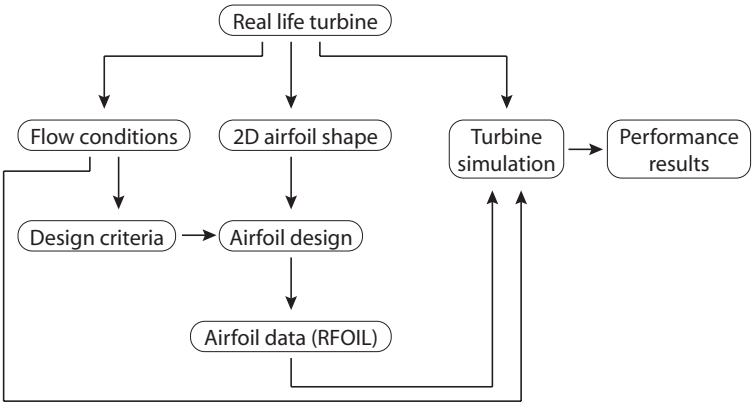

This design process resulted in a final design: the DU 06-W-200. The Du 06-W-200 airfoil is a laminar, 20% thick airfoil with 0.8% camber. The original NACA 0018 airfoil is a turbulent, symmetric airfoil with 18% thickness. To be able to compare both airfoils wind tunnel measurements were performed in the LTT wind tunnel at the Delft University of Technology. For the DU 06-W-200 airfoil the following conclusions are made:

- The added thickness of 2% will add to the blade strength and this is reached without decreasing the performance
- The added camber of 0.8% increases the performance with respect to a symmetric airfoil
- The DU 06-W-200 performance equals the NACA 0018 for negative angles of attack
- The DU 06-W-200 has a much higher $C_{L,max}$ for positive angles of attack, resulting in a wider drag bucket
- Deep stall occurs at higher angles of attack with a smaller drop in lift coefficient
- In contrast to the NACA 0018 the DU 06-W-200 does not have laminar separation bubbles which extend over the trailing edge
- The increase in turbine performance at the operating tip speed ratio of $\lambda = 3$ is 8% in clean conditions and twice as much when dirty

Table of Contents

List of Figures

List of Tables

List of Symbols

Abbreviations

CFD	Computational Fluid Dynamics
DMS	Double Multiple Streamtube model
DMSV	Double Multiple Streamtube model with variable interference factors
HAWT	Horizontal Axis Wind Turbine
LDV	Laser Doppler Velocimetry
NACA	National Advisory Committee for Aeronautics
NASA	National Aeronautics and Space Association
NLF	Natural Laminar Flow
VAWT	Vertical Axis Wind Turbine

Greek Symbols

α	Blade element angle of attack	$[^\circ]$
α_B	Effective blade angle of attack	$[^\circ]$
α_{ref}	Reference angle of attack	$[^\circ]$
Δ	Difference	$[-]$
Ω	Rotational speed	$\left[\frac{rad}{s}\right]$
π	Pi = 3.14159	$[-]$
ρ	Air density	$\left[\frac{kg}{m^3}\right]$
θ	Angle of the blade element with respect to the start position	$[^\circ]$

Latin Symbols

λ	Tip speed ratio	$[-]$
ν	Dynamic viscosity	$[\frac{kg}{ms}]$
B	Number of blades	$[-]$

c	Blade element chord	$[m]$
C_D	Drag coefficient	$[-]$
C_L	Lift coefficient	$[-]$
C_M	Moment coefficient	$[-]$
C_N	Normal force coefficient	$[-]$
C_P	Power coefficient	$[-]$
C_p	Pressure coefficient	$[-]$
C_T	Tangential force coefficient	$[-]$
D	Turbine diameter	$[m]$
F	Force	$[N]$
M	Mach number	$[-]$
N	Normal force	$[N]$
R	Maximum turbine blade radius	$[m]$
r	Local turbine blade radius	$[m]$
Re	Reynolds number	$[-]$
S	Swept turbine area	$\left[m^2\right]$
$S_{\dot{\alpha}}$	Sign of the instantaneous rate of change of α	$[-]$
T	Tangential force	$[N]$
u	Upwind interference factor	$[-]$
u'	Downwind interference factor	$[-]$
V	Airspeed	$\left[\frac{m}{s}\right]$
W	The local airspeed at the blade element	$\left[\frac{m}{s}\right]$

Subscripts

$_D$	Disk
$_e$	Equilibrium
$_{inf}$	Infinity
$_{max}$	Maximum
$_N$	In direction normal to the blade element
$_{ref}$	Reference
$_{ss}$	Steady stall
$_T$	In direction tangential to the blade element
$_x$	In direction of the x-axis

Superscripts

^{dyn}	Dynamic
^{mod}	Modificated

Chapter 1

Introduction

1.1 Wind turbines

In the history of mankind wind energy has played an important role. Among others wind energy was harnessed to grind grain. These so called wind mills are of the horizontal axis design (HAWT) and were also used for pumping water and later for sawing wood etc. Using multiple blades the wind energy generated by the atmosphere is converted to kinetic energy inside the turbine. As more attention was put on the environmental aspect of traditional (fossil) fuels the development of wind turbines for generating electricity became more interesting.

(a) HAWT **(b)** VAWT

Figure 1.1: The two main designs of lift driven wind turbines

In general there are two main categories of wind turbines: Horizontal Axis Wind Turbines (HAWT) and Vertical Axis Wind Turbines (VAWT), see figure 1.1. Although

HAWT designs are widely used, they have the disadvantage that they have to be positioned perpendicular to the wind direction. VAWT have the advantage that they are independent of wind direction for their operations. This latter group is divided again in two groups: lift driven VAWT (Darrieus) and drag driven VAWT (Savonius). As the maximum possible efficiency of lift driven turbines is larger then for drag driven turbines, the main attention today is focused on lift driven turbines. The first turbine of this design was patented in 1931 by G.J.M. Darrieus.

1.2 VAWT basics

The concept of VAWT can have differently shaped blades. As the forces of the blades can be large, the ideal blade has a Troposkien (nearly parabolic) shape with which the centrifugal force is translated through the blade to the shaft. This type of blade is mainly used in large turbines and prevents the blade from failing because of too large rotational speeds. A large disadvantage is the decreasing radius near the top and the bottom of the turbine. These parts experience only low rotational speeds and therefore generate almost no power.

Another concept is the H-Darrieus or Musgrove VAWT. The blades are straight and therefore the radius is equal over the total length of the blade, see figure 1.1(b). The power is now generated over the complete length of the blade. In contrast to the Troposkien shape blade extra strength is necessary to cope with the centrifugal forces. The blades can be rotated slightly to disperse the moment forces on the axis over a larger angle. The first prototypes of the H-Darrieus were developed in 1986.

The typical VAWT consists of the following parts:

- Supporting mast
- Rotational axis
- Supporting struts for the blades
- Blades
- Generator
- Converter

The blades of a VAWT have to develop lift and must have enough thickness to withstand the loads. To achieve this they have a certain shape, comparable to aircraft wings. This shape determines how the wind energy is conversed to forces on the blade. The goal of this study is to develop a new airfoil profile for an H-Darrieus vertical axis wind turbine. In most of the existing turbines of this type standard profiles like the NACA 0015 and NACA 0018 are used. These profiles were developed in the 1930's by the NACA as standard profile series for turbulent flow. Although these airfoils have

existed for a long time, not much experimental data is available. As the design involves a relatively small turbine, the Reynolds numbers are small. For most existing airfoils no data is available for these Reynolds numbers.

For this project the Turby is chosen as design case, a VAWT turbine developed in cooperation with the TU Delft (see figure 1.1(b)). This is a relatively small turbine designed to operate in urban environments on high buildings. The main characteristics are given in tables 1.1 and 1.2 below.

Table 1.1: The Turby geometry specifications

Overall height	2890 mm
Weight (inc. blades)	136 kg
Base flange Diameter	250 mm
Bolt circle	230 mm
Bolt holes	6 x M10
Rotor Diameter	1999 mm
Height	2650 mm
Rotor blades Number	3
Material	composite
Weight (3 blades)	14 kg

Table 1.2: The Turby operating specifications

Cut-in wind speed	4 $\frac{m}{s}$
Rated wind speed	14 $\frac{m}{s}$
Cut-out wind speed	14 $\frac{m}{s}$
Survival wind speed	55 $\frac{m}{s}$
Rated rotational speed	120 - 400 rpm
Rated blade speed	42 $\frac{m}{s}$
Rated power at 14 m/s	2.5 kW

1.3 Project overview

The main goal is to design a new airfoil for VAWT application using the Turby as design case. To be able to design this airfoil, the turbine has to be modeled. In figure 1.2 the flow diagram of the model is given.

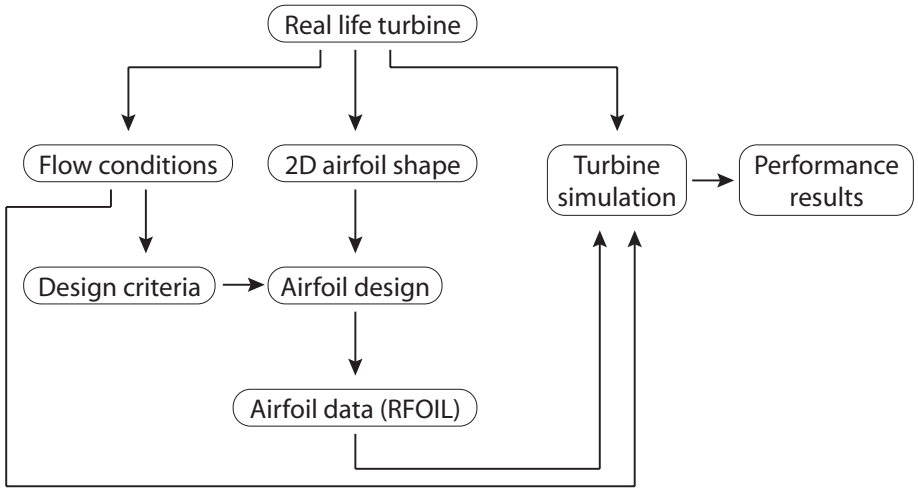

Figure 1.2: Flow diagram of the modeling of the turbine

In chapter 2 the flow conditions which are encountered in VAWT aerodynamics are discussed. These flow conditions determine for a large part the design criteria of the new airfoil and are used in making a sufficiently accurate simulation program. The simulation methods and the final simulation program are discussed in chapter 3. In the rest if the chapters the design of the new airfoil will be discussed. In figure 1.3 this process is shown in more detail.

During the development and testing of airfoils the NACA 0018 airfoil is used as reference. The RFOIL program is used to modify the blade shape and to calculate the characteristics of the new shape. Although RFOIL is a strong design tool, it has its limitations. The program is not able to predict all flow phenomena, resulting in limited accuracy and the angular range is limited until the airfoil is stalled. The RFOIL program is validated using wind tunnel data of the NACA 0018 airfoil and other profiles measured at the TU Delft. Starting from the NACA 0018 airfoil the RFOIL program is then used to investigate other airfoils, make adjustments and calculate their characteristics. In chapter 5 these characteristics are compared and used in the simulation program. The results of the simulation program and the airfoil characteristics are distilled into a general design of the airfoil. In chapter 6 this general design is fine tuned until the optimum design is reached. The characteristics of this design are measured in the wind tunnel and a comparison is made between this final design and the NACA 0018.

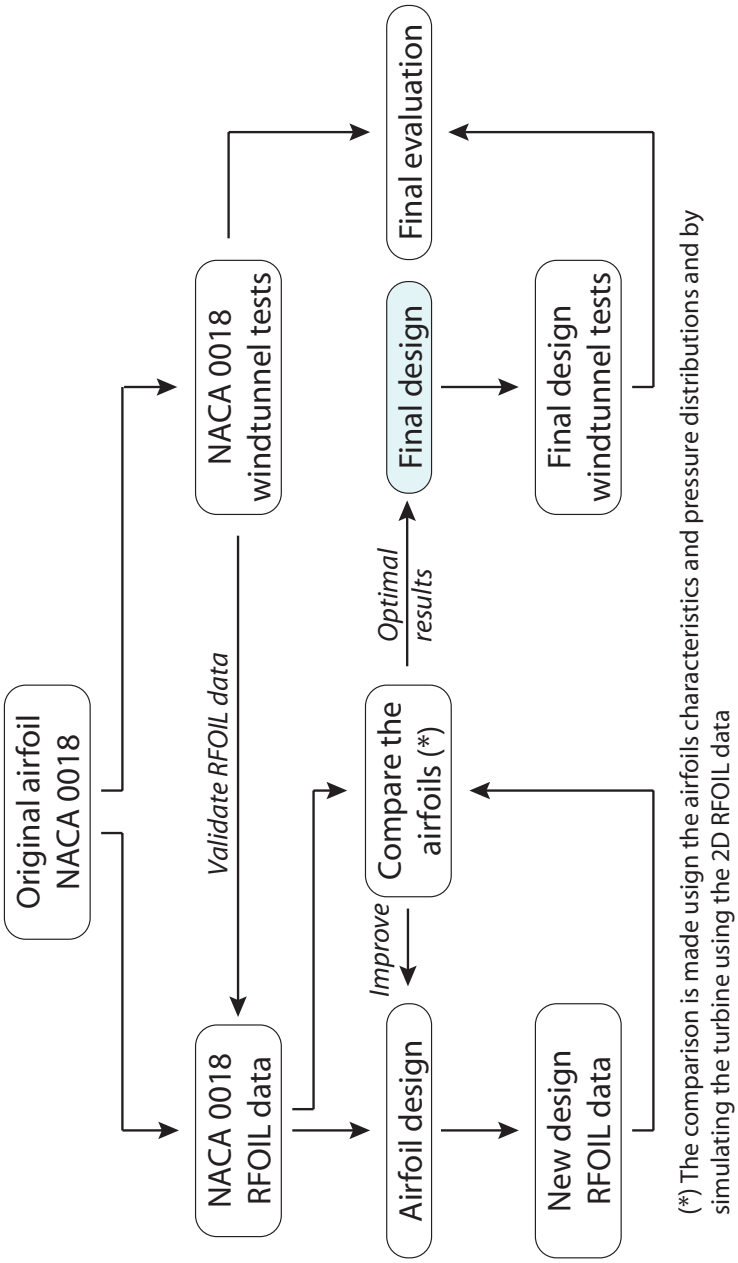

Figure 1.3: More detailed overview of the airfoil design

Chapter 2

VAWT aerodynamics

In this chapter the prevailing aerodynamic phenomena for the VAWT are discussed. In the first section the basics involved with the aerodynamic analysis are given. The flow conditions which are encountered by this turbine are given in the second section. The flow conditions determine for a large part the design criteria of the airfoil that has to be developed. These criteria are given in the last section. These phenomena also have to be incorporated in the simulation model of the turbine. The way in which this is done is discussed in chapter 3.

2.1 Basic aerodynamics

As the VAWT have a rotational axis perpendicular to the oncoming airflow, the aerodynamics involved are more complicated than of the more conventional HAWT. The main benefit of this layout is the independence of wind direction. The main disadvantages are the high local angles of attack involved and the wake coming from the blades in the upwind part and from the axis. If the turbine is represented in a two dimensional way (see figure 2.1) these characteristics are more obvious.

The rotational speed can be varied by the turbines controller for a certain wind speed. The rotational speed ω is therefore represented by the tip speed ratio λ. This parameter gives the tip speed $R\omega$ as factor of the free stream velocity V_{inf}:

$$\lambda = \frac{R\,\omega}{V_{inf}} \tag{2.1}$$

The Reynolds number is a measure of the viscous behavior of air:

$$Re = \frac{\rho V c}{\nu} \tag{2.2}$$

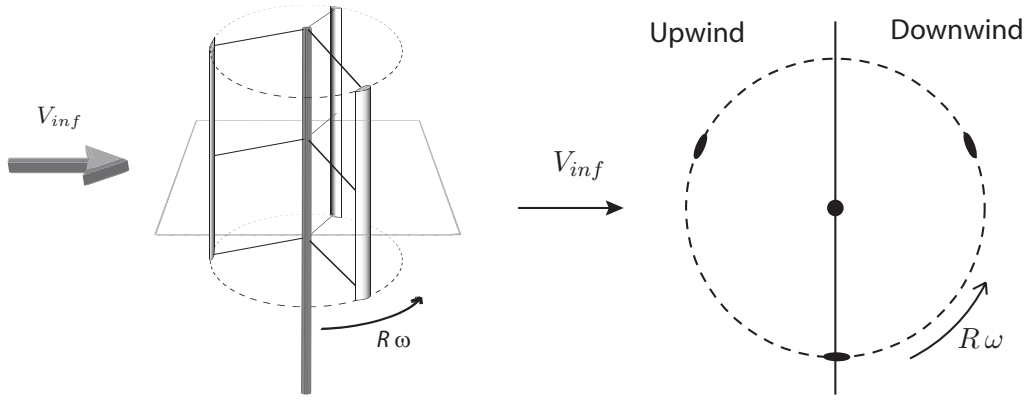

(a) 3D schematic **(b)** 2D cross section

Figure 2.1: 2D cross section from the turbine

The performance of the turbine is given by the power coefficient C_P. This coefficient represents the produced energy of the turbine as part of the total wind energy passing through the swept area of the turbine. This area equals the frontal area of the turbine given by the height times the diameter. This coefficient is normally plotted against the tip speed ratio λ at a certain Reynolds number, see figure 2.2. The tip speed ratio and Reynolds number are in this case both dependent of V_{inf}.

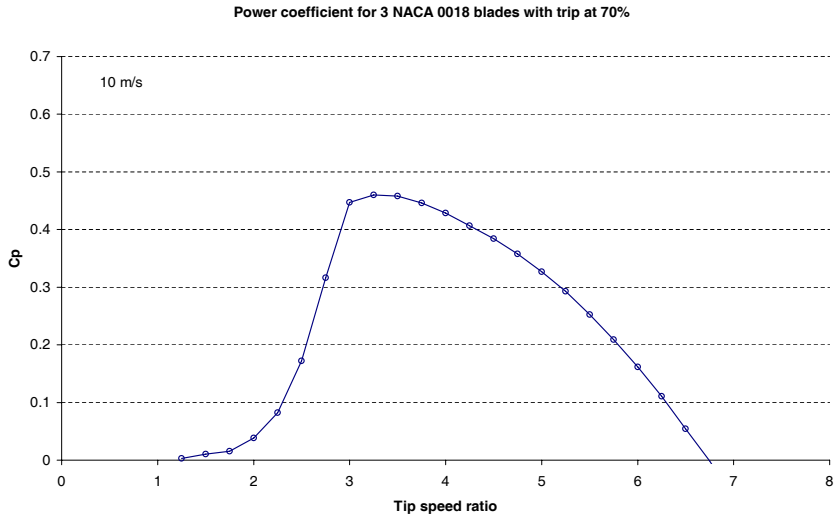

Figure 2.2: Power efficiency results for a VAWT at $V_{inf} = 10\frac{m}{s}$

2.2 Flow conditions

Below the prevailing flow conditions for a VAWT are described. These conditions are important to set the design goals and the correct boundary conditions for the design. The concluding design goals are given in the following section.

2.2.1 Angle of attack

One of the largest challenges of the VAWT is the wide range of angles of attack the blades experiences. When the turbine starts from zero rotational speed, the blades even experience back flow. With increasing rotational speed, the maximum angle of attack decreases. See figure 2.3. The larger the rotational speed, the smaller the influence of the free stream flow on the local speed W. The blade will be optimized for the Turby VAWT, which operates at a tip speed ratio of 3. As can be seen in figure 2.3 the maximum angle of attack in this situation equals 16.5°. The angle varies with the turbine azimuth angle θ. As dynamic and exterior effects can increase this angle, a larger angle of attack has to be taken into account in the design phase. In the interval where the angle of attack is negative, the maximum angle of attack is lower. The blades extract energy from the airflow at the upwind side, resulting in a lower air speed and thus a lower angle of attack at the downwind side.

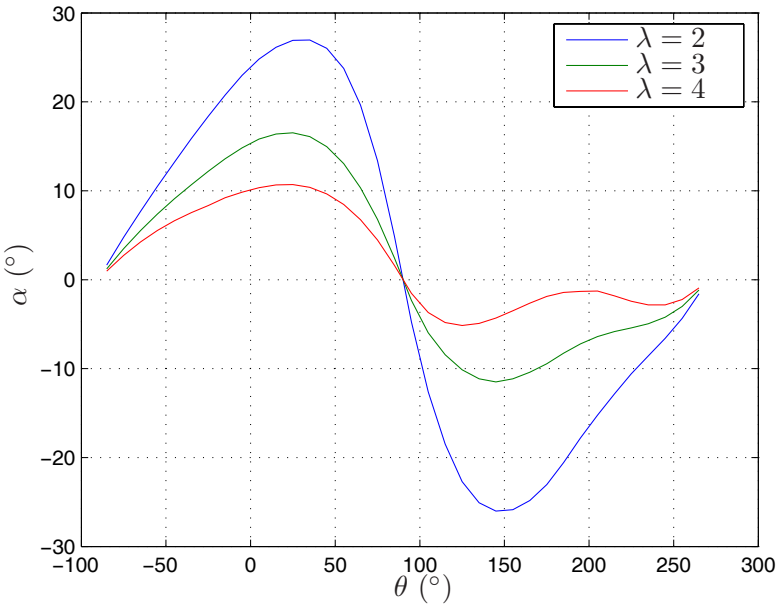

Figure 2.3: The angle of attack variation as function of θ at $V_{inf} = 10\frac{m}{s}$

2.2.2 Deep stall

If the angle of attack over a wing is increased, at some moment the airflow will separate. The separation starts at the trailing edge of the airfoil and shifts forward with increasing angle. If the angle is increased further the separation moves forward to the leading edge. This phenomenon is called deep stall. At very low Reynolds numbers separation can occur at the airfoils nose right away, but this is outside the scope of this research. If the airfoil is in deep stall, this condition will be maintained for some time, even if the angle is decreased again. This will cause a hysteresis loop, see figure 2.4. Here the deep stall starts at $\alpha = 21°$ and the hysteresis loop ends at $\alpha = 13.5°$. This phenomenon has a strong negative influence on the performance of the blade, because in the loop the lift is low and the drag remains high.

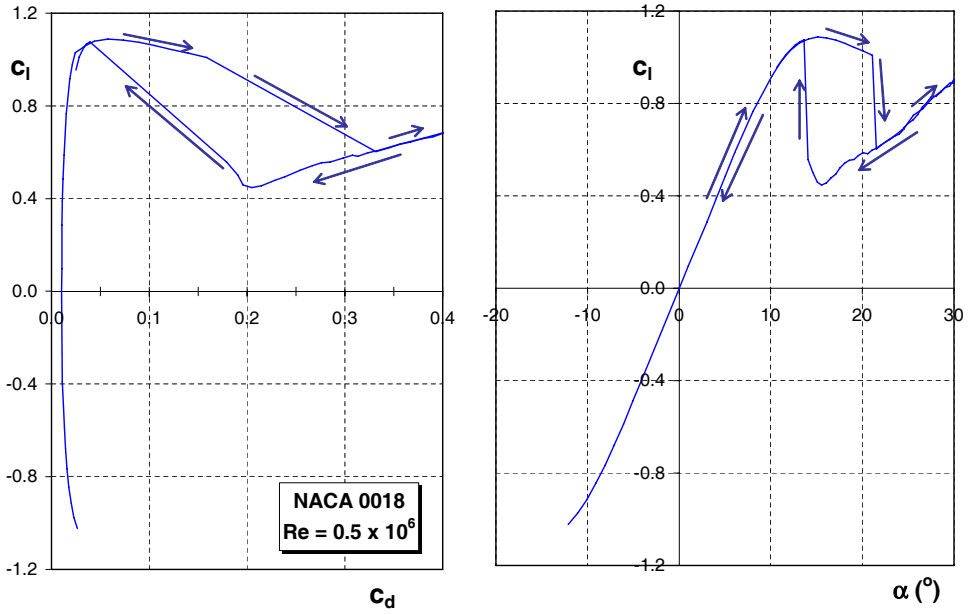

Figure 2.4: The deep stall characteristics of the NACA 0018 profile

The angle at which deep stall occurs dependents on the Reynolds number and the nose radius. In the VAWT application of airfoils large angles of attack are encountered. At the operating tip speed ratio this phenomenon therefore should be avoided or its influence should be kept as small as possible. Figure 2.5 shows the results for deep stall for different profiles measured at the TU Delft plotted against the parameter $\frac{y}{c}$ at $\frac{x}{c} = 0.0125$.

The negative values in figure 2.5 are the values for the lower side of the profile. All the test models had a chord of 60 cm, [W.A. Timmer, 2003]. The resulting straight line can be translated to the following relation between the thickness of the nose and the

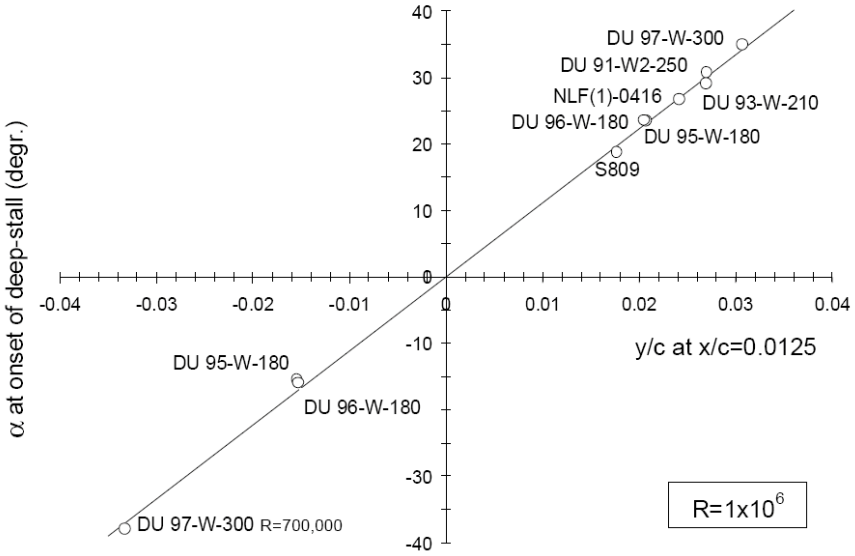

Figure 2.5: The deep stall characteristics of multiple profiles

deep stall angle:

$$\alpha_{deep-stall} = 1114 \left(\frac{y}{c}\right)_{\frac{x}{c}=0.0125} \tag{2.3}$$

2.2.3 Dynamic stall

Dynamic stall is a phenomenon that occurs at airfoils with rapid changing angle of incidence. The resulting effect of this changing angle is a difference, a hysteresis, in the lift, drag and moment characteristics between increasing and decreasing angle of incidence. Dynamic stall is characterized by the shedding and passage of a vortex-like disturbance over the low pressure surface of the lifting body. The main parameter of influence is related to the airfoil motion and the boundary layer separation. The main fields of research in dynamic stall are helicopter or fighter aircraft application. Some of those methods are modified for wind turbine applications and also research specifically in this field is performed.

The Darrieus type wind turbine is especially susceptible to dynamic stall, as the change in angle of incidence is large, especially at low tips speed ratios. As the blades perform a complete circle, the blades in the downstream part of the turbine are influenced by the wake resulting from the upstream blades. A good understanding of dynamic stall and the resulting wake is therefore important.

First visualization of the dynamic stall for the VAWT was done by [Brochier et al., 1986]. Using a water channel, visualizations were made with LDV and hydrogen bubbles at an Reynolds number of 10,000 and tip speed ratios

varying from 1 to 8 on a Darrieus turbine with two NACA 0018 blades. The results for $\lambda = 2.14$ are shown in figures 2.6(a) and 2.6(b).

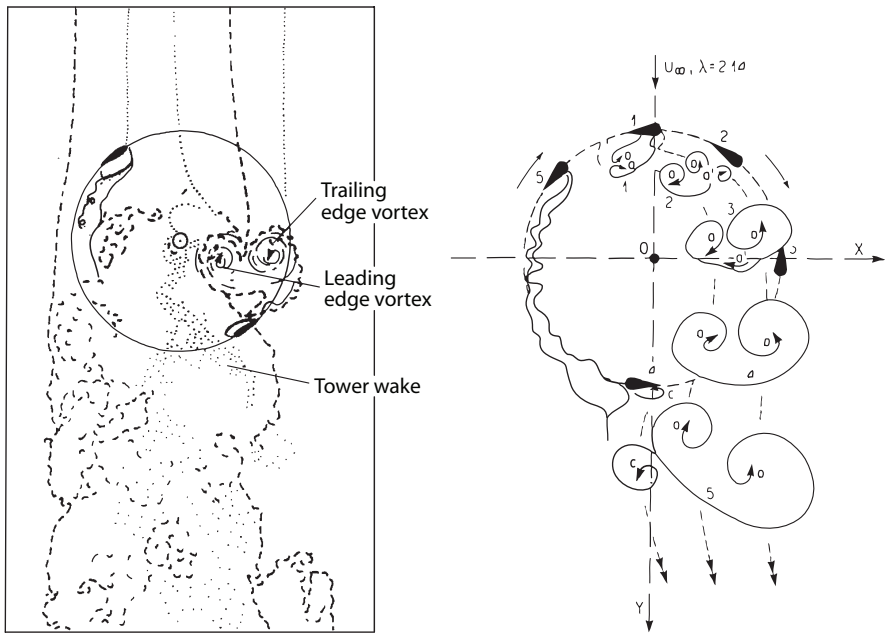

(a) Flow visualization **(b)** Schematic diagram

Figure 2.6: Visualization of dynamic stall at $\lambda = 2.14$, [Brochier et al., 1986]

The first vortex is formed at the leading edge of the airfoil. A second vortex, turning in the opposite direction, originates form the trailing edge. Together they form the characterizing doublet of two counter rotating vortices, which travels downstream to meet the second blade. This is confirmed by measurements made in a water channel using PIV by [Fujisawa and Shibuya, 2001] on a one NACA 0018 blade Darrieus turbine without central column. The flow visualization is showed in figure 2.7. The formation of the vortices is clearly visible. In this case two pairs of stall vortices are found. The first pair is formed at small blade angles and develops through the wake. The second pair is formed at large blade angles and will follow the blade at the inner side.

As the encountered angles of incidence are larger at lower tip speed ratios, the dynamic stall is more present. As can be seen in figure 2.8 the dynamic stall will start earlier and the vortices themselves are larger. The structure of the stall itself is independent of the tip speed ratio. At higher ratios, above 4, the dynamic stall will become of less importance. Although dynamic stall will increase the performance of the turbine, it includes also large disadvantages. It will cause an increase in noise, aero-elastic vibrations and blade fatigue.

Both studies show the strong asymmetry in the flow properties inside the turbine. The blades pass through the wake in only a part of the cycle. In this part they will experience highly turbulent flow.

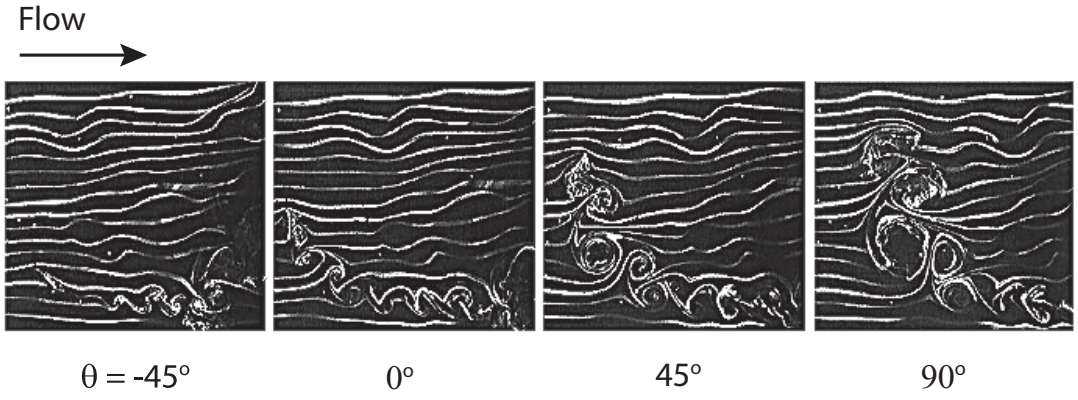

Figure 2.7: Flow visualization at four different positions, [Fujisawa and Shibuya, 2001]

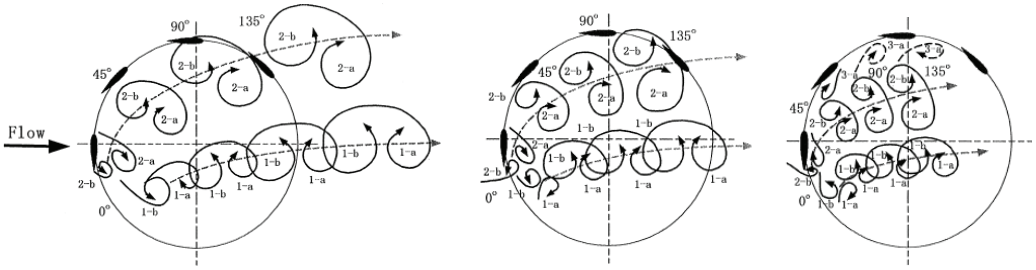

(a) $\lambda = 1$ **(b)** $\lambda = 2$ **(c)** $\lambda = 3$

Figure 2.8: Schematic illustration of the dynamic stall for different λ, [Fujisawa and Shibuya, 2001]

2.2.4 Reynolds number

A crucial factor for small turbine design is the low Reynolds range (< 1 million) in which they operate (see figure 2.9). Most studies in aerodynamics are performed for aircraft applications in which the Reynolds number lies above 3 million. It is very difficult and often impossible to find the right data for airfoils in this low Reynolds number range.

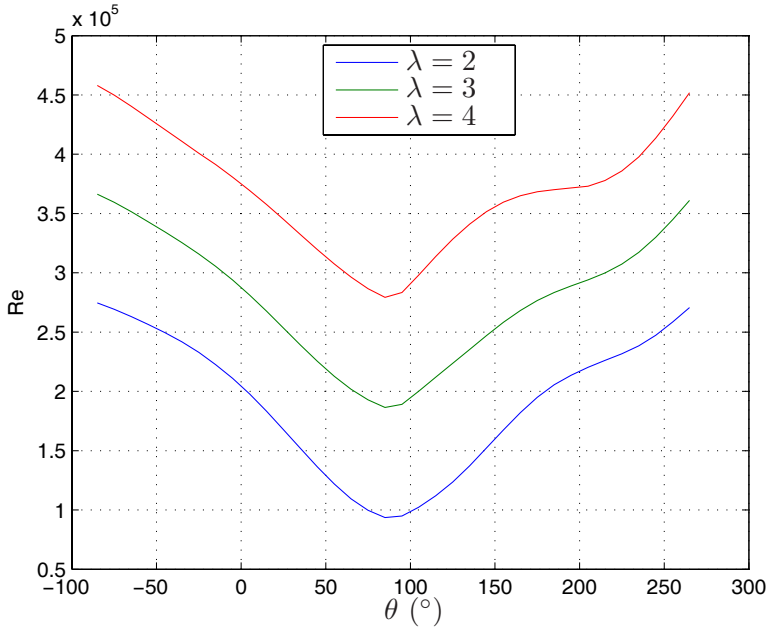

Figure 2.9: The Reynolds number variation at $V_{inf} = 10\,m/s$

In figures 2.10 to 2.13 the effects of the Reynolds number on the aerodynamics of an airfoil is shown. For the currently used NACA 0018 profile the maximum lift coefficient and the stall angle of attack drastically decreases with a decreasing Reynolds number (figure 2.10). These effects can be noticed for all turbulent NACA symmetric airfoils, see figure 2.11. The difference in maximum lift coefficient between Re = 3 million and Re = 0.3 million can be as much as 60%. The VAWT operates at low Reynolds numbers and high angles of attack, therefore the negative Reynolds number effects on the airfoils performance have to be taken into account when working with airfoil data of higher Reynolds number.

From experiments performed on VAWT by [Sheldahl et al., 1980] the influence of the Reynolds number is also shown. The chord Reynolds number was changed by altering the rotational speed of the turbine. Also the wind speed was changed to view the performance over the tip speed range, see figures 2.12 and 2.13.

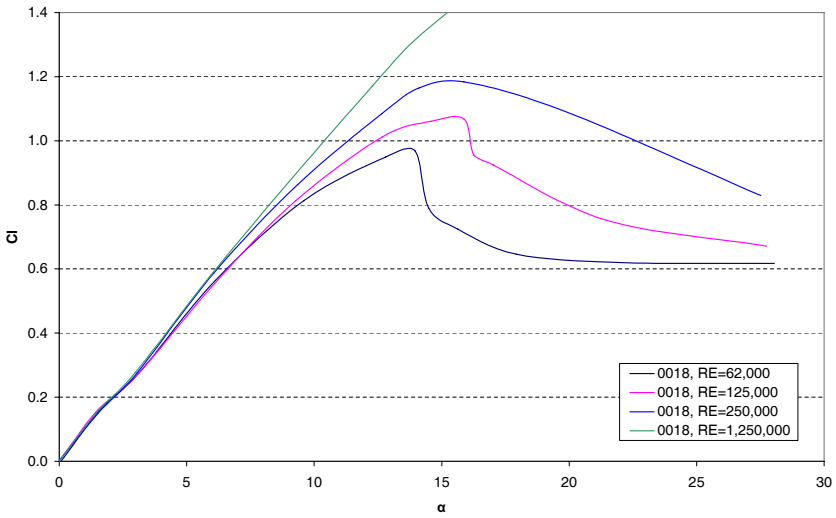

Figure 2.10: Reynolds effects on the lift curve of the NACA 0018 profile, [Jacobs and Sherman, 1937]

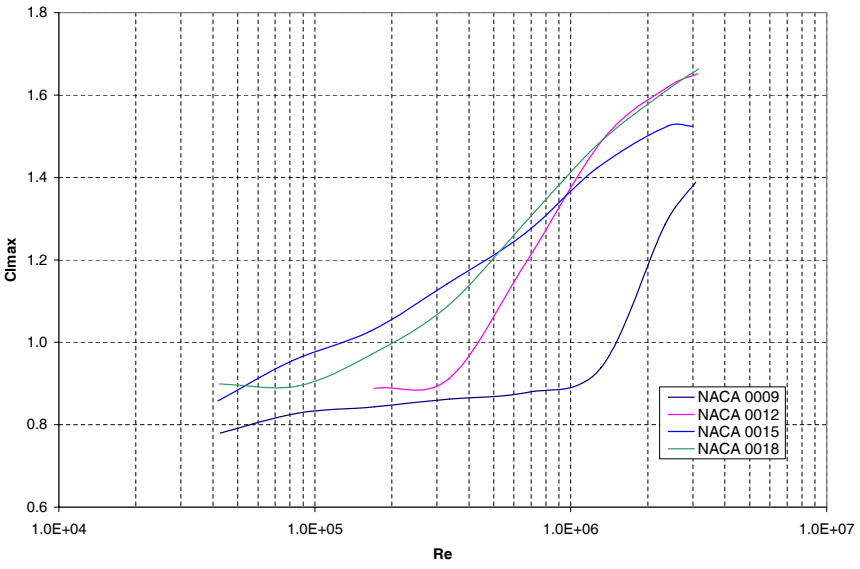

Figure 2.11: Reynolds effects on the maximum lift the NACA 00xx series profiles, [Jacobs and Sherman, 1937]

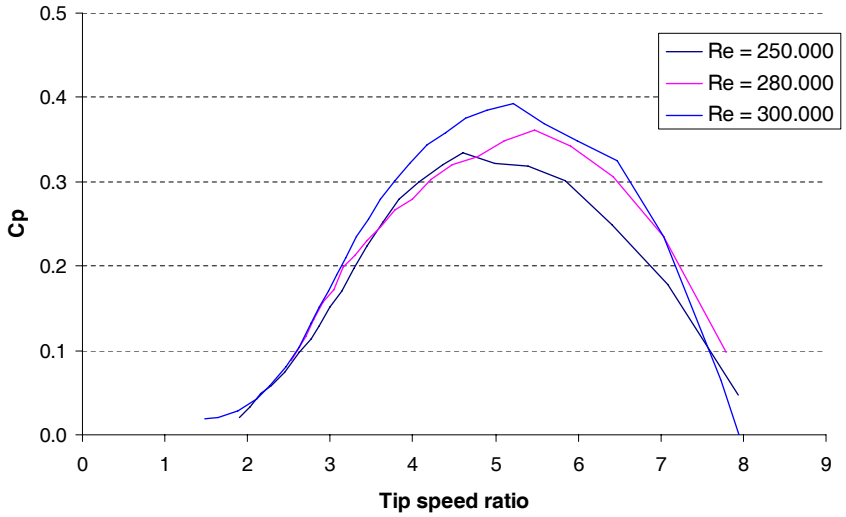

Figure 2.12: Reynolds number influence on the Sandia 5 meter turbine, [Sheldahl et al., 1980]

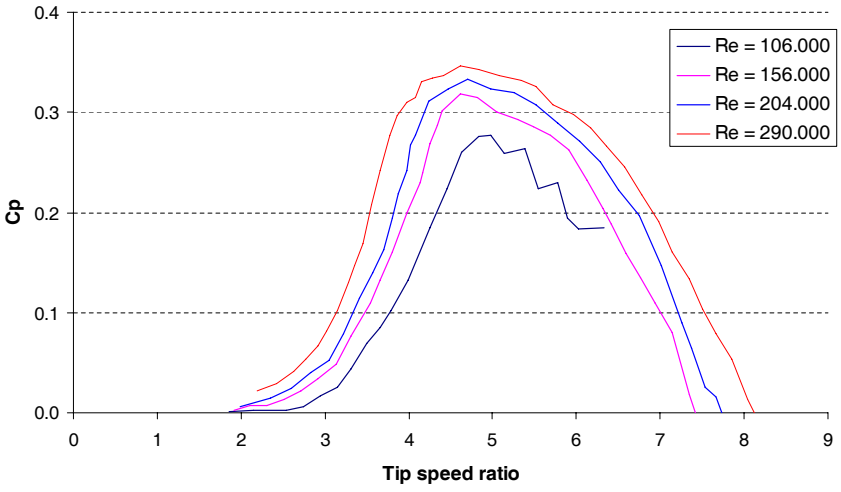

Figure 2.13: Reynolds number influence on the Sandia 2 meter test rotor, [Paraschivoiu, 2002]

2.2.5 Laminar separation bubbles

In low Reynolds conditions a specific feature called laminar separation bubbles is often present. The laminar boundary layer is no longer able to follow the contour of the airfoil as a result of the adverse pressure gradient. At the same time the instabilities in the boundary layer have not developed enough to cause the layer to become turbulent. Therefore the laminar boundary separates. This flow can turn turbulent and reattach itself to the airfoil again, forming the so called laminar separation bubble. In some cases the bubble can extend over the trailing edge of the airfoil because the adverse gradient is too large for the turbulent layer to reattach. The latter occurred in the case of the NACA 0018 airfoil at lower Reynolds numbers, see figure 2.14. At higher Reynolds numbers the appearance of separation bubbles shifts to higher angles of attack. The most effective solution is to apply a turbulator, e.g. zigzag tape, at a position before the laminar layer separates.

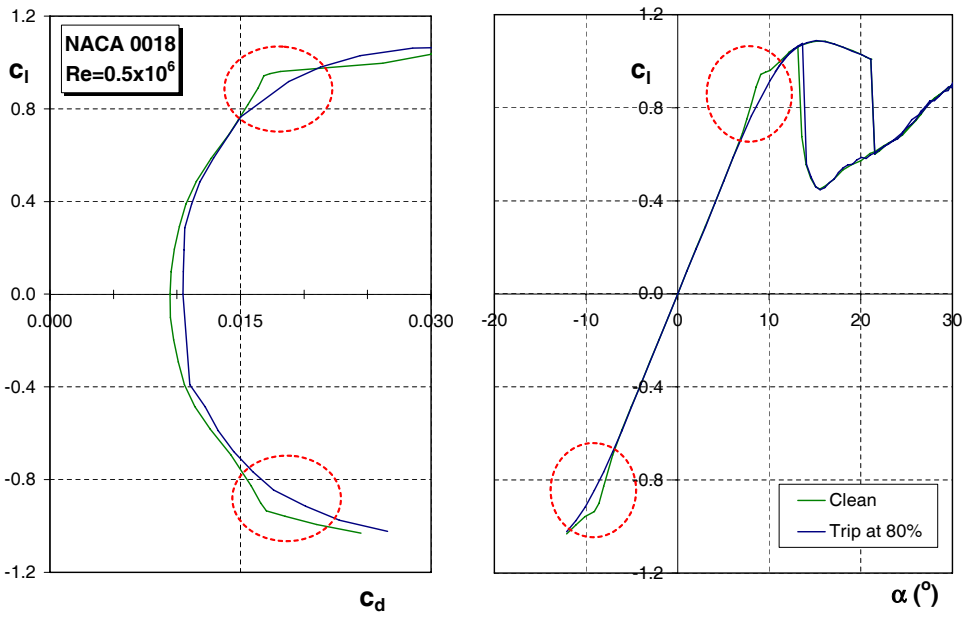

Figure 2.14: Laminar separation bubbles for the NACA 0018

2.2.6 Virtual camber

Research performed by [Migliore et al., 1980] shows that the aerodynamic characteristics of an airfoil differ between situations of curvilinear flow fields and rectilinear flow fields. Due to the fact that the airfoil is rotating the symmetric airfoil behaves like an airfoil in rectilinear flow with camber and with a virtual angle of incidence (see figure 2.15). The influence of the curvilinear flow field on the aerodynamic characteristics depends very much on the blade chord to turbine radius ratio $\frac{c}{R}$. If this ratio becomes larger, the influence of curvilinear flow increases as well. Virtual camber causes an upward shift of the lift curve and introduces an aerodynamic moment. Virtual incidence causes the lift curve to shift to the left. The exact impact of these phenomena on the airfoil performance in VAWT is not yet established.

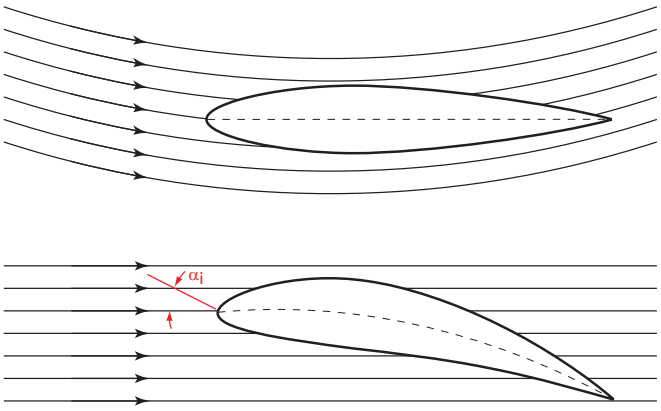

Figure 2.15: The principal of virtual camber as a result of curvilinear flow, [Migliore et al., 1980]

2.3 Design criteria

From the flow conditions in which the VAWT turbine operates, described in the previous section, certain airfoil design parameters can be established. Optimum values for these parameters may be conflicting and compromises should be made. The design is made using the NACA 0018 airfoil as reference. In chapter 5 more information about the design of the new airfoil is given.

The parameters of interest are:

- Designed to perform well at Reynolds numbers between 150,000 and 700,000
- Low zero drag coefficient
- Increased width of the drag bucket to maintain performance over a larger range of α
- Increased thickness to improve structural strength
- Smooth stall characteristics to reduce noise
- Large separation bubbles which extend over the trailing edge are a source of noise

Also deep stall characteristics are important with regard to airfoil design:

- Postpone deep stall to a larger angle of attack; a thicker airfoil will in general also have deep stall at a higher angle of attack
- The deep stall hysteresis loop should be as small as possible. Thicker airfoils have generally a larger drop in lift at deep stall
- The lift coefficient drop at deep stall should be as small as possible

Furthermore the use of cambered airfoils instead of symmetrical ones is investigated.

Chapter 3

Simulation methods

The shape of the turbine blade has to be connected to the performance of the turbine. A simulation program was made using 2D airfoil data to predict the performance of the turbine. The way in which 2D airfoil data is generated will be discussed in the following chapters. In this chapter the different methods in which the turbine can be simulated and the way in which the 2D characteristics are implemented in these methods is discussed.

Different methods are possible for simulating the VAWT, each with its own benefits and drawbacks. The three main directions in modeling are: momentum based models, vortex models and CFD modeling. Each of these methods has its own benefits and drawbacks in terms of accuracy and complexity. In the sections below these methods will be explained in more detail.

3.1 Momentum theory based models

Momentum based models are based on of the actuator disk theory, which is generally used for rotor aerodynamics, adjusted for the VAWT. The basic model is called the single streamtube model. This model was developed in two directions. The first one was splitting the single streamtube in a number of parallel streamtubes, resulting in the multiple streamtube model. The other direction was the double actuator disc analysis for the VAWT. This model places two actuator disks is tandem formation, resulting in two interference factors; one for the upwind side and one for the downwind side. These models were eventually combined in the Double Multiple Streamtube (DMS) model. One disadvantage of this model is that the interference factors are fixed for the upwind and downwind side, as such they can not be adjusted for each streamtube. By modifying the DMS model this is made possible. The only major improvement since was the implementation of a dynamic stall model. There are many different dynamic stall models, with different accuracy and complexity, see section 3.3.

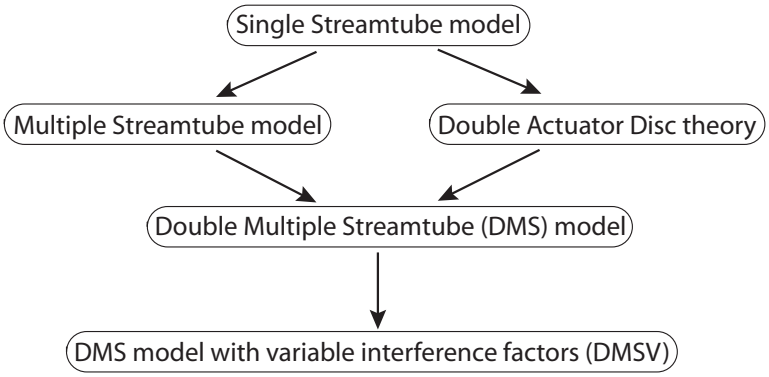

Figure 3.1: Overview of the development of the streamtube models

The momentum based models are limited to smaller tip speed ratios and to a solidity below 0.2, because the Glauert momentum theory is not valid outside this range. Also quasi-steady flow through the turbine and constant streamwise velocity as function of free stream velocity is assumed. The velocities normal to the free stream velocity are neglected.

3.1.1 Single Streamtube Model

This model was first developed by Templin ([Templin, 1974]) for the VAWT. It is based on the actuator disk theories applicable for propellers and is the most basic model based on the momentum theory. The flow through the turbine is assumed to have one constant velocity.

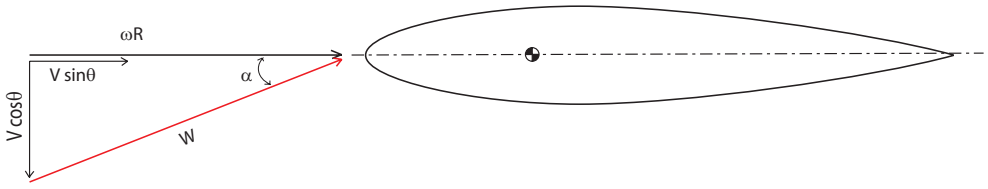

Figure 3.2: Components of the local angle of attack

The local angle of attack is given by:

$$\alpha = arctan\left(\frac{cos(\theta)}{\frac{R\omega}{V} - sin(\theta)}\right) \tag{3.1}$$

The forces on the blade elements are based on available experimental 2D airfoil data:

$$C_N = C_L\, cos(\alpha) + C_D\, sin(\alpha) \tag{3.2}$$
$$C_T = C_L\, sin(\alpha) - C_D\, cos(\alpha) \tag{3.3}$$

$$dN = C_N \, q \, c \, dz \tag{3.4}$$

$$dT = C_T \, q \, c \, dz \tag{3.5}$$

The drag experienced by one element, or the force in the direction of the airflow, is:

$$dD = qc \left(C_N \, sin(\theta) - C_T \, cos(\theta) \right) \tag{3.6}$$

The total drag for a turbine with N blades with chord C on the complete interval $(0 < \theta < 2\pi)$ and $(-H < z < H)$ results in:

$$D = \frac{Nc}{2\pi} \int_{z=-H}^{H} \int_{\theta=0}^{2\pi} q \left(C_N \, sin(\theta) - C_T \, cos(\theta) \right) d\theta dz \tag{3.7}$$

3.1.2 Multiple Streamtubes Model

This model is developed by Strickland [Strickland, 1975] and is also based on the momentum theory. The main improvement with respect to the single streamtube model is that more streamtubes make different induced velocities possible (see figure 3.3). Each streamtube has its own velocity, allowing a change in velocity depending on the direction perpendicular to the freestream flow. The accuracy is dependent on the number of streamtubes used. It gives good results for low tip speed ratios and low solidity.

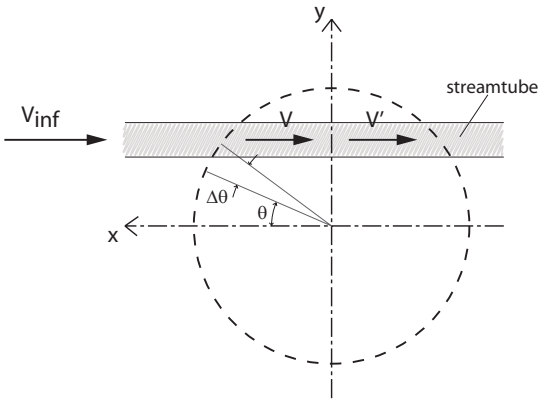

Figure 3.3: 2D schematic of the streamtube model

The total span of the single streamtube is divided in multiple streamtubes using a fixed angle $\Delta\theta$ as width.

$$\Delta\theta = \frac{2\pi}{N_\theta} \tag{3.8}$$

For each of these streamtubes the momentum equations and blade elements have to be calculated, resulting in N interference factors $u_i\,, i = 1 \rightarrow N$.

3.1.3 Double actuator disc theory

The main disadvantages of the previous models is the inability to make a distinction between the upwind and downwind part of the turbine. To make this possible, two actuator discs are placed behind each other, connected at the center of the turbine (see figure 3.4).

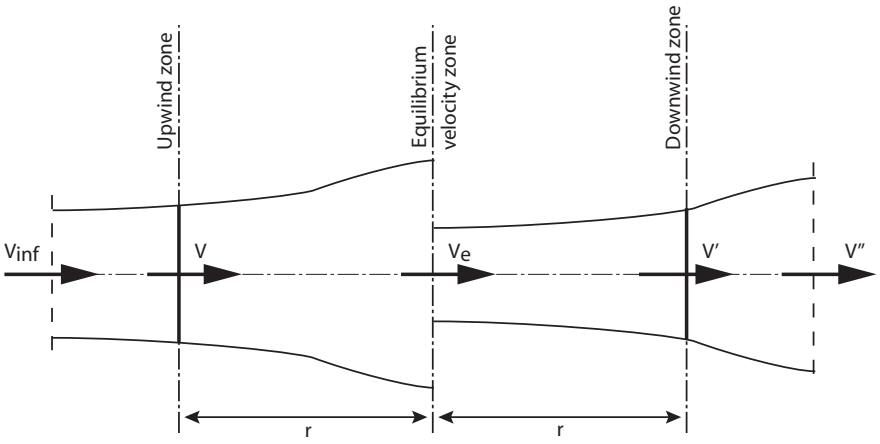

Figure 3.4: Schematic of the two actuator discs behind each other

The velocities are determined by two interference factors, u and u':

$$V = u\,V_{inf} \tag{3.9}$$

$$V_e = (2u - 1)\,V_{inf} \tag{3.10}$$

$$V' = u'\,V_e = u'\,(2u - 1)\,V_{inf} \tag{3.11}$$

3.1.4 Double-Multiple Streamtubes Model

The DMS model described by [Loth and McCoy, 1983] and [Paraschivoiu and Delclaux, 1983] combines the multiple streamtubes model with the double actuator disc theory. This allows to model velocity variations in the direction perpendicular to the freestream flow and between the upwind and downwind part of the turbine. The previous models were not able to calculate the influence of the upwind part on the downwind part. As a result non-symmetrical airfoils, which depend on this difference, could not be simulated accurately. It is easily understood that the wind velocities at the upwind part are larger than these at the downwind part, because the blades have already extracted energy from the wind.

The flow is divided horizontally into tubes, each with the angular width of:

$$\Delta\theta = \frac{2\pi}{N_\theta} \tag{3.12}$$

The streamwise force acting on one blade element is:

$$\Delta F_x = \Delta F_N cos\theta + \Delta F_T sin\theta \tag{3.13}$$

The tangential and normal force components ΔF_N and ΔF_T are linked to the airfoil characteristics in the following way:

$$C_N = \frac{\Delta F_N}{\frac{1}{2}\rho W^2 c\Delta z} \tag{3.14}$$

$$C_T = \frac{\Delta F_T}{\frac{1}{2}\rho W^2 c\Delta z} \tag{3.15}$$

Resulting in the equation:

$$\Delta F_x = \frac{1}{2}\rho W^2 c\Delta z[C_N cos\theta + C_T sin\theta] \tag{3.16}$$

This is the force which is experienced by one blade element. Each element passes through the stream tube of $\frac{\Delta\theta}{2\pi}$ and there are B number of blades, so the averaged force equals:

$$\overline{\Delta F_x} = \frac{1}{2}\rho W^2 \frac{B\Delta\theta}{2\pi} c\Delta z[C_N cos\theta + C_T sin\theta] \tag{3.17}$$

The local velocity W is the resultant of the rotational speed ΩR and the airspeed at the rotor V. These variables can be transformed to the single variable, tip speed ratio λ:

$$\lambda = \frac{\Omega r}{V} \tag{3.18}$$

$$W = V\sqrt{[\lambda - sin\theta]^2 + [cos\theta]^2} \tag{3.19}$$

The local angle of attack depends on the tip speed ratio λ and the position of the element θ:

$$\alpha = tan^{-1}\left[\frac{cos\theta}{\lambda - sin\theta}\right] \tag{3.20}$$

Upwind half $-\frac{\pi}{2} \leq \theta \leq \frac{\pi}{2}$:

$$W^2 = V^2 \left[\left(\frac{\omega R}{V} - \sin\theta \right)^2 + \cos^2\theta \right] \tag{3.21}$$

$$\alpha = \arctan \left[\frac{\cos\theta}{\frac{\omega R}{V} - \sin\theta} \right] \tag{3.22}$$

Downwind half $\frac{\pi}{2} \leq \theta \leq \frac{3\pi}{2}$:

$$W'^2 = V'^2 \left[\left(\frac{\omega R}{V'} - \sin\theta \right)^2 + \cos^2\theta \right] \tag{3.23}$$

$$\alpha = \arctan \left[\frac{\cos\theta}{\frac{\omega R}{V'} - \sin\theta} \right] \tag{3.24}$$

The resulting force on the blade element can be calculated by first calculating C_N and C_T and the resulting force in streamwise direction $\overline{\Delta F_x}$ with equation (3.17). Using the momentum theory the streamwise force also can be written as:

$$\overline{\Delta F_x} = 2\rho S U (U_\infty - U) \tag{3.25}$$

Filling in the calculated value of $\overline{\Delta F_x}$ the factor $\frac{U}{U_\infty}$ is found, which equals the interference factor a. By starting with $U = U_\infty$ after one calculation the interference factor a is found. The next iteration round the following airspeed is used:

$$U = aU_\infty \tag{3.26}$$

These iteration steps can be continued until the value of the interference factor reaches the requested accuracy.

3.2 Non - momentum theory based models

Besides momentum based models different models are available for simulating vertical axis wind turbines. The two most important are vortex models and CFD. For this study these models were not applicable because they are too time consuming for the design process. To give a complete overview of the available simulation models both models will be explained in brief below.

3.2.1 Vortex models

Vortex models are based on vorticity equations. The blade element is replaced by a lifting line which represents the flow field at distances more then one chord away from the airfoil. The benefit is that pressure field values are not needed to obtain a velocity field. In contrast to momentum based models this method is also applicable for VAWT turbines with high solidity and at large tip speed ratios. Furthermore the momentum based models are not capable of giving information of the wake structure near the turbine, as velocity normal to the airflow is neglected. The main vortex models for the VAWT turbine are the free-wake vortex model and fixed-wake momentum theory (combination of vortex theory and momentum method).

As for our study both the solidity and tip speed ratios are not large and only the overall performance of the turbine is needed, the vortex models offer no benefits over the momentum based models. As the amount of work needed for the vortex models is substantially more, this type of models is neglected.

3.2.2 CFD models

If even more accuracy and details are needed, Computational Fluid Dynamics (CFD) offers the best solution in comparison to momentum and vortex models. Even unsteady calculations are a possibility. This method uses a grid around a 3D model of the turbine to calculate the complete airflow around it. The mesh size and computational models determine the accuracy of the result. A lot of computer power and time is required for CFD and the generation of the 3D model and mesh take a lot of time. Also implementing any airfoil changes require a lot of time. As both the computational time and airfoil changes are very important for the model used during this project, CFD is not a feasible option.

3.3 Dynamic stall models

Dynamic stall is a phenomenon which occurs on airfoils with a rapidly changing angle of incidence. The effect of this changing angle is a difference, a hysteresis, in the lift, drag and moment characteristics between increasing and decreasing angle of incidence. Dynamic stall is characterized by the shedding and passage of a vortex-like disturbance over the low pressure surface of the lifting surface. The main parameters of influence are related to the airfoil motion and the boundary layer separation. The main fields of research in dynamic stall are concentrated on helicopter or fighter aircraft applications. Some of those methods are modified for wind turbine applications and also research specific for this field is performed. The models can be split in (semi-)empirical and theoretical models. For the implementation in the streamtube models the semi-empirical methods are most useful, although these models are very crude.

3.3.1 Gormonts model

A model which empirically approaches the dynamic stall behavior for helicopter application was developed by [Gormont, 1973]. It models the hysteresis effect by defining a reference angle of attack at which static airfoil data is taken. The difference between the geometrical angle α and the reference angle α_{ref} determines the influence of the dynamic stall.

$$\alpha_{ref} = \alpha - K_1 \, \Delta\alpha \tag{3.27}$$

The reference angle of attack is off course different for increasing and decreasing α:

$$K_1 = \begin{cases} 1 & \text{when} \quad \dot{\alpha} \geq 0 \\ -0.5 & \text{when} \quad \dot{\alpha} < 0 \end{cases} \tag{3.28}$$

$$\Delta\alpha = \begin{cases} \gamma_1 & \text{when} \quad S \leq S_c \\ \gamma_1 S_c + \gamma_2 (S - S_c) & \text{when} \quad S > S_c \end{cases} \tag{3.29}$$

$$S = \sqrt{\left| \frac{c\dot{\alpha}}{2W} \right|} \tag{3.30}$$

$$S_c = 0.06 + 1.5 \left(0.06 - \frac{t}{c} \right) \tag{3.31}$$

$$\gamma_1 = \begin{cases} \frac{\gamma_2}{2} & \text{for lift characteristic} \\ 0 & \text{for drag characteristic} \end{cases} \tag{3.32}$$

$$\gamma_2 = \gamma_{max} max \left\{ 0, min \left[1, \frac{M - M_2}{M_1 - M_2} \right] \right\} \tag{3.33}$$

The resulting dynamic coefficients are given by:

$$C_L^{dyn} = C_L(\alpha_0) + m(\alpha + \alpha_0) \tag{3.34}$$

$$C_D^{dyn} = C_D(\alpha_{ref}) \tag{3.35}$$

$$m = min\left[\frac{C_L(\alpha_{ref}) - C_L(\alpha_0)}{\alpha_{ref} - \alpha_0}, \frac{C_L(\alpha_{ss}) - C_L(\alpha_0)}{\alpha_{ss} - \alpha_0}\right] \tag{3.36}$$

The values for M_1, M_2 and γ_{max} are dependent on whether the lift or drag is calculated (see table 3.1).

Table 3.1: Gormont values for M_1, M_2 and γ_{max}

	Lift characteristics	Drag characteristics
M1	0.4+5.0(0.06-t/c)	0.2
M2	0.9+2.5(0.06-t/c)	0.7+2.5(0.06-t/c)
γ_{max}	1.4+6.0(0.06-t/c)	1.0+2.5(0.06-t/c)

3.3.2 Strickland et al. modification

The Gormont method hase been adjusted for VAWT application by [Strickland, 1975]. The following assumptions were made:

- S_c is equal to 0, because the thickness used in VAWT application is usually larger then 12%
- The flow is incompressible, no Mach number dependency
- The dynamic stall model is only applied if $\alpha \geq \alpha_{ss}$
- The lift curve curve slope and zero lift angle remain the same
- The dynamic stall only effects the angle at which stall occurs

$$\alpha_{ref} = \alpha_B - \gamma\, K_1 \left(\left|\frac{c\dot{\alpha_B}}{2W}\right|\right)^{1/2} S_{\dot{\alpha}} \tag{3.37}$$

K_1 is again dependent on the sign of the instantaneous rate of change of the angle of attack:

$$K_1 = 0.75 + 0.25 S_{\dot{\alpha}} \tag{3.38}$$

Table 3.2: Strickland values for γ

	γ
Lift	$1.4 - 6.0\,(0.06 - t/c)$
Drag	$1.0 - 2.5\,(0.06 - t/c)$
Moment	$1.0 - 2.5\,(0.06 - t/c)$

The final values of the lift, drag and moment coefficients are given by:

$$C_L = \left(\frac{\alpha_B}{\alpha_M - \alpha_{B0}}\right) C_L(\alpha_M) \tag{3.39}$$

$$C_M = C_M(\alpha_M) \tag{3.40}$$

$$C_D = C_D(\alpha_M) \tag{3.41}$$

See figures 3.5(a) and 3.5(b) for the results of the Strickland dynamic stall model when applied to the NACA 0018 wind tunnel data.

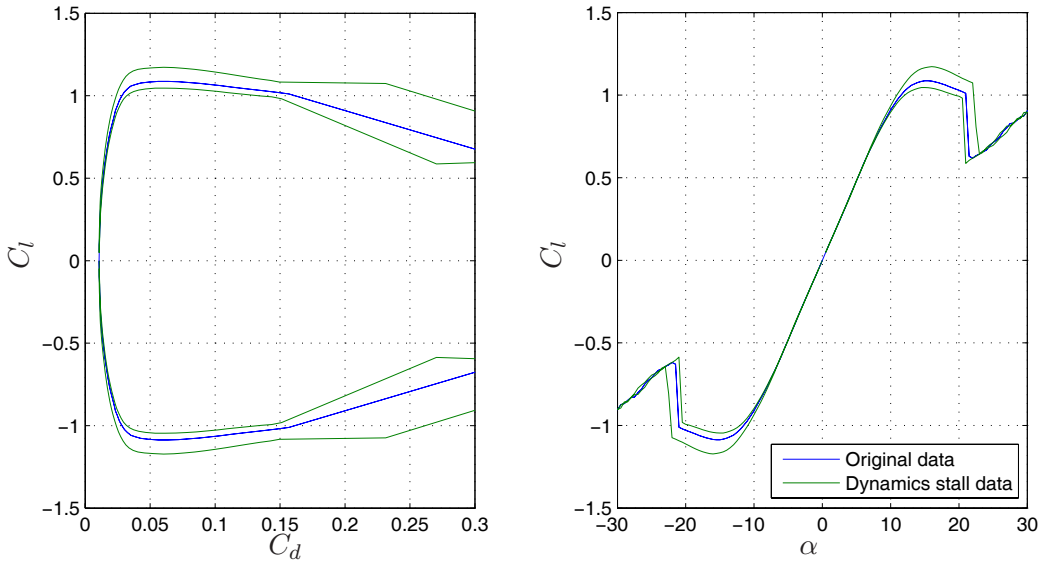

(a) Dynamic stall drag

(b) Dynamic stall lift

Figure 3.5: The Strickland dynamic stall model applied to the NACA 0018

3.3.3 Paraschivoiu et al. modification

In the Darrieus type wind turbines there are regions with large scale turbulence, see figure 2.6(b). Turbulence stabilizes the boundary layer of the airfoil. Dynamic stall therefore occurs at higher angles of attack then at regions without large scale turbulence. The main modification that [Paraschivoiu, 2002] made to the Gormont method modified by [Strickland, 1975] is limiting its application to a certain area of the wind turbine at which the turbulence is low, between the azimuth angles of 135 and 15 degrees.

3.3.4 Massé and Berg modification

In practice it was found that the model over predicts the effects of dynamic stall at large angles of attack. For the original Gormont model in section 3.3.1 this is not a problem, as in helicopter applications these large angles are not encountered. To solve this problem Massé as described by [Paraschivoiu, 2002] introduced a modification in which linearly interpolates between the static lift and drag values and the dynamic values. The influence decreases at larger angles until the static values are restored at $\alpha = A_M\,\alpha_{ss}$. In this modification the Mach number is still present, in contrast with the modification by Strickland.

$$C_L^{mod} = \begin{cases} C_L + \left[\frac{A_M\alpha_{ss}-\alpha}{A_M\alpha_{ss}-\alpha_{ss}}\right]\left(C_L^{dyn} - C_L\right) & \text{when} \quad \alpha \leq A_M\alpha_{ss} \\ C_L & \text{when} \quad \alpha > A_M\alpha_{ss} \end{cases} \tag{3.42}$$

$$C_D^{mod} = \begin{cases} C_D + \left[\frac{A_M\alpha_{ss}-\alpha}{A_M\alpha_{ss}-\alpha ss}\right]\left(C_D^{dyn} - C_D\right) & \text{when} \quad \alpha \leq A_M\alpha ss \\ C_D & \text{when} \quad \alpha > A_M\alpha_{ss} \end{cases} \tag{3.43}$$

The value of A_M is empirically determined for VAWT by Berg as described by [Paraschivoiu, 2002]. According to his research the best value for VAWT equals:

$$A_M = 6 \tag{3.44}$$

Also the static angle of stall α_{ss} is proposed to be the angle at which the lift curve no longer follows the linear lift behavior.

3.4 Simulation model

In this chapter different methods of modeling VAWT are discussed. The goal of the simulation program is the possibility to use 2D blade shape characteristics and calculate their performance in a VAWT. Fast blade shape adjustment and short calculation time are essential to incorporate the simulation program into the airfoil design process. CFD and vortex models are too time consuming to use for this purpose. Therefore the choice is made for momentum based models which are incorporated into the simulation program, which is built in MATLAB.

For this project it is important to have a simulation model which can differentiate between the upwind and downwind side of the turbine. This enables the program to take into account airfoils with camber. For the final simulation program the Double Multiple Streamtubes model was chosen. As dynamic stall model the [Strickland, 1975] modification to the Gormont model is chosen. As all these models are relatively crude, the option is left to chose whether to enable or disable dynamic stall. To be able to compare the different models, in the program it is possible to also choose for the Multiple Streamtubes model. The program allows to swiftly implement adjusted blade shapes by inserting the RFOIL data for these changed airfoils. Also the airfoils which were subject to the design process are available for implementation in the model.

Chapter 4

RFOIL

The simulation program discussed in the previous chapter uses 2D airfoil data to calculate the VAWT performance. The 2D data can be determined by wind tunnel testing, only this is not a feasible option for the design process since wind tunnel testing and the airfoil models are expensive. It is not economic to manufacture a model from each design and analyze it in the tunnel. For the practical design process the RFOIL program is used. This is based on the XFOIL program and uses the panel method in combination with boundary layer equations to calculate 2D airfoil characteristics. It is a fast design tool which offers the possibility to make changes in pressure distributions and geometries. Different computational options, like CFD, are too time consuming to be considered for use within the scope of this study.

To validate the RFOIL results, the data of four airfoils is available. These airfoils are divided into two groups: laminar and turbulent. The following airfoils or airfoils of the same family will be used later on in the design process. For the NACA 0018 data is available for Re = 300,000, 500,000 and 700,000. For the NACA 64-418 no data at Re = 500,000 is available and for the NLF-0416 profile only data at Re=500,000 is present.

- NACA 0018 (turbulent)
- NACA 64-418 (laminar)
- NFL-0416 (laminar)

All these profiles are compared at lower Reynolds numbers (< 1,000,000). RFOIL has problems to accurately predict the behavior of airfoils at these numbers, as laminar separation and reattachment play an important role. These aerodynamic phenomena are difficult to predict with high accuracy by computational methods. At higher Reynolds numbers the RFOIL performance is more accurate. Two examples at Re=3,000,000 are given in section 4.3.

4.1 Turbulent profiles

For this study tests on the turbulent NACA 0018 were performed at the TU Delft. Good data sets are not available in literature for the NACA 0018 profile. That is why tests were performed on the profile as part of this study. An overview of the test results can be found in Appendix B. The lift and drag of the NACA 0018 are determined using a balance. As the balance measures the forces on the total model, 3D effects as tunnel wall interference are accounted for. The results for the drag are corrected for these effects. The calculated RFOIL data is corrected for the wind tunnel data by adjusting the critical amplification factor N_{crit}. The amplification factor is a measure of the growth of instabilities in the boundary layer. The critical value is the value at which RFOIL decides the boundary layer turns turbulent. By adjusting this value, the RFOIL data can be adjusted for the different turbulence levels at different Reynold numbers of the wind tunnel. In the wind tunnel the turbulence level increases with increasing Reynolds number, the same trend can be viewed in the used critical amplification factor for RFOIL modeling.

In figure 4.1 it can be seen that the predicted RFOIL lift at Re = 300,000 is almost equal to the measurements using $N_{crit} = 12$. The RFOIL lift slope is equal to the corrected lift slope of the measurements. The drag is in good agreement with wind tunnel data (see figure 4.1).

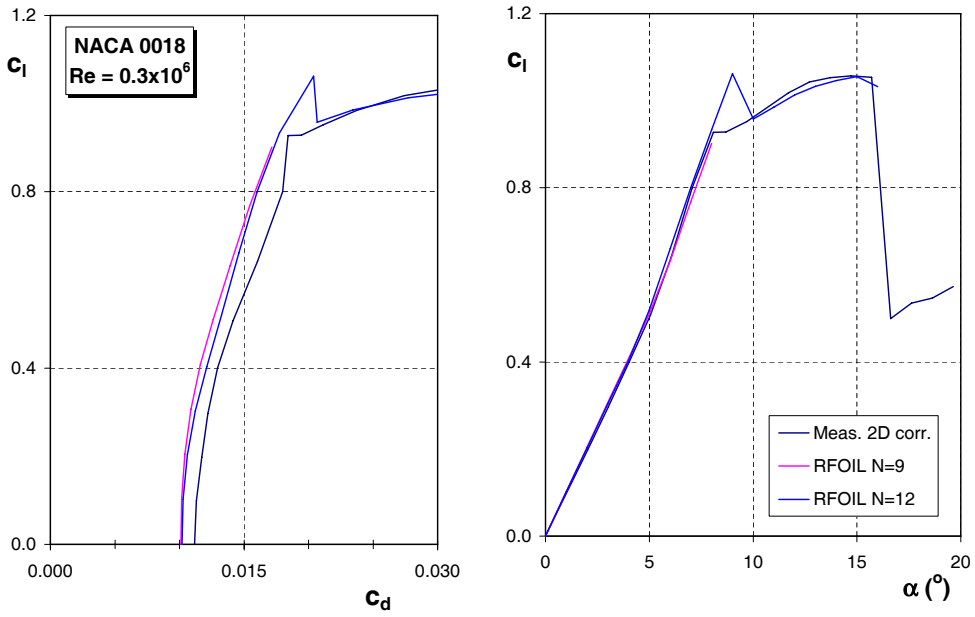

Figure 4.1: NACA 0018 characteristics at Re=300,000 trip at 70%

For Re = 500,000 the differences between measured and calculated lift slope become larger. The lift slope of the RFOIL data is steeper than the measurements, see fig-

ure 4.2. The lift is overpredicted until stall occurs. After $\alpha = 13$ the RFOIL lift decreases slightly, where the measured lift does not. RFOIL under predicts the lift at high angles of attack, but the validity of RFOIL at such large angles of attack is doubtful. The drag is underpredicted over the whole range, see figure 4.2. A drag increase starts later, resulting in too optimistic L/D values at $\alpha \geq 10$. The value for N_{crit} is chosen equal to 12, as the results more closely resemble the measured data.

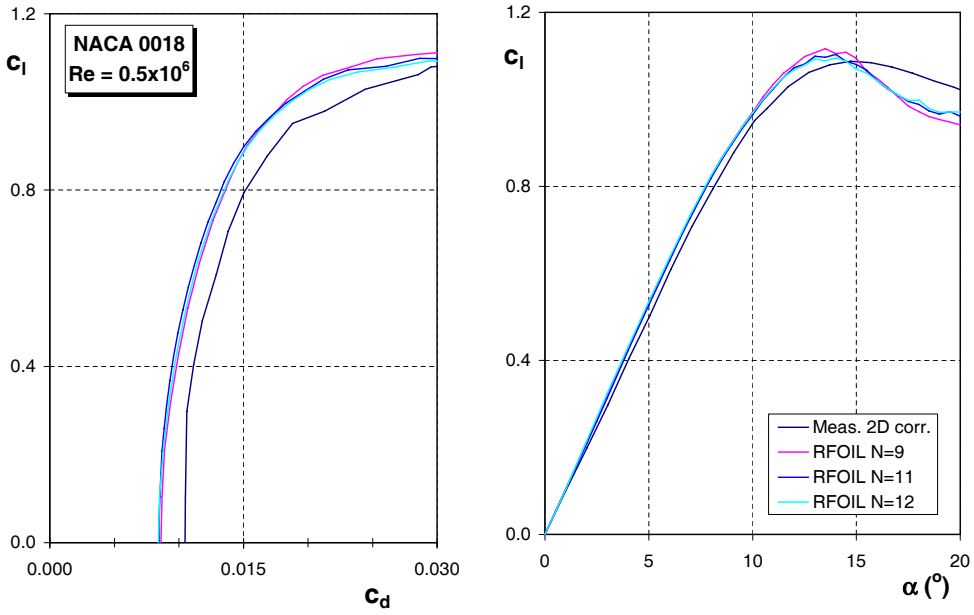

Figure 4.2: NACA 0018 characteristics at Re=500,000 trip at 80%

At Re = 700,000 the same phenomena are present as at Re = 500,000. In this case the differences are even larger, resulting in a larger overprediction of L/D (see figure 4.3). The drag bucket of the RFOIL data is again wider than that of the measured data. Also here the RFOIL data using $N_{crit} = 12$ is slightly more similar to the measured data for larger angles. In this case however this gives problems with convergence after $\alpha = 16$. For smaller angles the drag coefficient for $N_{crit} = 9$ is more accurate. As it is important to be able to gather data at high angles of attack, a value of $N_{crit} = 9$ is preferred.

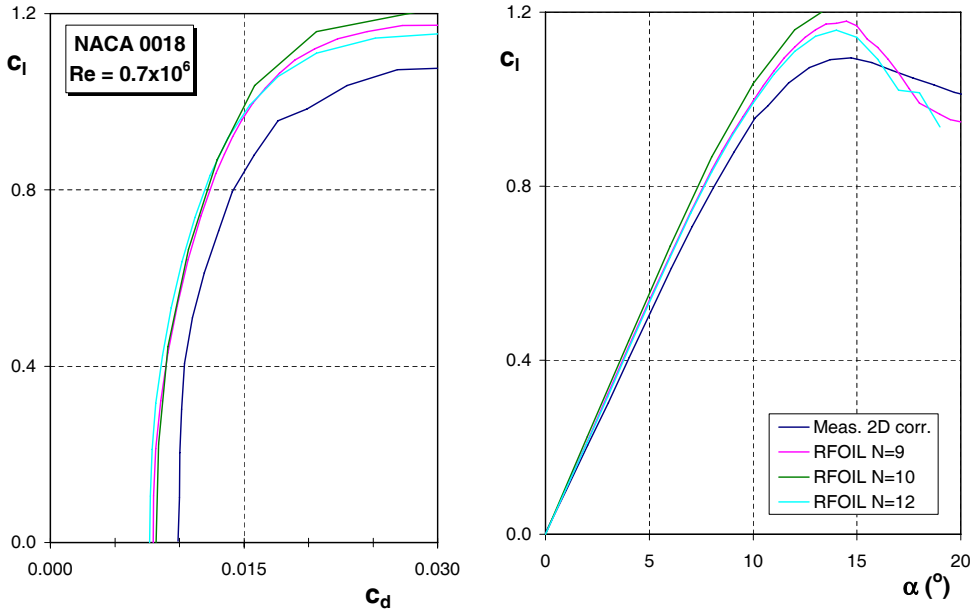

Figure 4.3: NACA 0018 characteristics at Re=700,000 trip at 80%

4.2 Laminar profiles

For the laminar airfoils two different types are reviewed, the NACA 6-series and the NLF-series. The NACA series are developed after the turbulent NACA series. The NLF profiles are more modern laminar profiles developed by NASA in the 1980's. Furthermore the S824 profile is reviewed as a symmetric laminar airfoil, although the measurements on this profiles were not conducted at the TU Delft.

4.2.1 NACA 64-418

The result for the NACA 64-418 at Re = 280,000 using RFOIL is given in figure 4.4. The experimental data is measured using pressure holes in the model. No corrections for 3D effects are necessary. The lift data are almost the same using $N_{crit} = 12$. Only the maximum lift coefficient is lower for the RFOIL data. The drag is at low α's is slightly higher and the drag bucket at positive C_l is wider.

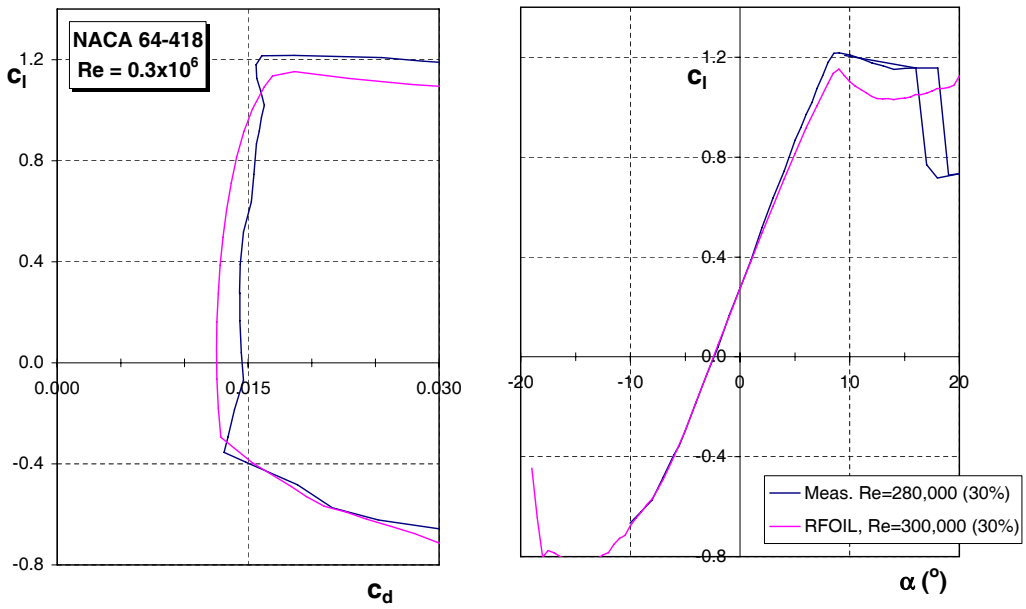

Figure 4.4: NACA 64-418 characteristics at Re=280,000

The result for simulating the NACA 64-418 at Re = 700,000 using RFOIL is given in figure 4.5. Again the RFOIL results are very close to the measurements using $N_{crit} = 9$. For the negative C_l the airfoil stalls smoother and later. This also results in a wider drag bucket. For positive C_l, however, the results are very good. Only the lift is slightly lower for $\alpha \geq 10$.

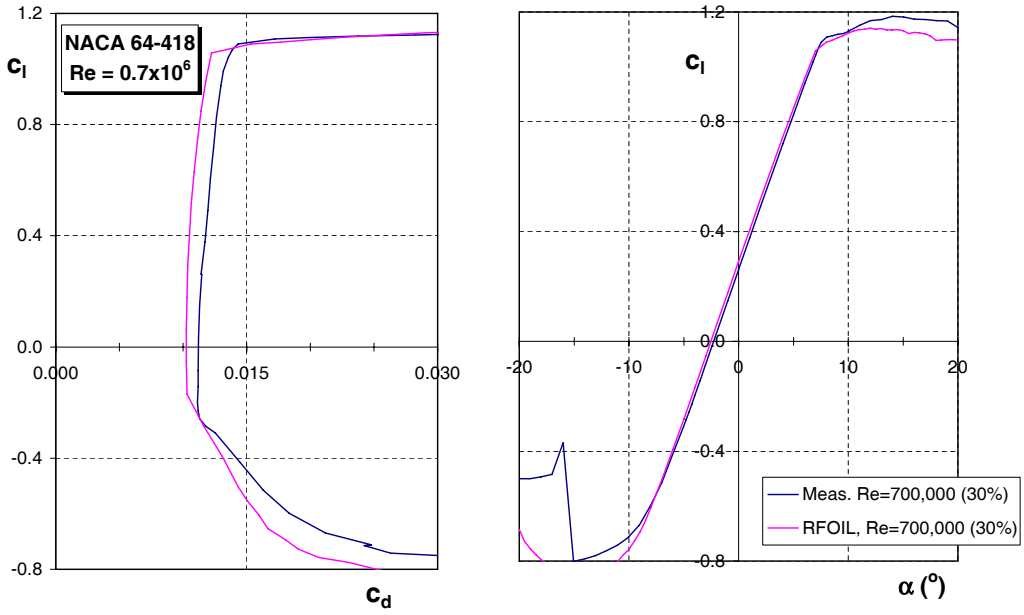

Figure 4.5: NACA 64-418 characteristics at Re=700,000

4.2.2 NLF-0416

Unfortunately not much data is available for NLF profiles at low Reynold numbers. Data is available for Re=500,000, measured at the DUT, faculty of Aerospace Engineering. The angle of attack ranges from -4° to 15°, see figure 4.6. The RFOIL lift data has a flatter slope compared to the measured data. Also the maximum measured lift coefficient is much larger. The same goes for the drag: the measured drag is larger and the drag bucket is wider.

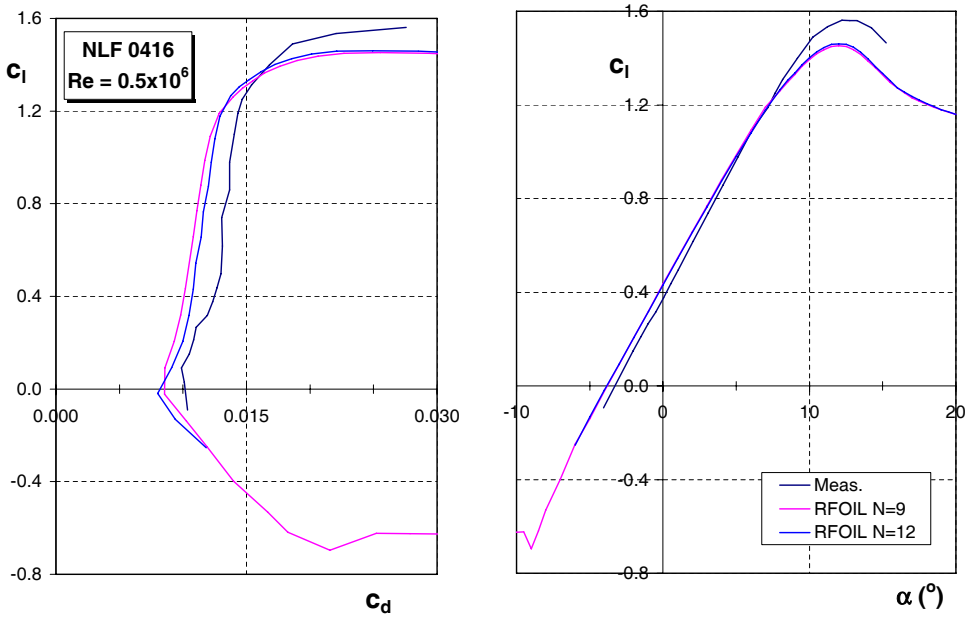

Figure 4.6: NLF 0416 characteristics at Re=500,000

4.2.3 S824

The symmetric S824 is also a laminar profile and was measured by [Maughmer, 1999]. In this case the RFOIL data is again very close to the measurements using $N_{crit} = 9$. Only now, instead of under predicting the lift, the lift is over predicted for $\alpha \geq 10$.

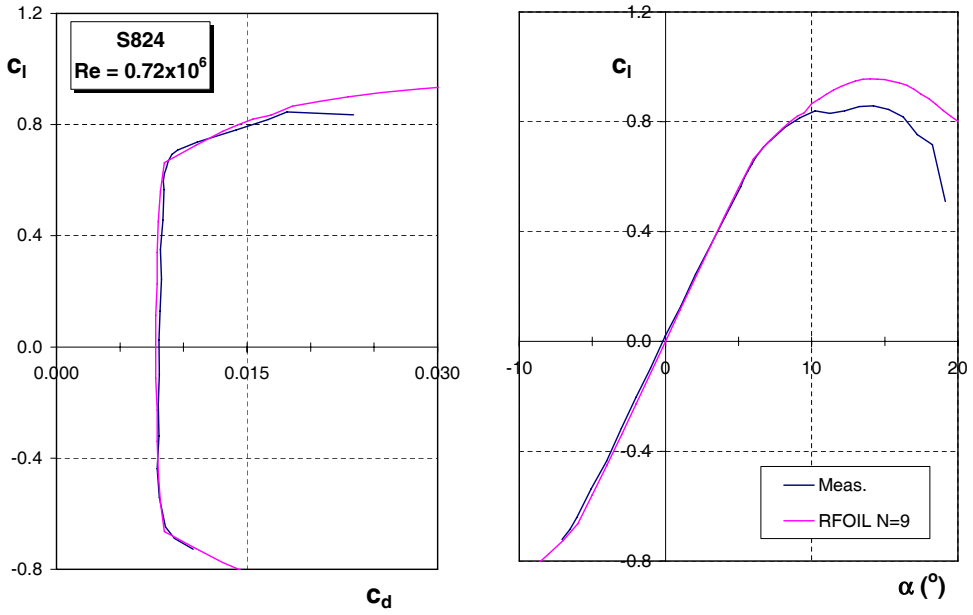

Figure 4.7: S824 characteristics at Re=720,000

4.3 Higher Reynolds numbers

As stated earlier, RFOIL has some difficulties to calculate airfoil behavior at lower Reynolds numbers. To illustrate this the results at higher Re for one turbulent airfoil (NACA 4418) and one laminar airfoil (NACA 64-218) will be discussed in this section. For the turbulent profile RFOIL tends to underestimate the drag over the whole range, see figure 4.8. The qualitative behavior is almost the same, only the lift slope of the measured data from [Abbott and Doenhoff, 1949] is lower. As a results the RFOIL data has a higher $C_{L,max}$. So even at higher Reynolds numbers RFOIL has some trouble predicting turbulent profiles very accurately. Still the RFOIL program is a fast and qualitatively correct design tool for 2D airfoils.

For the laminar profiles RFOIL is an accurate design tool for predicting the drag over the whole range, see figure 4.9. The behavior is almost the same, only at $\alpha > 8$ again the lift slope of the measured data from [Abbott and Doenhoff, 1949] decreases. RFOIL proves to be a powerful design tool for laminar profiles.

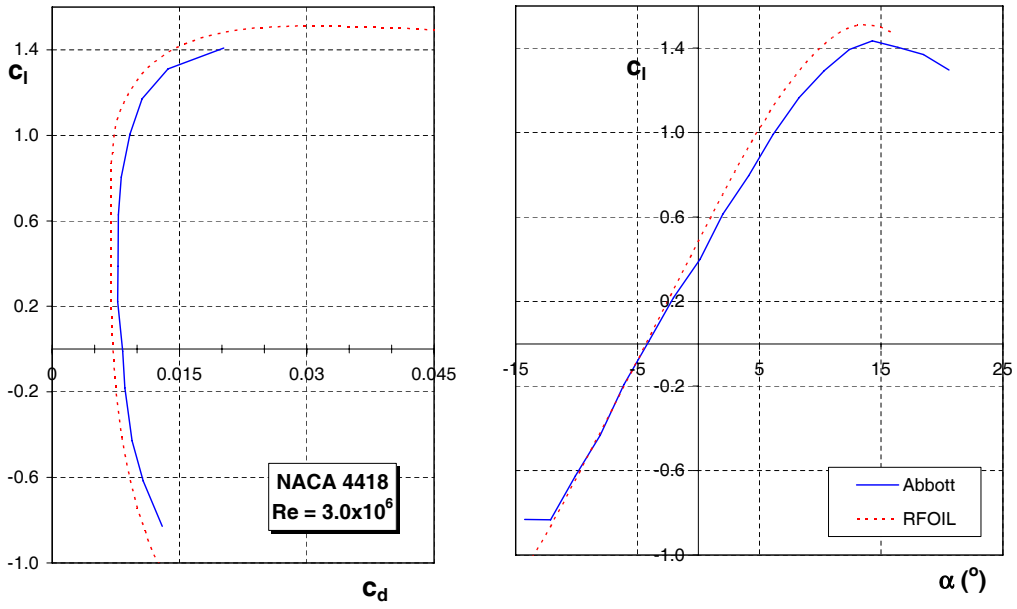

Figure 4.8: NACA 4418 characteristics at Re=3,000,000

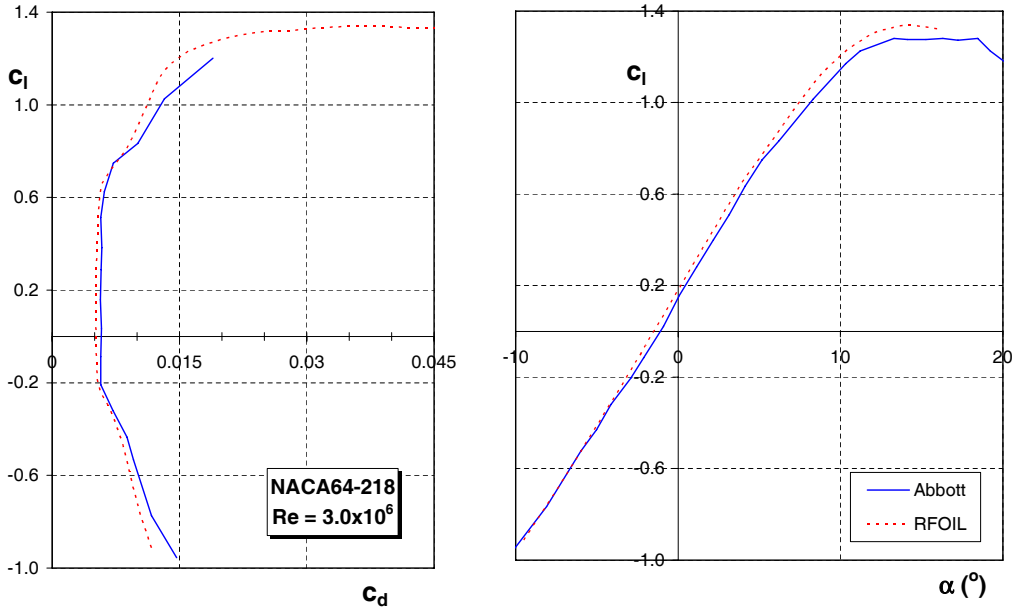

Figure 4.9: NACA 64-218 characteristics at Re=3,000,000

4.4 Fixed transition at 5% chord

If a turbine operates in the field the blades will eventually get dirty from particles and insects in the air. As a consequence the boundary layer will turn turbulent at the nose of the blade, which results in a turbulent boundary layer over the airfoil. To mimic this situation in the wind tunnel, zigzag tape is applied at 5% chord of the airfoil. The resulting turbulent boundary layer will imediately have some thickness as a result of the thickness of the tape. In RFOIL it is only possible to apply a trip to the boundary layer without physical height. To get comparable boundary layer thickness at 5% chord the trip is applied further near the nose. RFOIL has problems at higher angles of attack when the stagnation point at the pressure side moves past this trip point. To avoid this from happening the trip is applied at 1% at the suction side and 5% at the pressure side of the airfoil. If negative angles are investigated, the trips are applied the other way around.

To validate RFOIL performance for fixed transition airfoils, the RFOIL values are compared to the measured values for the NACA 0018 at Re=300,000, see figure 4.10 and Re=700,000, see figure 4.11.

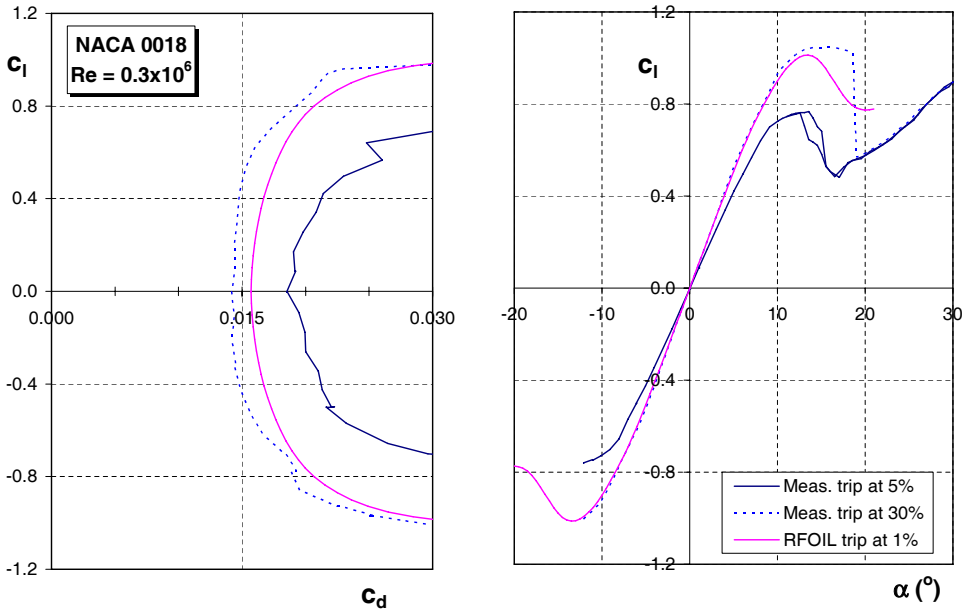

Figure 4.10: Comparison between 5% trip RFOIL and measured data at Re=300,000

The results of RFOIL deviate substantially from the measured values. The wind tunnel results with zigzag tape applied at 30% are also added. It is clear that the lift results of RFOIL are almost the same as for these last wind tunnel meaurements. The drag values for both Reynolds numbers are also closer to zigzag tape applied to 30% chord. Therefore the RFOIL results for "dirty airfoils" have to be viewed with some scepticism.

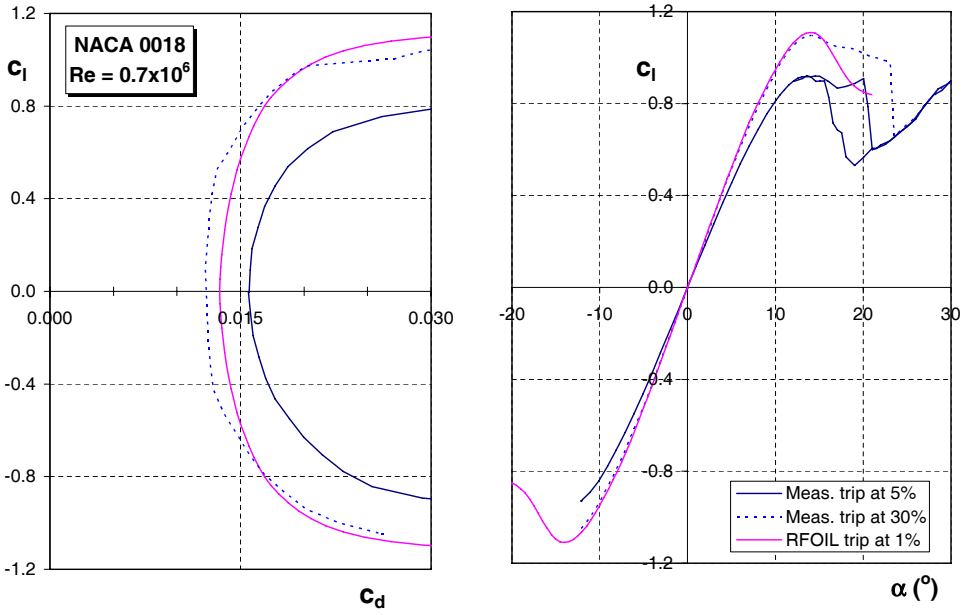

Figure 4.11: Comparison between 5% trip RFOIL and measured data at Re=700,000

The fixed transition airfoil charateristics will not be used in the airfoil comparisons.

4.5 Conclusions

After the validation the following conclusions are drawn concerning the RFOIL results:

- For the turbulent profiles RFOIL predicts the behavior accurately for Re=300,000 to an angle of attack of 15°. For Re=500,000 and 700,000 RFOIL tends to overestimate the maximum lift coefficient, at 700,000 even by 10%. Also the calculated lift slope is too steep.
- For the laminar NACA 6-series profiles RFOIL underestimates the drag at low angles of attack and underestimates the maximum lift coefficient. For Re=500,000 the drag prediction is accurate but the maximum lift coefficient is under predicted. For Re=700,000 the drag is again under predicted, but the lift prediction is accurate to $\alpha = 10°$. The lift slope is in all cases accurate.
- For the laminar NLF profiles only a data set for Re=500,000 is available. In this case RFOIL under predicts the drag, the lift slope and the maximum lift coefficient.
- For fixed transition airfoils RFOIL is incapable of producing good results. The RFOIL values for a tip at 5% chord are more similar to applying zigzag tape at 30% chord. This can be the results the thickness of the applied rougness which can not be simulated by the RFOIL program
- The calculated RFOIL data is compared to the measured wind tunnel data. To compensate for the low turbulence it the tunnel the critical amplification number of 12 should be used at Reynolds number 300,000. At Reynolds number of 500,000 N_{crit} is equal to 11 and at 700,000 it equals 9

The RFOIL program is a design tool which allows changes to the airfoils geometry and the pressure distributions. It is a fast program and gives qualitatively good results compared to wind tunnel data. The quantitative values show differences with measured wind tunnel data. The differences are larger at lower Reynolds numbers than at higher Reynolds numbers. These discrepancies should be kept in mind when designing the new airfoil. As during this project the RFOIL data of one airfoil is compared to the RFOIL data of another airfoil, complete similarity between RFOIL and wind tunnel data is not necessary. However, to compare the results of the design process with the NACA 0018 airfoil wind tunnel tests should be performed.

Chapter 5

Airfoil design parameters

In the previous two chapters the design tools are introduced; the RFOIL program to generate 2D airfoil data and the simulation program to use the 2D data to calculate the VAWT performance. In chapter 2 the design goals for the new airfoil are constructed. In this chapter the design tools are used to generate a general design of the new airfoil that complies with the design goals. The fine tuning and validation of this model will be performed in the next chapter. To comply with the design goals the following parameters can be altered: thickness, camber, type of airfoil (laminar or turbulent) and noise emission. Also the possibility to design an airfoil which can make the turbine self-starting is investigated. First in section 5.1 a study of each of these parameters is given.

As RFOIL is used, the new designs will be compared to the RFOIL values of the current airfoil, the NACA 0018. As stated before, there are two main groups of airfoils which may be applicable for VAWT use. These groups are: turbulent profiles (NACA 4-series) and laminar profiles (NACA 6-series and NLF profiles). First these groups will be compared to choose which one provides the most potential for a good airfoil. The comparisons will be done at the Reynolds numbers 300,000 and 700,000.

5.1 Design variables

In this section an overview will be given of the influence of thickness and camber on the aerodynamic properties. Also the relevance of boundary layer tripping and noise emissions are treated. Finally a short comment about design parameter influence on the self starting properties of turbines is given.

5.1.1 Thickness

The current airfoil used on the Turby is the NACA 0018. The thickness has been chosen to give enough structural strength with respect to the loads on the blades. A thicker airfoil of 20% can be an option.

The advantage of higher thickness:

- Increase of the drag bucket
- Increase of structural strength

The disadvantages:

- Higher drag coefficient at lower angles of attack
- Chance of 'overshooting' the maximum, past a certain unknown point more thickness will result in a lower efficiency

The optimum of the thickness is difficult to find. In older VAWT less thick airfoils were used of 12% or 15%. The 18% thick airfoils also produce very good results. The question is how much the thickness can be increased without performance loss. From figure 5.1 the increase of thickness from 9% to 15% results in a wider drag bucket. But if the thickness is increased form 15% to 18% the drag bucket does not increase anymore. Figure 5.2 shows for a lower Reynolds number the same results.

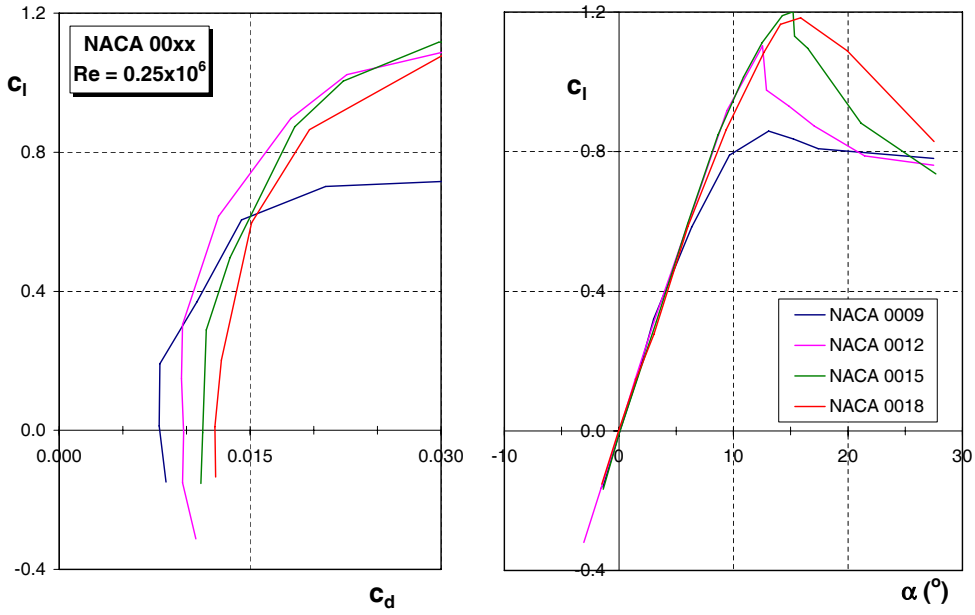

Figure 5.1: NACA characteristics with different thickness at Re≈250,000, [Jacobs and Sherman, 1937]

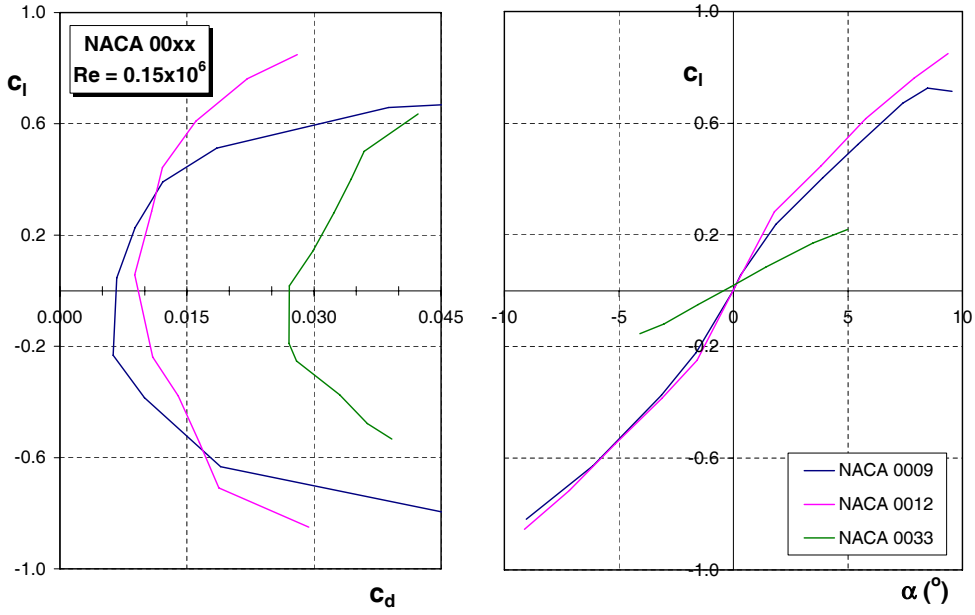

Figure 5.2: Symmetric NACA characteristics with varying thickness at Re=150,000, [Althaus, 1980]

If the airfoil reaches a certain thickness, more thickness will decrease instead of increase the performance of the turbine. Most turbines are not tested with airfoils of varying thickness, but the results of one test is given in figure 5.3. It is clear that the 15% thick airfoil performs better then the 12% thick airfoil, with a $C_{P,max}$ increase of 44%.

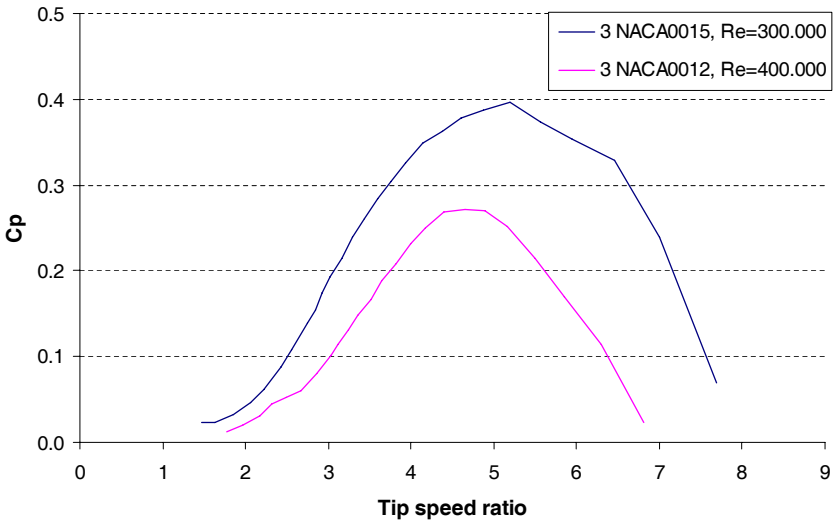

Figure 5.3: The Sandia 5m turbine with NACA 0015 and 0012 blades, [Sheldahl et al., 1980]

5.1.2 Camber

Until now in almost all vertical axis wind turbines only symmetrical airfoils have been applied (mostly NACA 0015 and NACA 0018). From a physical point it is clear that the velocity at the upwind side of the turbine will be higher than at the downwind side, as the blade extracts energy from the air at the first passage. The lower airspeeds result in lower angles of attack at the downwind side, as these two parameters are directly related. The power extraction from the wind is a function of V^3. Only a small variation in wind speed gives a large difference in possible power extraction. Therefore an optimal power extraction at the upwind side is preferable. This will have as negative result that the velocity, and therefore the extracted power, at the downwind side will decrease even more.

To increase the efficiency of the turbine camber can be added to the profile. In this case the profile will be more efficient at the upwind side. Even more energy will be extracted from the wind, and the angle of attack at the downwind side will be even lower. This is very important, because the efficiency at the downwind side will be much lower. With a lower negative maximal a.o.a. the drag bucket can be moved more easily to higher lift coefficient values.

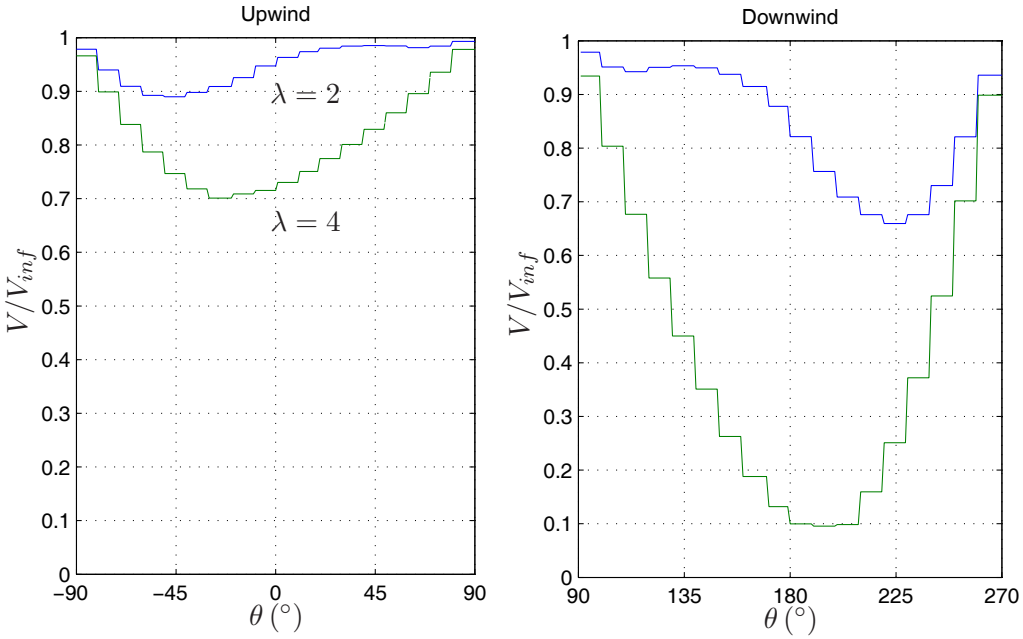

Figure 5.4: Variation of wind speed in the VAWT

The increase in camber results in a shift of the lift curve in upwards direction. The stall angle and the maximum lift coefficient increase, see figure 5.5.

The lift over drag curve shifts to the right with increasing camber. The performance at higher lift coefficients is increasing, but at negative lift coefficients the performance decreases at the same time.

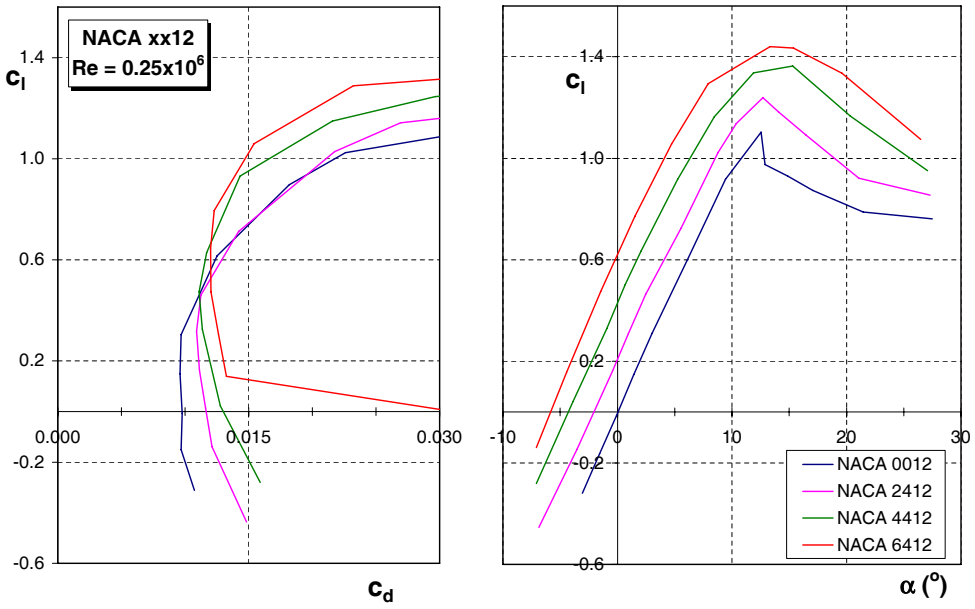

Figure 5.5: NACA characteristics with different camber at Re≈250,000, [Jacobs and Sherman, 1937]

5.1.3 Boundary layer tripping

At low Reynolds numbers the laminar boundary layer can separate before it turns turbulent. This causes the laminar separation bubbles to appear. These bubbles alter the effective shape of the profile and influence the lift curves, see section 2.2.5. If the boundary layer is made turbulent artificially before the starting point of these bubbles, the formation of the bubbles is prevented. This tripping of the boundary layer has a large influence on the performance at low Reynolds numbers.

In [Gopalarathnam et al., 2001] an extensive study is made on the effects of boundary layer tripping. The drag is decreased in the high lift, low Reynolds number condition, compared to the clean airfoils. This is at a cost in the low lift, high Reynolds number condition. For lower Reynolds numbers, 100,000 and smaller, and situations with thicker airfoils, tripping can improve the performance substantially. Research into the SA7026 profile shows the effect of applying a fixed transition, see figures 5.6 and 5.7.

The effects are much more significant at low Reynolds numbers. At higher Reynolds numbers the tripping of the boundary layer gives a slight shift in the lift over drag curve. If the Reynolds number is high enough, the flow will become turbulent naturally before laminar separation bubbles can appear.

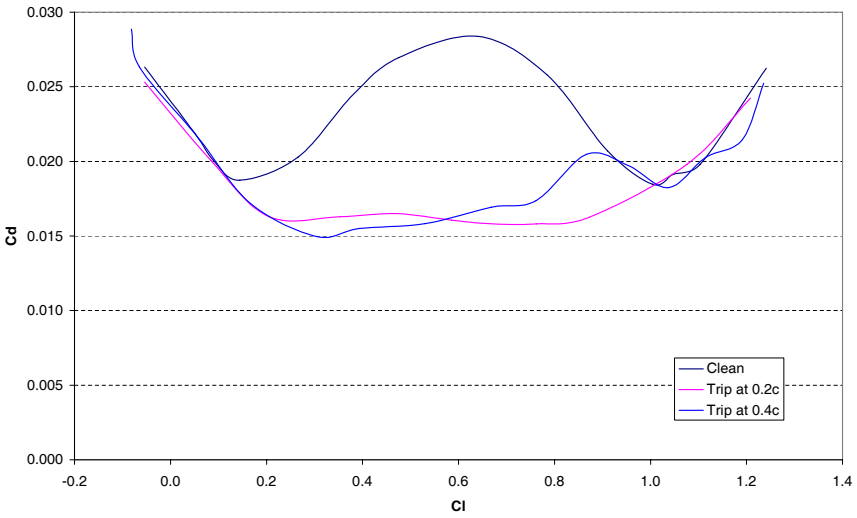

Figure 5.6: SA7026 airfoil characteristics at Re=100,000, [Gopalarathnam et al., 2001]

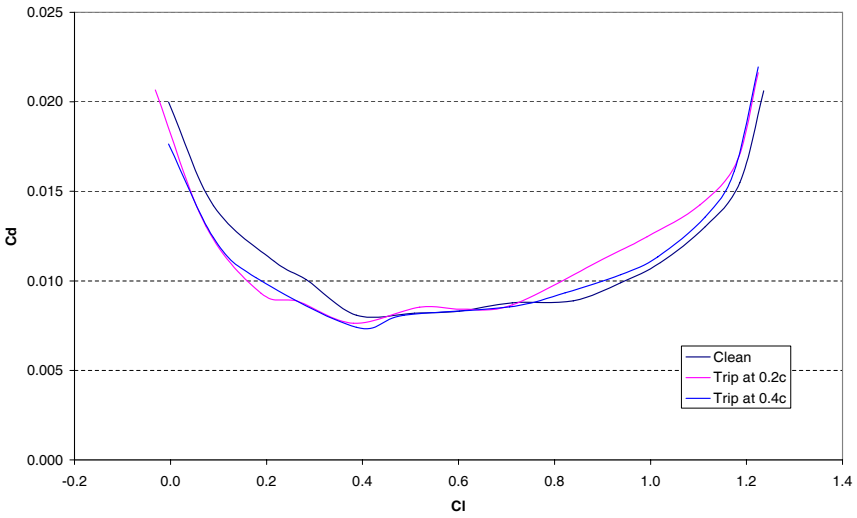

Figure 5.7: SA7026 airfoil characteristics at Re=300,000, [Gopalarathnam et al., 2001]

5.1.4 Noise

Not much research is performed on the noise emission of the VAWT. Form [Iida et al., 2004] a the aerodynamic sound of a VAWT is numerically modeled using discreet vortex methods. The complicated wake structure can be captured using this method. It shows that the VAWT produces less sound than a horizontal axis wind turbine with the same power coefficient at normal operating speed. The simulated sound against the tip speed ratio is given below in figure 5.8. The operating tip seed ratio is 3, which results in a produced aerodynamic noise of 60 dB.

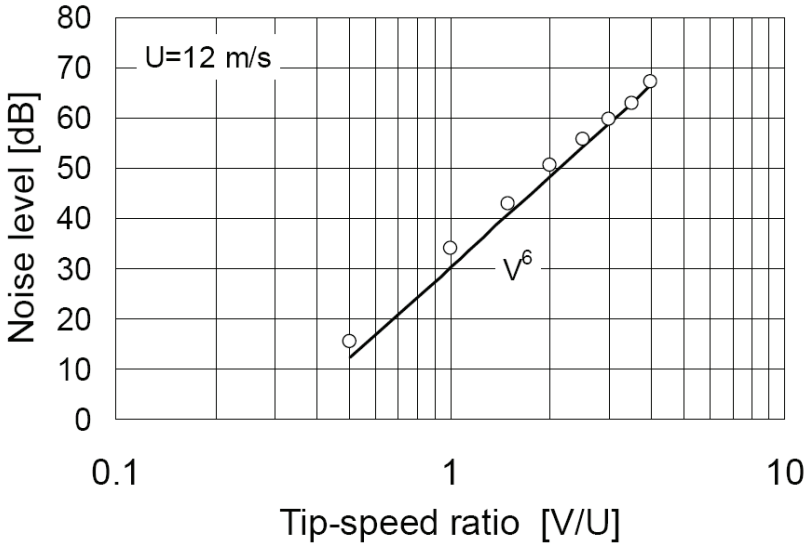

Figure 5.8: The radiated aerodynamic noise from a VAWT, [Iida et al., 2004]

5.1.5 Self starting turbines

In general a VAWT with fixed pitch blades is unable to start on itself. The main problem for Darrieus turbines is the negative power coefficient at low tip speed ratios. If the power coefficient is positive, the turbine is able to rotate independently and produce power. If the coefficient is negative, the turbine needs extra power to be able to rotate.

The region of negative C_P is influenced by the blade camber, thickness and turbine solidity. The influence of these parameters was investigated by [Kirke and Lazauskas, 1991]. By adding 4% camber the negative coefficients are completely avoided, see figure 5.9. Kirke and Lazauskas have also predicted that a turbine with cambered NACA 4415 blades of 0.32 m chord should easily self-start in a 10 m/s wind (Re = 200,000), unlike an otherwise identical turbine with symmetrical NACA 0015 blades. However the maximum efficiency of the turbine would be significantly lower with cambered blades.

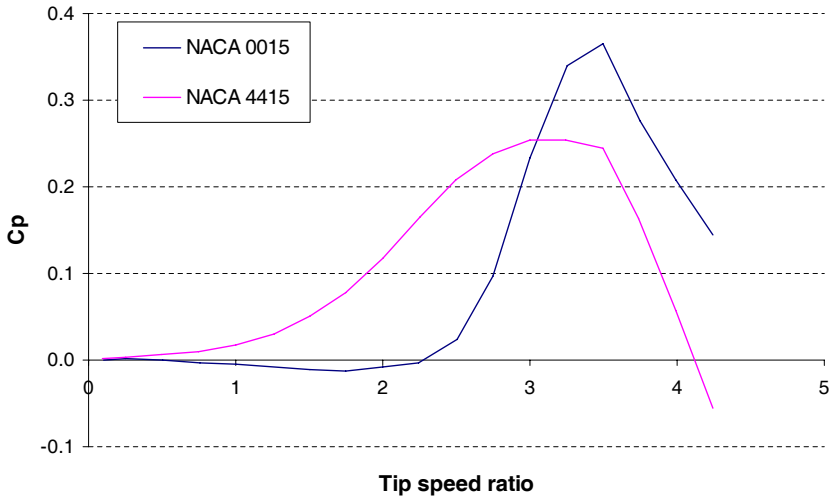

Figure 5.9: Camber influence on the performance coefficient at Re=200,000, [Kirke and Lazauskas, 1991]

By increasing the thickness, the region with negative C_P coefficients is drastically decreased, see figure 5.10. [Kirke and Lazauskas, 1991] have predicted the performance of a turbine at Re = 200,000 with symmetrical NACA blades of thickness ranging from 12% to 21% and found that increasing the blade thickness reduces the severity of the dead band of negative torque between $\lambda = 1$ to 3 but does not eliminate it, i.e. increased thickness is an improvement but does not in itself ensure self-starting.

The increase of solidity also diminishes the region of negative C_P and even makes the C_P values completely positive. This is only applied at high solidity values of 0.6 and higher. As this will result in very large and expensive blades, so this is not an option in this research.

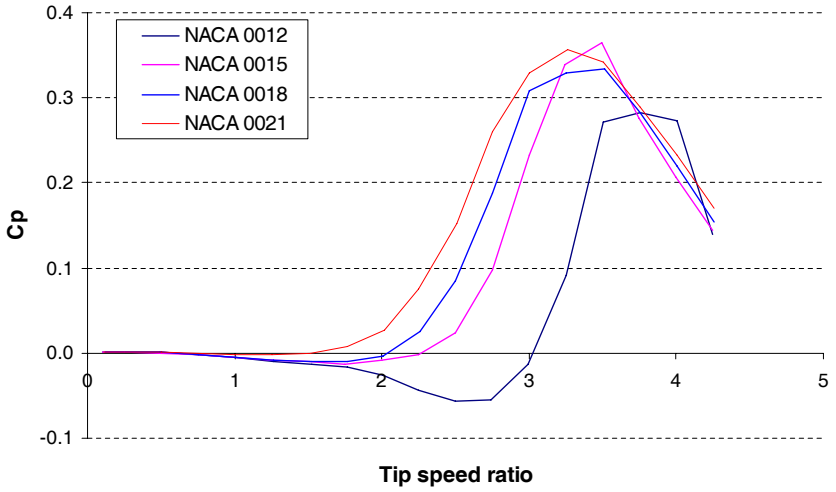

Figure 5.10: Influence of airfoil thickness on the turbine performance at Re=200,000, [Kirke and Lazauskas, 1991]

5.2 Turbulent profiles

Most vertical axis wind turbines built so far use airfoil profiles from the NACA 4-series and most of them use symmetric airfoils. The turbulent NACA 4-series were developed in the 1930's. Also the NACA 0018 belongs to this group. The main characteristic of the profiles is a large nose radius. This results in a high pressure peak followed by a steep pressure slope. The flow will turn turbulent very fast, as the laminar boundary layer can not follow this pressure rise. Because of the large nose radius the stall occurs very gentle. The drag bucket is not a real bucket, but a slowly increasing line, see figure 5.11. First will be investigated if the NACA 0018 profile can be adjusted by changing thickness or adding camber in such a way that the performance for the VAWT will be improved. The airfoils are constructed from a fixed thickness distribution:

$$\pm y_t = \frac{t}{0.20}\left(0.29690\sqrt{x} - 0.12600x - 0.35160x^2 + 0.28430x^3 - 0.10150x^4\right) \tag{5.1}$$

To this thickness distribution camber can be added in the form of a mean line:

$$y_c = \frac{m}{p^2}(2px - x^2) \quad \text{if} \quad y < y_{max} \tag{5.2}$$

$$y_c = \frac{m}{p^2}\left[(1-2p) + 2px - x^2\right] \quad \text{if} \quad y \geq y_{max} \tag{5.3}$$

5.2.1 Thickness

The extra thickness causes the airfoil to have more drag at smaller α. This is caused by the extra friction drag resulting from a larger surface. In some airfoil series a larger thickness makes a wider drag bucket. For the turbulent profiles the drag bucket becomes smaller and the maximum lift coefficient decreases as well, see figures 5.11 and 5.12.

5.2.2 Camber

Adding camber shifts the lift curve and therefore also the drag bucket up, see figures 5.13 and 5.14. As the VAWT operates at higher positive angles then lower angles this could result in better performance.

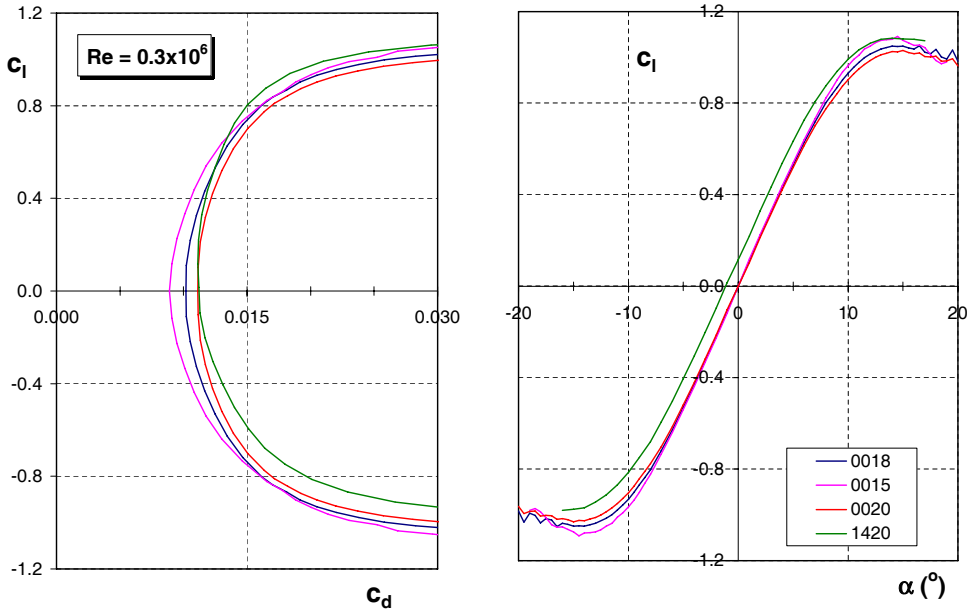

Figure 5.11: Calculated characteristics of different turbulent profiles at Re=300,000

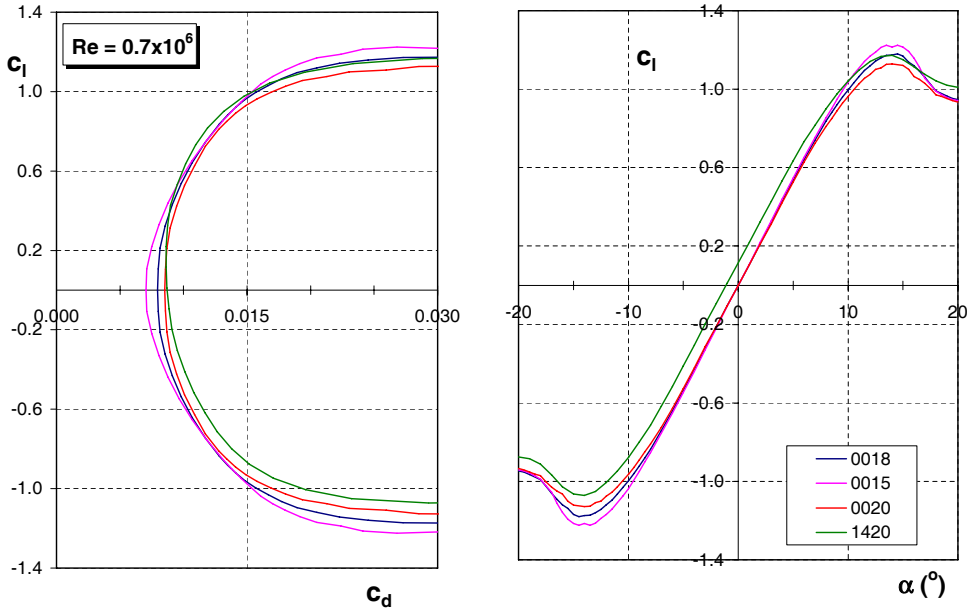

Figure 5.12: Calculated characteristics of different turbulent profiles at Re=700,000

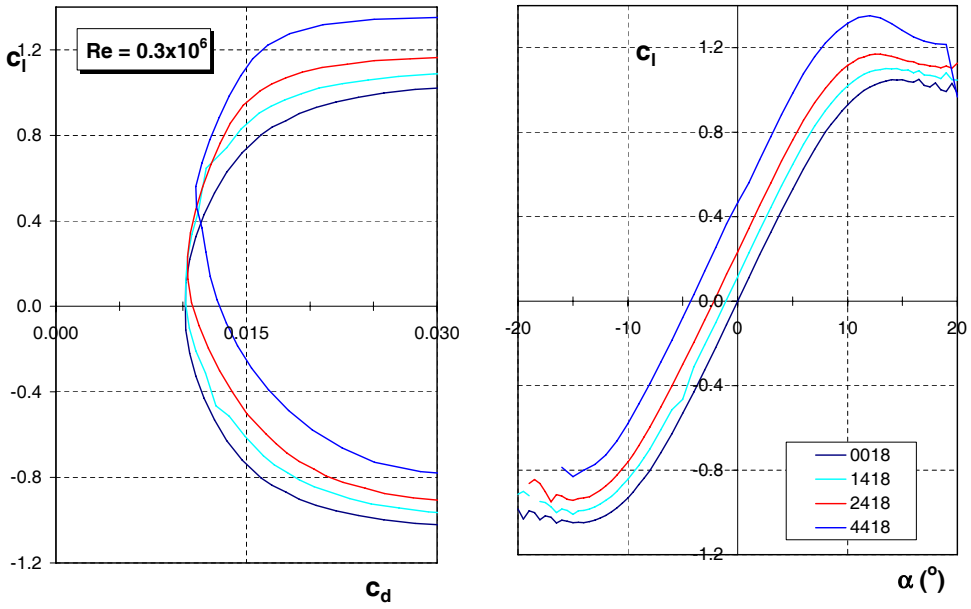

Figure 5.13: Calculated characteristics of different cambered profiles at Re=300,000

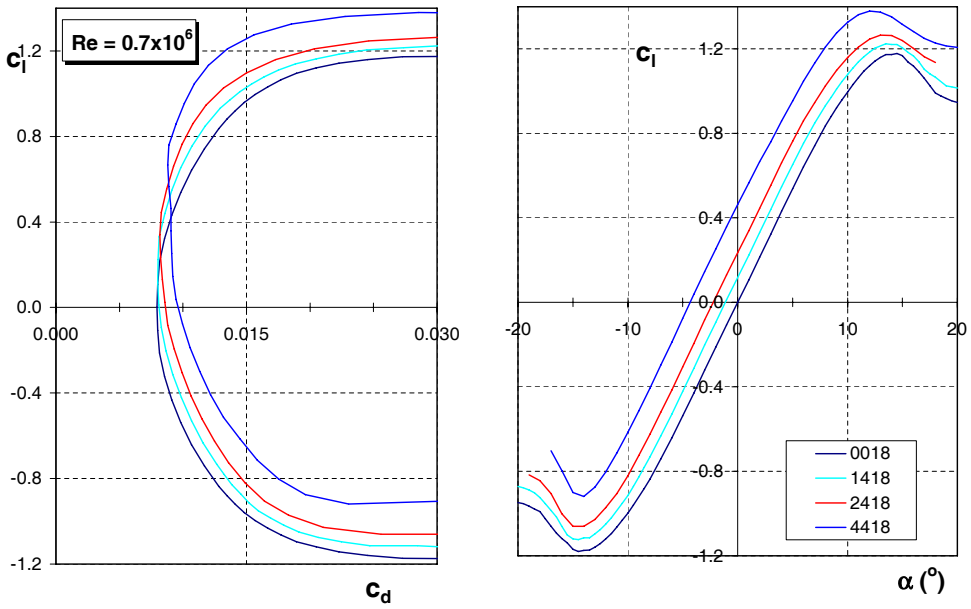

Figure 5.14: Calculated characteristics of different cambered profiles at Re=700,000

5.2.3 Simulation

The influence of the changes in camber and thickness on the performance of the VAWT is found by using the simulation. The results for changing the thickness can be found in figure 5.15, and changing the camber in figure 5.16. The extra thickness results in performance loss over the complete interval. A thickness decrease would improve performance, but because of structural demands this is not an option.

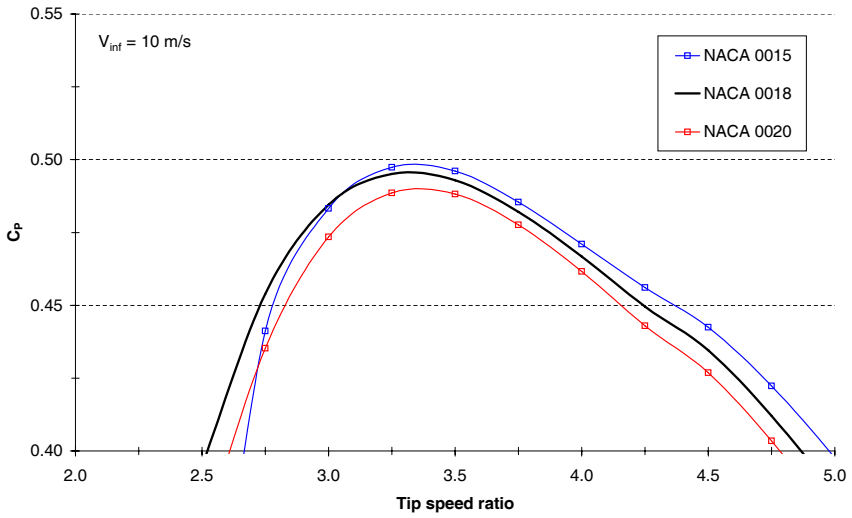

Figure 5.15: Turbulent profile characteristics for thickness variation

If camber is added the performance also declines. This decline is not consistent over the complete interval. If only 1% is added, the decline in $C_{P,max}$ is very little. At tip speed ratios larger than 3.5 the performans is a little better. However this region is not important, as the VAWT operates at a ratio of 3 and during start up the ratios are even lower.

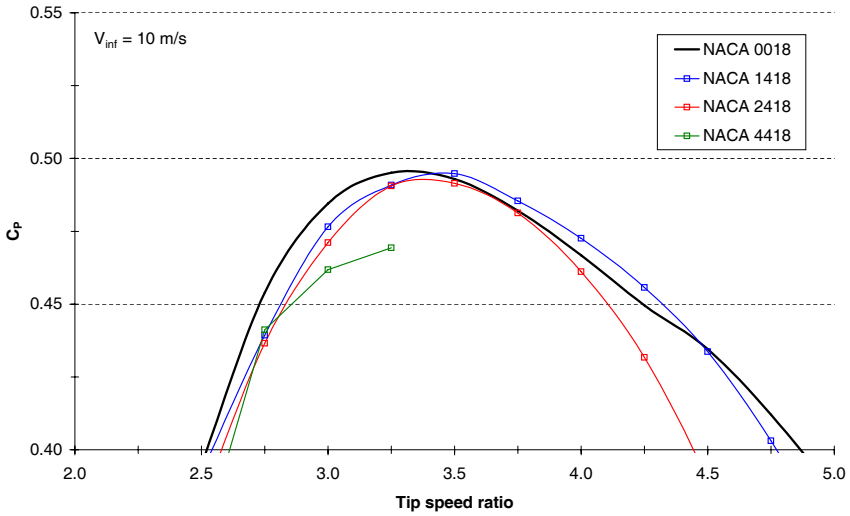

Figure 5.16: Turbulent profile characteristics for camber variation

5.3 Laminar profiles

As the turbine operates at low Reynolds numbers, the flow tends to be laminar over a larger part of the airfoil. The amount of disturbance needed to make the flow transition to turbulent is larger at lower Reynolds numbers. A logical choice would be to look at laminar profiles. These profiles have a sharper nose and the point of maximum thickness lies more aft. This enables a larger part with laminar flow and therefore lower drag at small angles of attack. The stall behavior is more rigorous compared to turbulent profiles. At stall the drag increases sharply, which results in a typical sharp drag bucket, see figure 5.17. At higher angles of attack the drag will be higher. For the comparison the NACA 6-series and the more modern NFL-series are used.

5.3.1 The NACA 6-series

If the turbine operates for a longer time in the field the blades get dirty and laminar flow is prevented. The 6-series are known to perform better than the turbulent profiles in laminar flow, but generally perform almost just as well when dirty. There is not one thickness distribution and mean line in this series, so the airfoils can not simply be scaled to the desired characteristics. However, some airfoils of this series have the same camber line in common and have thickness distributions that are similar.

Increasing the thickness or introducing camber has predictable influence on the airfoil characteristics. The laminar airfoils profit form lower drag in the range from $[-9^\circ \leq \alpha \leq 9^\circ]$ for Re=300,000 and $[-7^\circ \leq \alpha \leq 7^\circ]$ at Re=700,000, see figures 5.17 and 5.18. At higher angles the turbulent profile clearly performs better.

Simulation

The characteristics of the laminar profiles are inserted into the simulation program. The results are given in figure 5.19 below. The laminar counterpart of the NACA 0018 profile, the NACA 63018, performs worse over the complete interval. Especially at lower tip speed ratios the laminar profile can not compete with the turbulent one. This is caused by the fact that laminar profiles perform worse at higher angles of attack. At higher tip speed ratios the maximum angle of attack decreases and the performance of laminar profiles equals that of the turbulent. Changing the thickness or introducing camber does not have a beneficial effect on this performance.

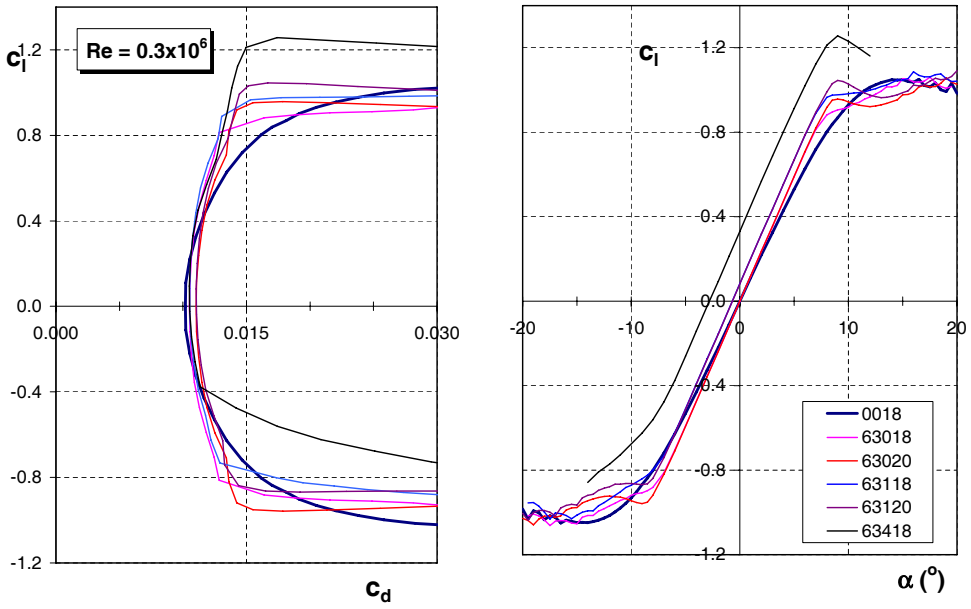

Figure 5.17: Calculated characteristics of different laminar profiles at Re=300,000

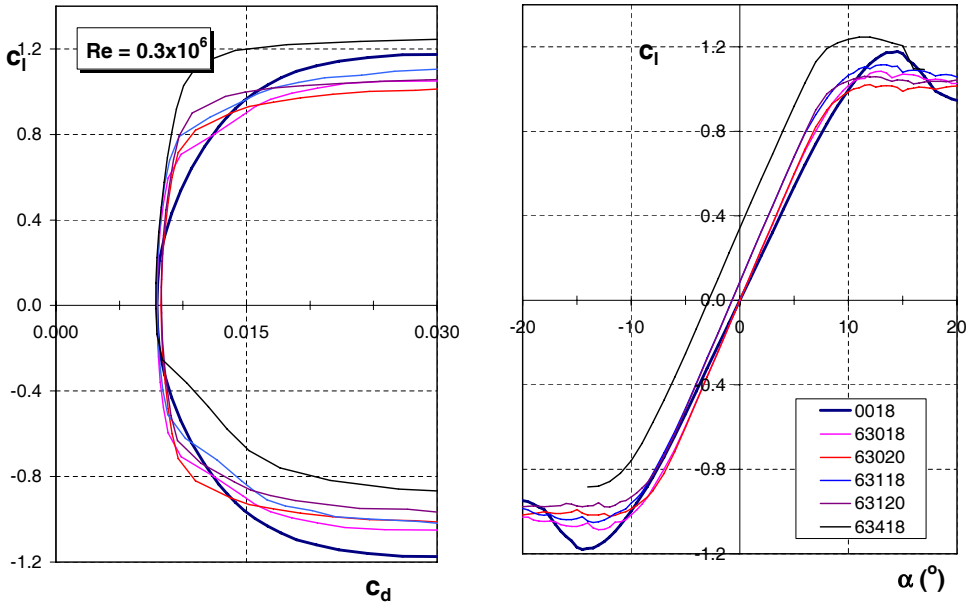

Figure 5.18: Calculated characteristics of different laminar profiles at Re=700,000

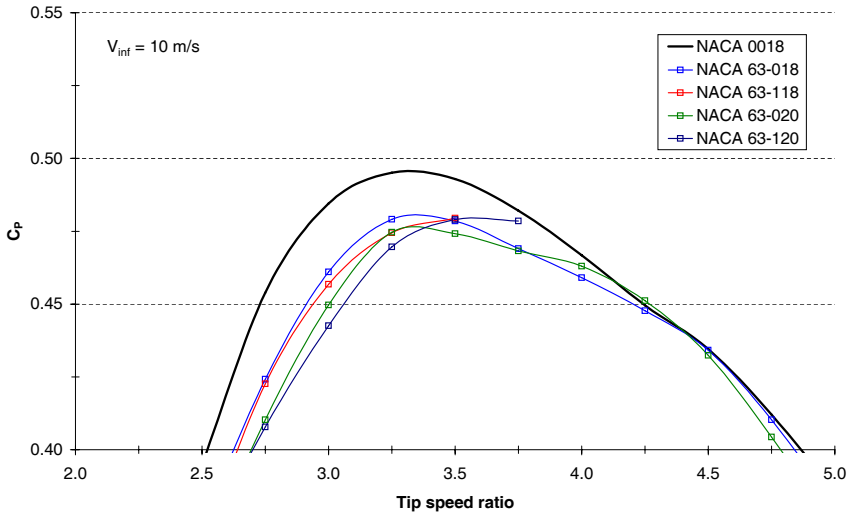

Figure 5.19: Simulation of laminar profiles compared to the NACA 0018

5.3.2 NLF profiles

Since 1980 the focus on airfoil designed shifted more to the laminar flow airfoils. It was found that the laminar profiles when dirty can perform just as well as the turbulent profiles in dirty conditions. But if the airfoils are clean, the laminar profiles perform much better. New construction methods and materials like composites made more smooth and accurate blades possible. This ensured that the laminar design can perform as calculated in practice. The emphasis of NASA also focused on these natural-laminar-flow (NLF) while retaining the high lift coefficients on turbulent NASA airfoils. Three airfoils were designed: the NLF-0416 and the flapped NLF-0215F and NLF-0414F. The laminar flow and the resulting low drag at small angles attack combined with good high lift performance should give improvements in the VAWT case in comparison with the NACA 0018.

The NLF-416 is used as the basis, which is transformed to a NLF-0018 profile by increasing thickness and removing camber in RFOIL. Besides the symmetrical airfoil also cambered airfoils with 0.5, 0.8 and 1 percent camber are investigated. In figure 5.20 the results for Re=300,000 are given. The NLF 0018 profile clearly performs better then the NACA 0018. The NLF profiles have a much larger drag bucket then the NACA 6-series. The 6-series does have lower drag at low angles of attack, but also a small drag bucket. The NLF series have overcome this and produce lower drag at low angles combined with a wider drag bucket. But if the Reynolds number is increased to 700,000, see figure 5.21 the benefits are smaller. The NACA 0018 has in this case a higher $C_{L,max}$ and drag bucket, although the NLF profile still performs better for $-10 < \alpha < 10$. The simulation program will have to decide which has the most effect on the performance.

If the 2D data used in the simulation program the symmetrical NLF 0018 profile is

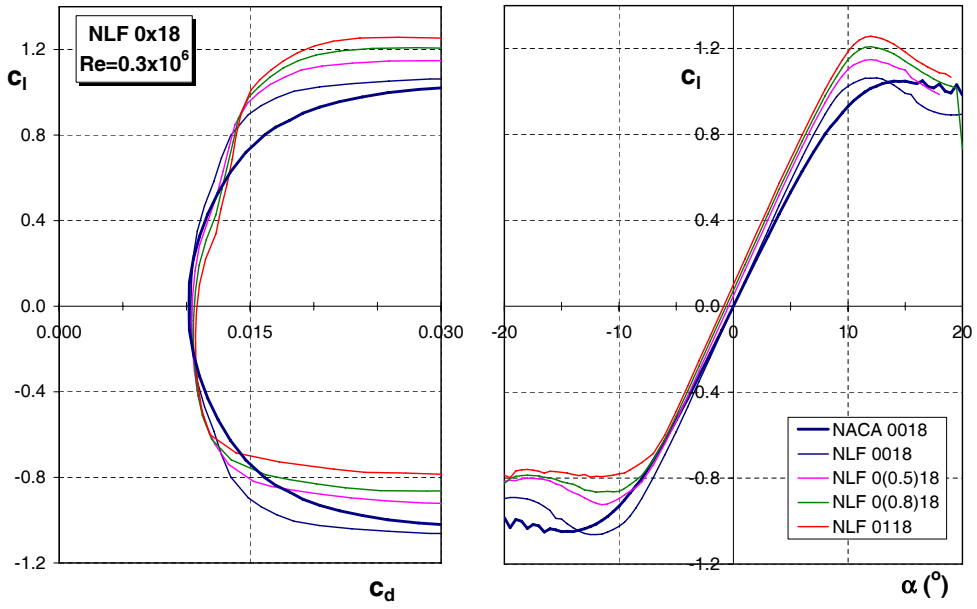

Figure 5.20: Characteristics for NLF airfoils with increasing camber at Re=300,000

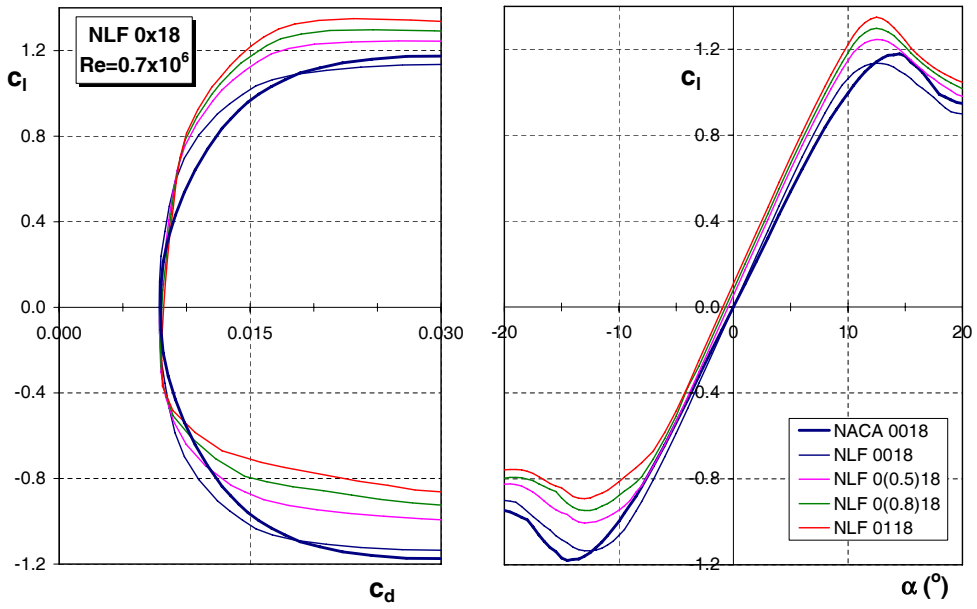

Figure 5.21: Characteristics for NLF airfoils with increasing camber at Re=700,000

more efficient at tip speed ratios of 3.5 and higher. The normal operating conditions are however around $\lambda = 3$. If camber is added the maximum efficiency increases, but the profile becomes more peaky. Efficiency is lost at lower and higher tip speed ratios, see figure 5.22. If the thickness is increased the C_P curve shifts to lower tip speed ratio's, which is very beneficial.

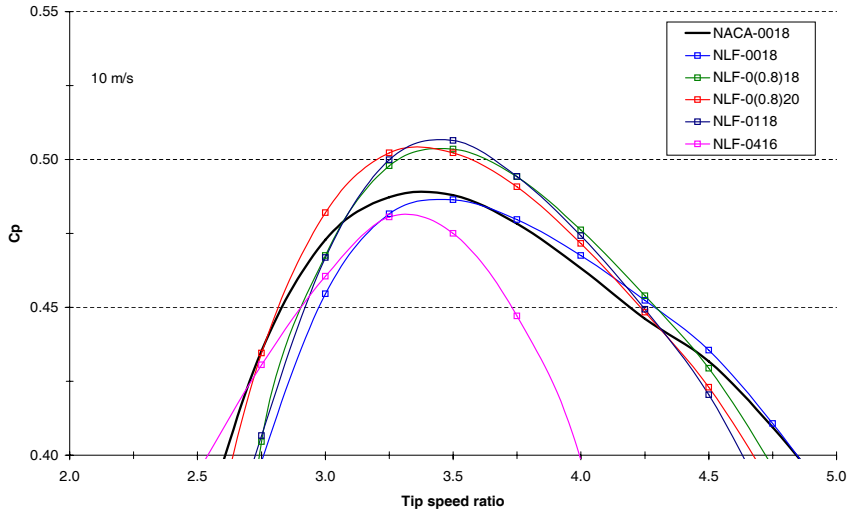

Figure 5.22: Simulation of NLF profiles compared to the NACA 0018

5.3.3 Experimental results

Unfortunately only one investigation into the usefulness of laminar profiles for VAWT applications is performed see [Leclerce, 1997]. The developed airfoil had to comply with the following goals:

1. Modest values of $C_{L,max}$ with sharp stall characteristics
2. Low zero lift drag coefficient
3. Wide drag bucket
4. Operating at Re = $1 * 10^6$ - $3 * 10^6$
5. Large laminar flow region (50%)
6. Symmetrical airfoil

The Sandia 34 meter VAWT, which is originally equipped with two NACA 0018/0021 blades was compared to the same turbine with two SNLA 0018/NACA 0021 profile blades. The SNLA 0018 profile is a modified NACA 0018 profile to produce a larger laminar flow region, see figure 5.23.

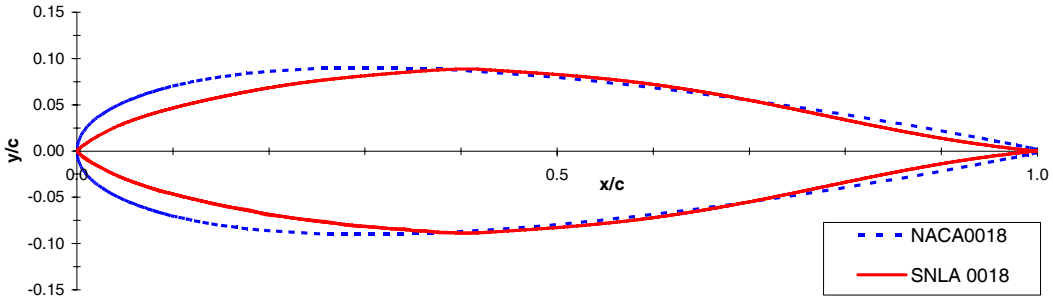

Figure 5.23: Comparison of the SNLA 0018 profile with the NACA 0018, [Berg, 1985]

If the characteristics of both airfoils are compared, the only benefit of the SNLA profile is the lower drag coefficient at lower angles of attack, see figure 5.24. The drag bucket is smaller and the maximum lift coefficient and stall angle are smaller then for the NACA 0018 profile. The characteristics match those of the NACA 6-series.

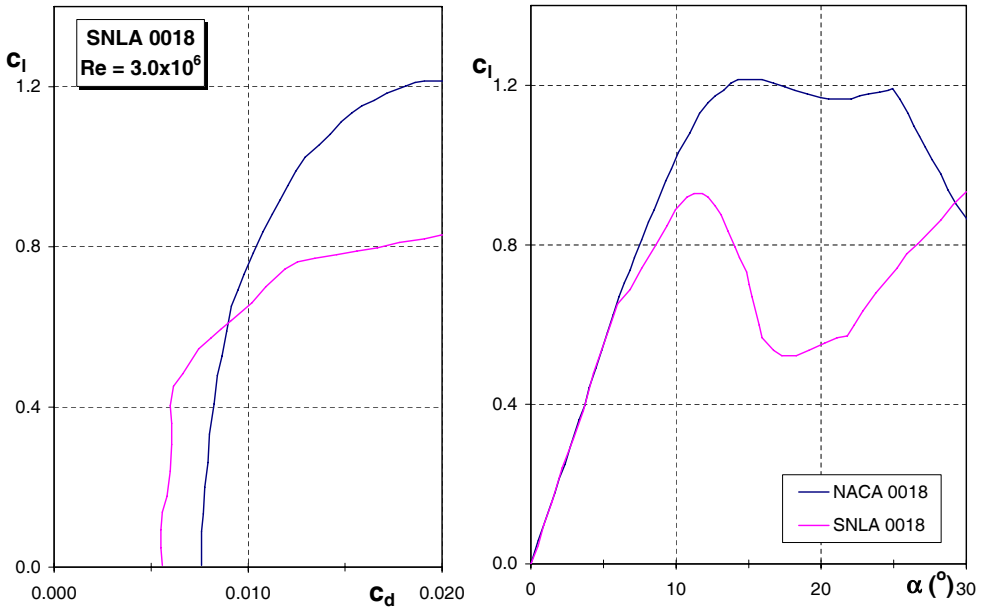

Figure 5.24: The NACA 0018 and SNLA 0018 lift characteristics for Re=3 million, [Berg, 1985]

The results for the 34 meter turbine, equipped with both profiles, are shown in figure 5.25. The turbine was operated at a constant rotational speed, the wind speed was altered. At lower wind speeds the maximum angle of attack of the profiles is very low. With increasing wind speed this angle is increased. The low drag coefficients at

low angles of attack of the SNLA profile are only beneficial at very low airspeeds. At higher speeds the SNLA profile is according to these experiments less efficient as the turbulent NACA 4 series airfoil.

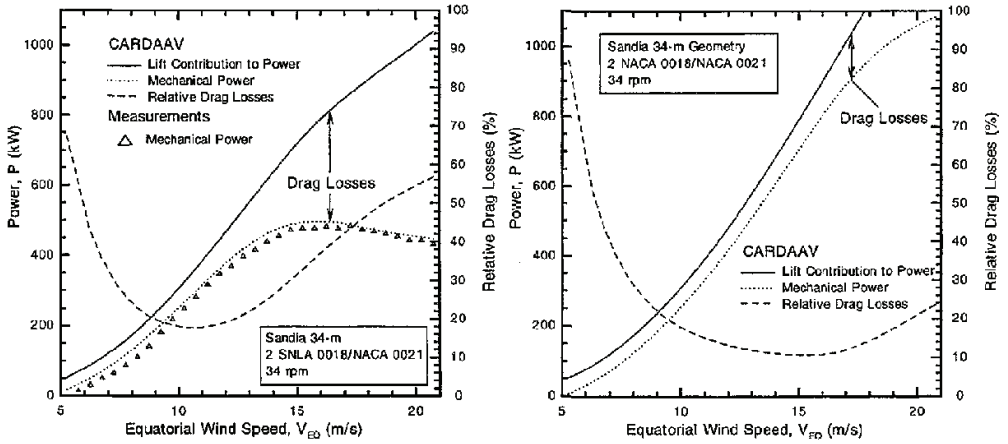

(a) SNLA profile **(b)** Turbulent profile

Figure 5.25: Results of the Sandia 34m turbine blades at 34rpm. [Berg, 1985]

The higher efficiency of the SNLA profile at low air speeds does improve the self starting qualities of the turbine. See section 5.1.5 for more information about the self starting properties. According to [Leclerce, 1997] and [Berg, 1985] the dynamic stall behavior of SNLA profiles are better than the NACA 4-series as a result of the steeper stall characteristics. The vibratory loads are reduced, therefore increasing the lifetime of the turbine and possibly the noise. It is also mentioned by [Berg, 1985] that the NLF airfoils perform better then the NACA 00xx in the Re range from 1 to 5 million, below 1 million it is the other way around. However no prove is given to support this theory. Unfortunately not enough data is available to check the results with the Matlab simulation program. The Troposkien shaped blades can not be calculated, the program is only applicable to VAWT with straight blades.

5.4 Conclusions

Form the comparisons made in this chapter the following conclusions are made:

- For turbulent profiles little improvement possible. A decrease of thickness to 15% would be benificial, but from structural point of view this is not an option
- Large increase in camber does not have beneficial results
- More thickness is not beneficial for turbulent and laminar profiles
- NACA 6-series does decrease drag at low Cl, but the drag bucket is too narrow: the total performance is less
- NLF profiles have low drag at low C_L, but also good performance at higher C_L
- Laminar NLF profiles are the most promising

The optimal results for an airfoil for VAWT applications has low drag at small angles of attack combined with a wide drag bucket. Turbulent profiles generally have a wide drag bucket and laminar profiles have low drag at low angles of attack. The NLF laminar profiles combine these both characteristics and therefore prove to be the best basis for the airfoil design.

Chapter 6

Airfoil design

In the previous chapter is was established that the laminar NLF profiles are the most promising airfoil series for a new VAWT profile. In this chapter the NLF 0018 profile will be taken as basis to investigate thickness (section 6.1) and camber changes (section 6.2). When these parameters are fixed, more detailed changes to the airfoil geometry and pressure distribution are investigated in section 6.3, resulting in the final design given in section 6.4.

The final design is measured in the wind tunnel. The RFOIL data is compared with the measured data to see whether the real airfoil complies with the expected results in section 6.5. Finally the design will be compared to the NACA 0018 profile in section 6.6 to see how and where the improvements are made.

6.1 Thickness

If the thickness is increased, the drag bucket becomes smaller. The minimum thickness with respect to structural demands is 18%. If thickness can be added, it would be a great benefit. This would result in more structural strength and effectively a larger operating envelope. In figure 6.1 the results for NLF profiles with different thickness is given. The decrease in drag bucket between 18% and 20% is only small. If the thickness is increased further, the zero lift drag increases and the drag bucket becomes smaller. Although this leads to a strong blade, the negative effects on performance will be too high.

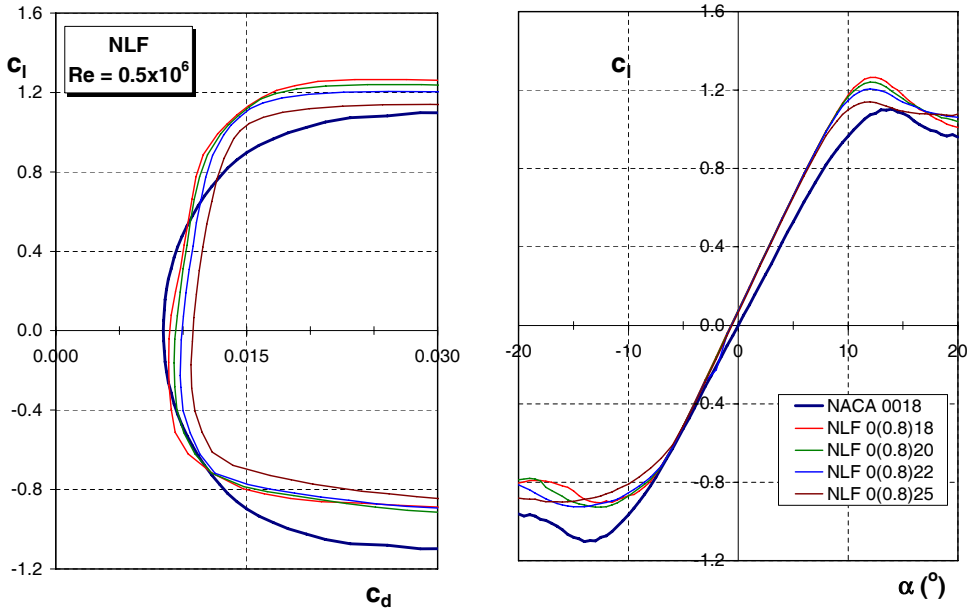

Figure 6.1: Variation in thickness at Re=500,000

From the performance graph (see figure 6.2) the results of increasing thickness are given. The increase in thickness leads to a forward shift of the power curve. If the thickness is increased from 18% to 20% the maximum powercoefficient remains the same, but is reached at lower tip speed ratios. If the thickness is increased further, the $C_{P,max}$ decreases and the forward shift of the curve is only small. The optimum is a thickness of 20%, as the $C_{P,max}$ is at its highest value and the efficiency curve lies more forward than for 18%.

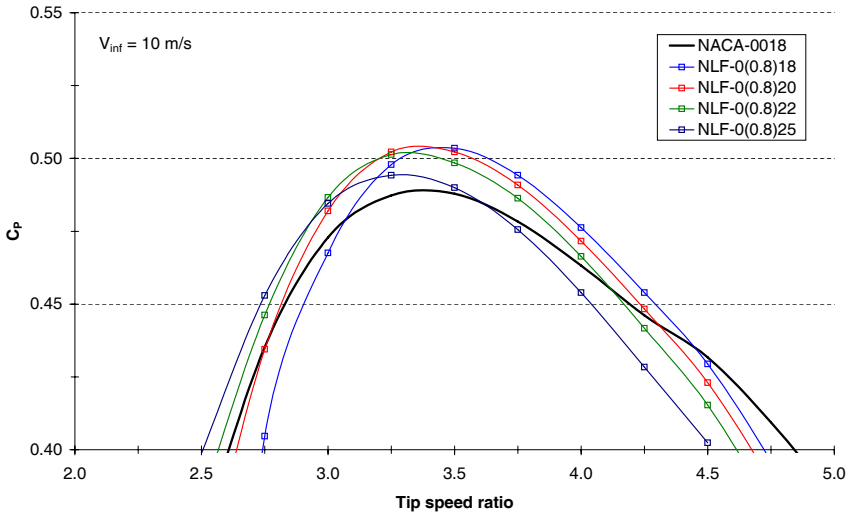

Figure 6.2: Performance results for NLF profiles with different thickness

6.2 Camber

In the previous chapter the concept of camber has been discussed. In this new airfoil design it was important to implement some camber to use the fact that the wind speed are higher at the upwind side of the turbine.

In figure 6.4 the simulation results for varying camber are given. The addition of camber to the airfoil does improve the performance significantly. when increasing camber from 0 to 0.5% and 0.8% the $C_{P,max}$ increase is relatively high. If the camber is increased further to 1%, the $C_{P,max}$ does increase, but at the cost of a smaller interval. The optimum percentage of camber is chosen to be 0,8%.

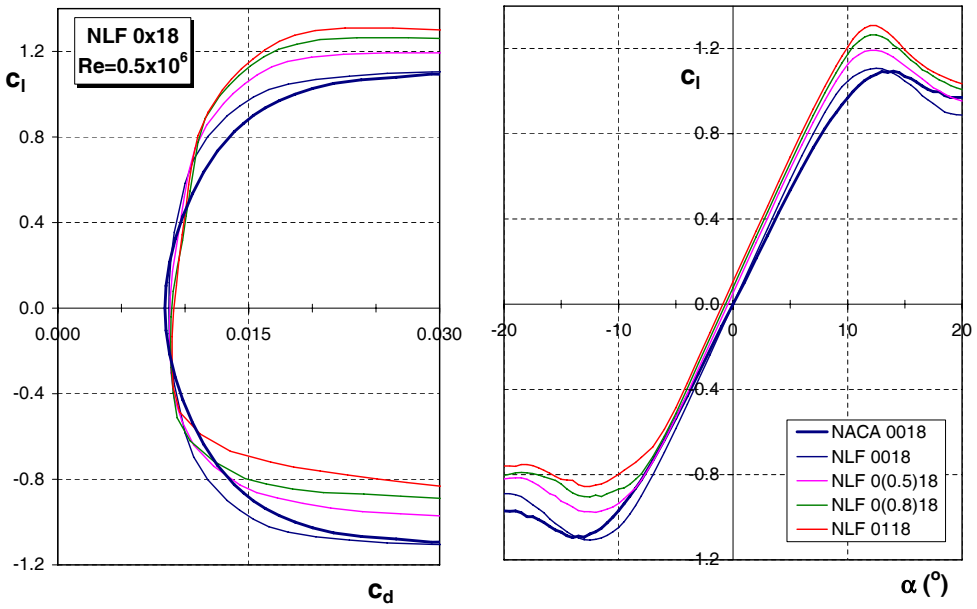

Figure 6.3: Variation in camber at Re=500,000

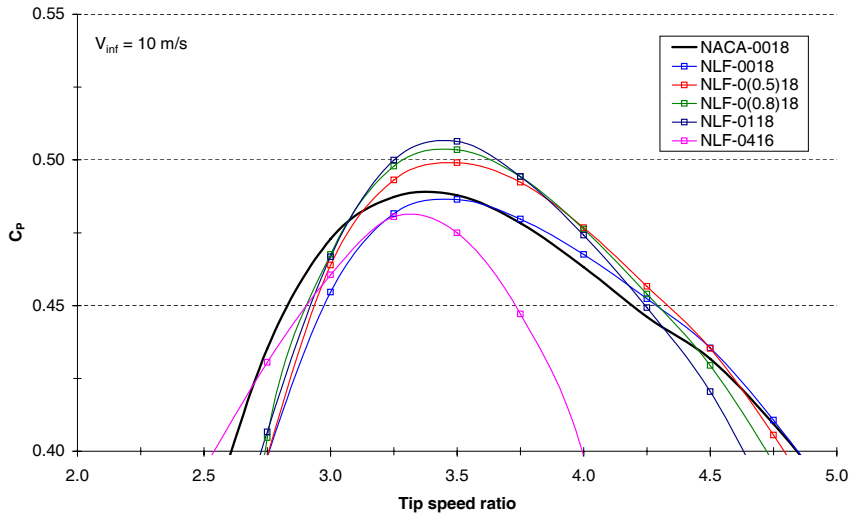

Figure 6.4: Performance results for NLF profiles with different camber

6.3 Fine tuning

In this stage the thickness and camber values are set. Improvements are still possible by fine tuning the pressure distribution and geometry of the airfoil in more detail.

In figure 6.5 the result of a nose radius adjustment is shown. For revision x of the airfoil the nose radius is increased slightly. The result is an increase in $C_{L,max}$ and the drag bucket is substantially wider (see the highlighted areas).

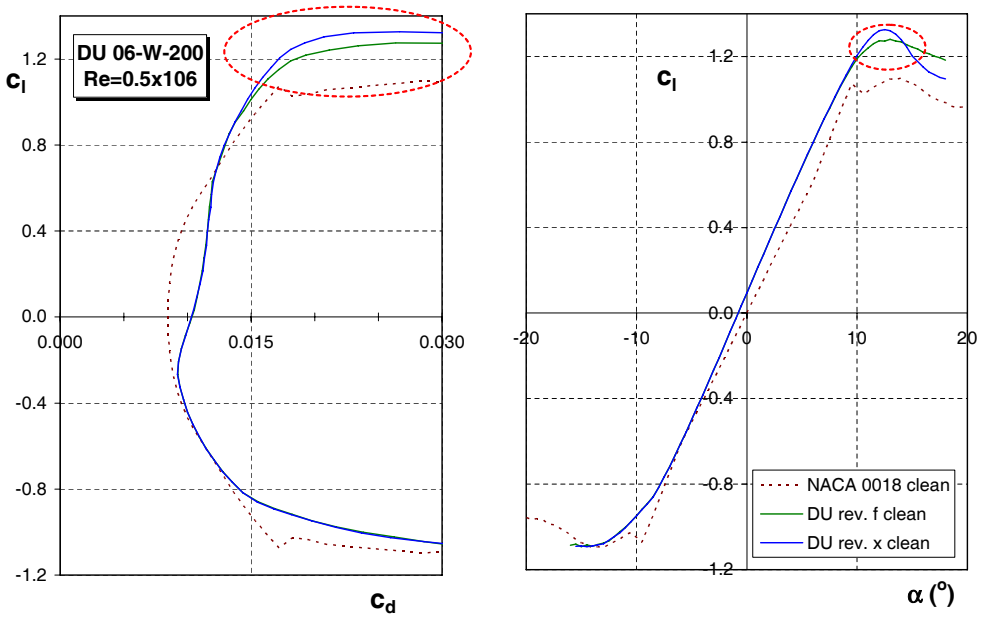

Figure 6.5: Airfoil nose radius optimization

In figure 6.6 the airfoil is modified for a "bump" in the pressure distribution which is present in the left pictures. By smoothing the pressure distribution the bump is removed, see the results at the right pictures.

Numerous adjustments to the airfoil result in the final design of the airfoil. This shape is given in the next section.

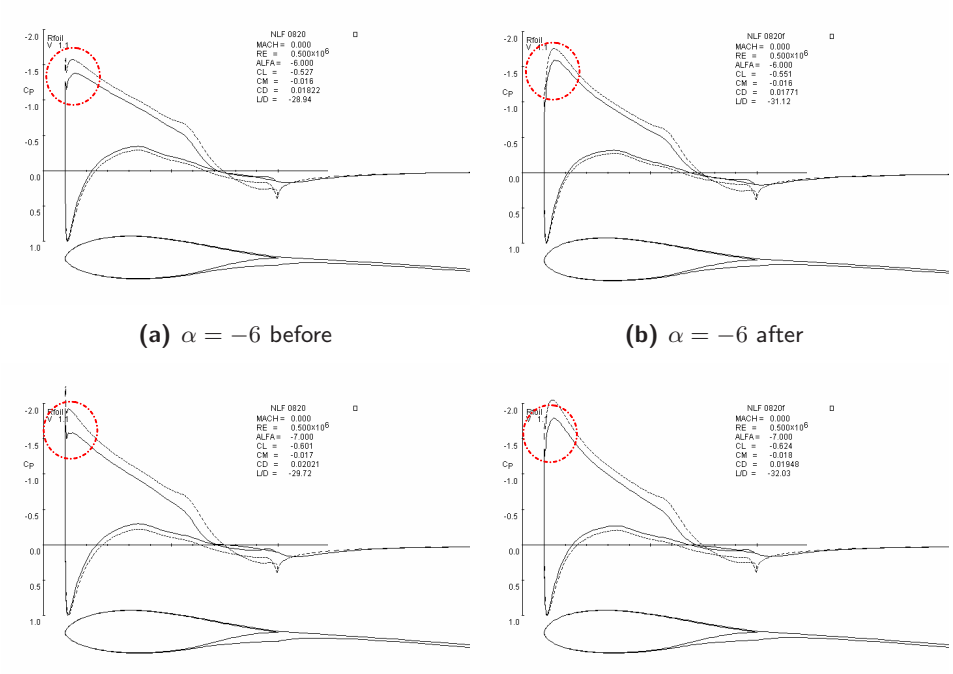

(a) $\alpha = -6$ before **(b)** $\alpha = -6$ after

(c) $\alpha = -7$ before **(d)** $\alpha = -7$ after

Figure 6.6: Removal of bump in the pressure distribution

6.4 Final design

In the previous sections the final design of the new airfoil was established. The name of the airfoil is determined by the conventions of the Aerospace Engineering faculty:

DU 06-W-200

The "DU" stands for Delft University, the "06" for the year 2006, the "W" for the Wind turbine application and the "200" for the thickness of 20,0%. In figure 6.7 the shape of the DU 06-W-200 airfoil is given. The coordinates from the RFOIL and the wind tunnel model are given in appendix A.2.

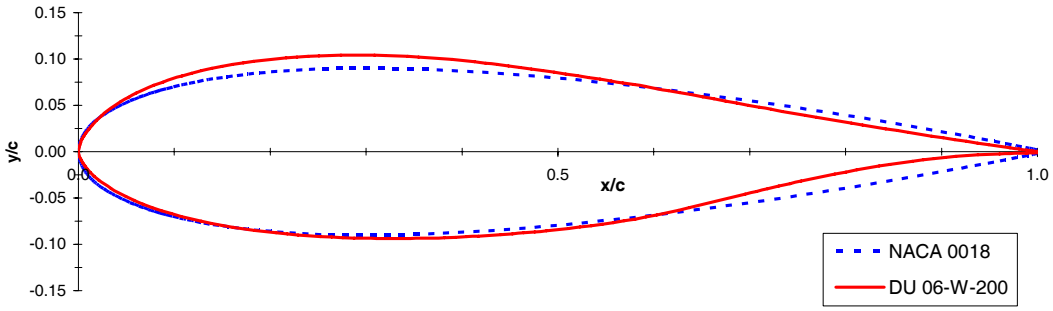

Figure 6.7: Final shape of the DU 06-W-200 compared with the NACA 0018

6.5 RFOIL comparison

In this section the computational results from RFOIL will be compared to the measured wind tunnel data. The RFOIL data for the DU 06-W-200 airfoil is given in appendix C and the data of the wind tunnel tests is given in appendix D. First the free transition data will be compared. Also a comparison is made for the fixed transition airfoil data, only the RFOIL data in this case should be viewed with skepticism (see section 4.4).

6.5.1 Free transition

In figures 6.8 to 6.10 the results for the comparison between RFOIL and measurement data for the clean DU 06-W-200 airfoil are given. The RFOIL $C_{L,max}$ for Re=300,000 and 500,000 are a slightly too low and the drag is underestimated for all Reynolds numbers. The qualitative aspects of the characteristics match however. For negative angles of attack the lift curves fit exactly, for the positive angles of attack the RFOIL lift curve slope is slightly steeper. The graphs show that the RFOIL program indeed has problems to predict the characteristics when the airfoil stalls. When stall begins, RFOIL has is no longer able to cope with the aerodynamic phenomena involved. The solution becomes more and more instable until RFOIL is incapable of giving a result. However, before the airfoil stalls the RFOIL results are very accurate.

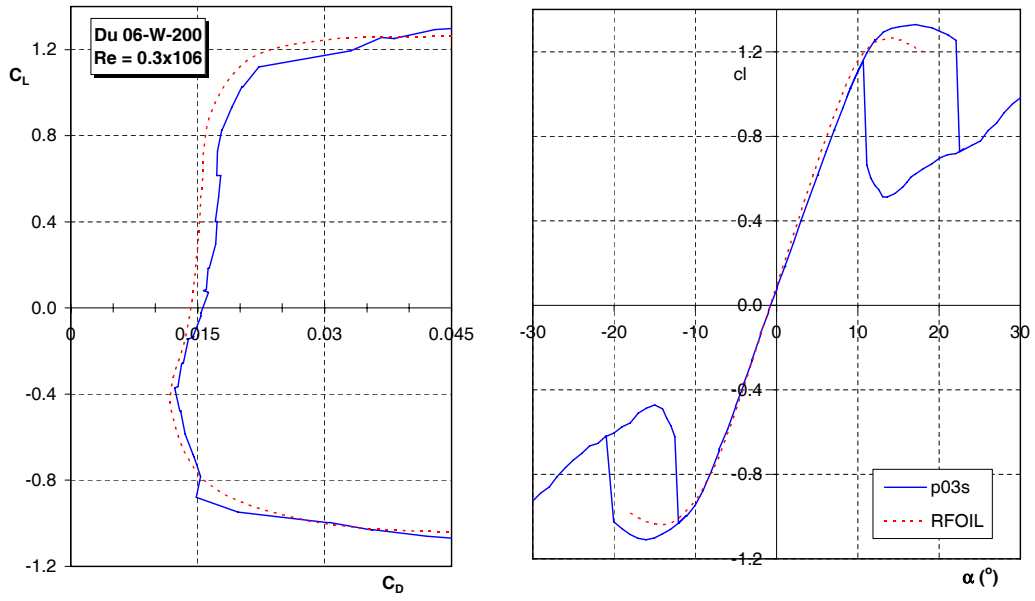

Figure 6.8: Comparison clean RFOIL and wind tunnel data for Re=300,000

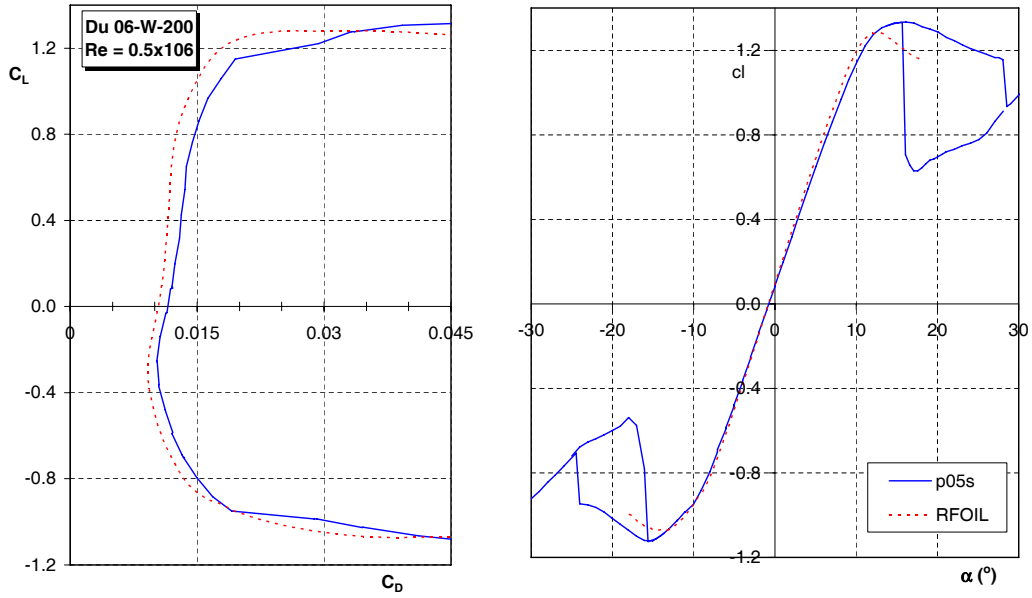

Figure 6.9: Comparison clean RFOIL and wind tunnel data for Re=500,000

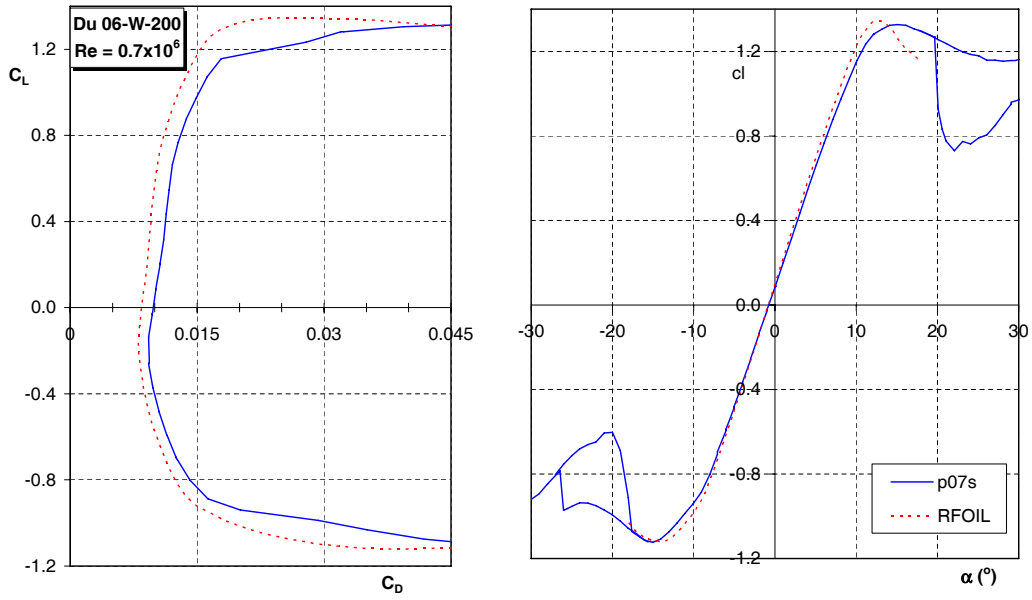

Figure 6.10: Comparison clean RFOIL and wind tunnel data for Re=700,000

6.5.2 Fixed transition

As stated in chapter 3 the RFOIL data for fixed transition conditions is not very reliable. In figure 6.11 a comparison between the RFOIL data for the DU 06-W-200 is compared to the measured data at Re=300,000 and 700,000. The zigzag tape in the measurement is applied at 5% chord and for the RFOIL calculations the trip is applied at 1%. The RFOIL data overpredicts the results of the DU 06-W-200. the same results were visible for the NACA 0018. This data can be found in section 6.6.2. The drag is much lower and the drag bucket wider than for the measured data. The real characteristics of the airfoils in dirty conditions can only be determined using wind tunnel tests.

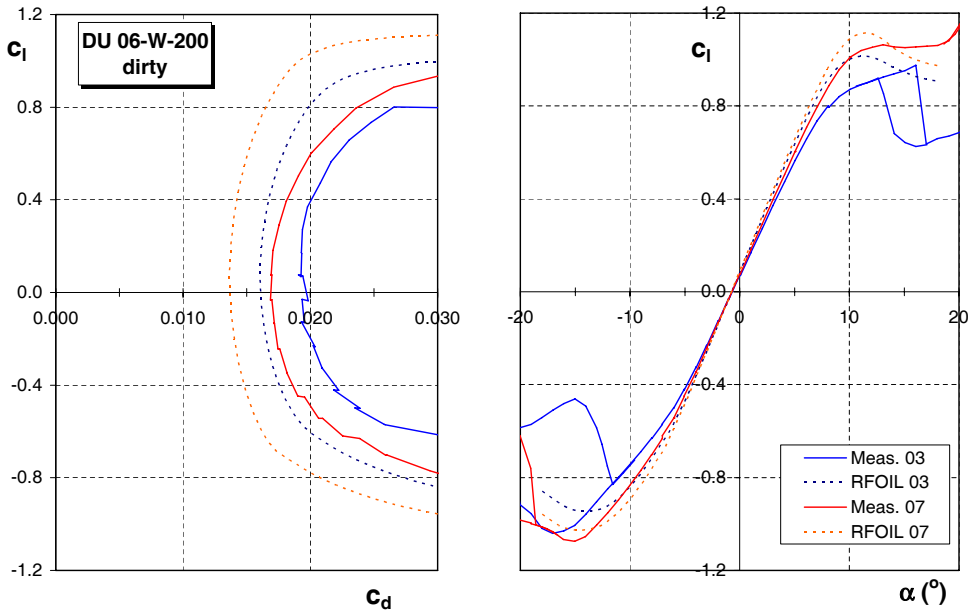

Figure 6.11: Comparison fixed transition RFOIL and measured data for Du 06-W-200

6.6 Measurement comparison

The goal is to improve the performance at positive angles by adding camber and keep the performance at negative angles equal to the NACA 0018. Furthermore 2% extra thickness is added to improve the strength of the blades. In this section the wind tunnel results from the Du 06-W-200 will be compared to the NACA 0018 wind tunnel data. The wind tunnel data for the DU 06-W-200 airfoil is given in appendix D and the data of the NACA 0018 wind tunnel tests is given in appendix B.

6.6.1 Free transition

In figures 6.12 to 6.15 the results for the comparison of the clean NACA 0018 and DU 06-W-200 airfoils are given. The measurement results for the clean airfoil match the predictions made using RFOIL. The zero lift drag of the DU 06-W-200 is slightly higher than for the NACA 0018 as a results of the extra thickness. The performance for the negative angles is the same for Re=300,000 and 500,000. For Re=700,000 and 1,000,000 the drag bucket is slightly smaller for the negative angles, but the $C_{L,max}$ remains as high as for the NACA 0018.

For positive angles of attack the drag bucket is wider as a result of the added camber. The $C_{L,max}$ occurs at the same angle of attack as for the NACA 0018, only the values are much higher.

A characteristic that is difficult to predict is the deep stall angle of attack. For the Reynolds numbers from 300,000 to 700,000 these angles are much higher for the Du 06-W-200 than for the NACA 0018. For Re=1,000,000 no measurements were made for the DU 06-W-200 because of possible balance overload.

To give an indication of the difference in efficiency of both airfoils the lift over drag data is given, for Re=500,000 in figure 6.16 and for Re=700,000 in figure 6.17. The DU 06-W-200 clearly has a higher lift over drag ratio for positive angles of attack. For negative angles the efficiency of both airfoils is nearly the same.

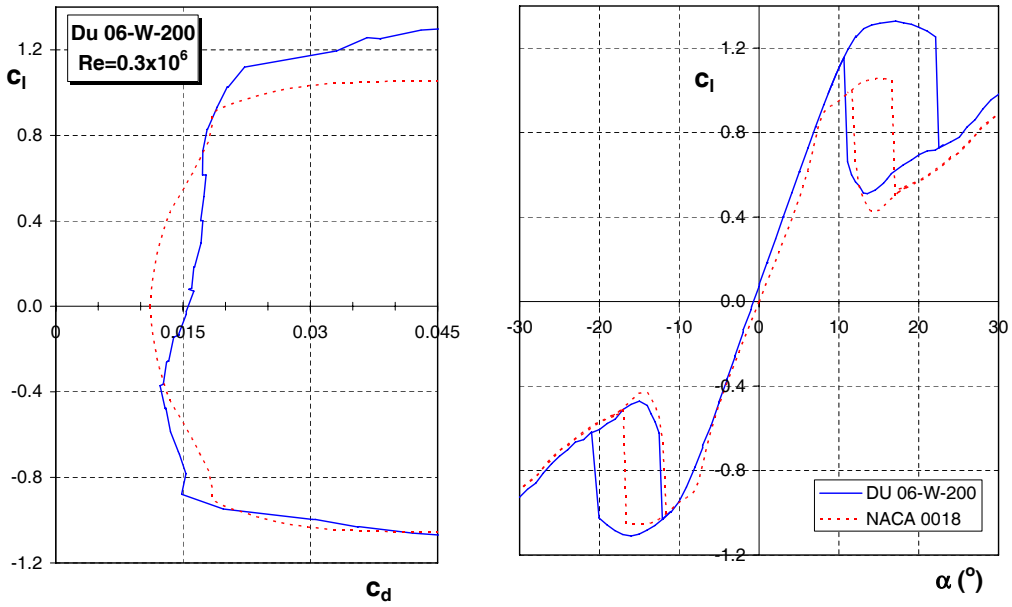

Figure 6.12: Comparison clean wind tunnel data for Re=300,000

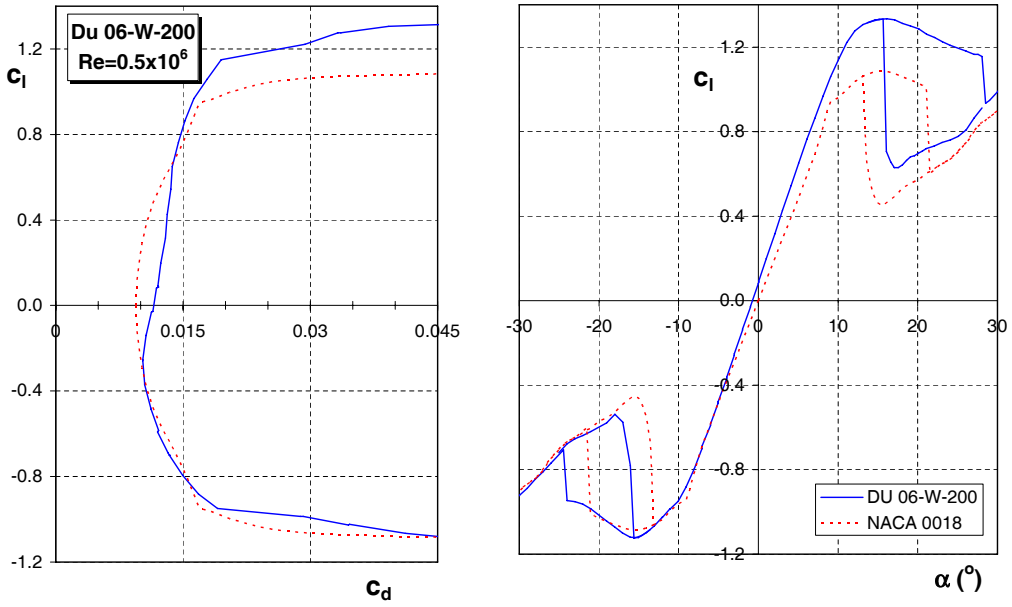

Figure 6.13: Comparison clean wind tunnel data for Re=500,000

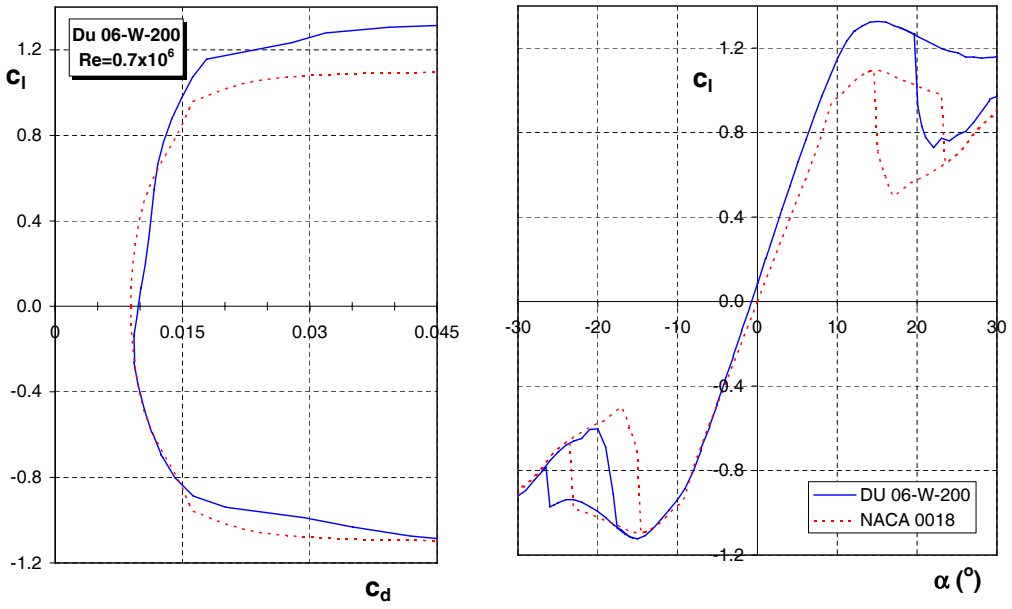

Figure 6.14: Comparison clean wind tunnel data for Re=700,000

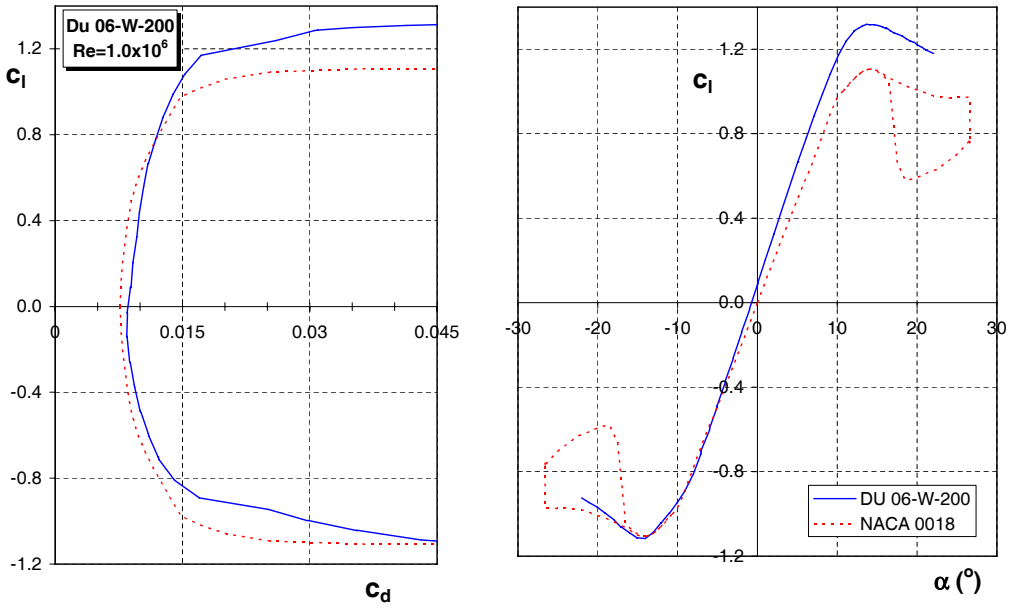

Figure 6.15: Comparison clean wind tunnel data for Re=1,000,000

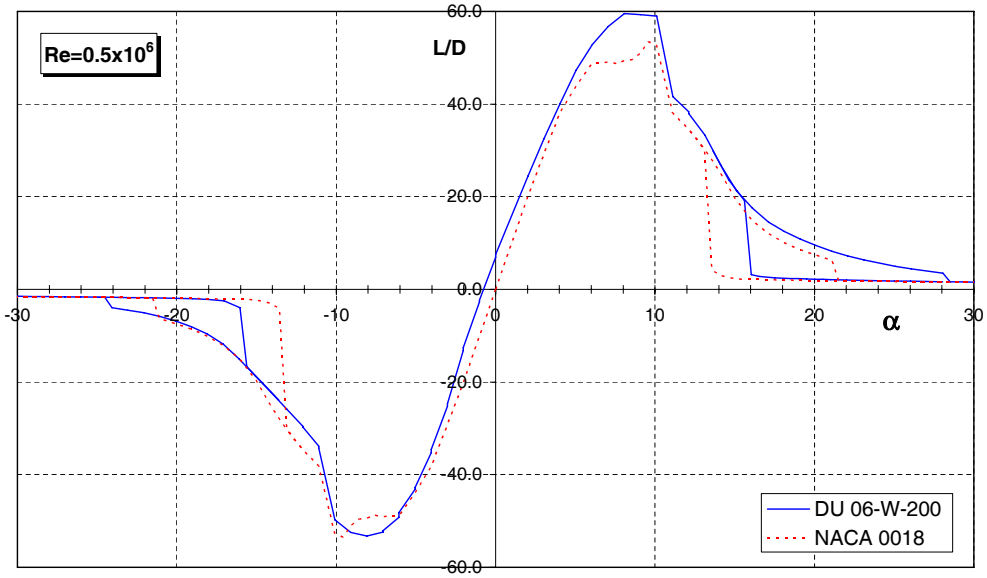

Figure 6.16: Comparison clean lift over drag data for Re=500,000

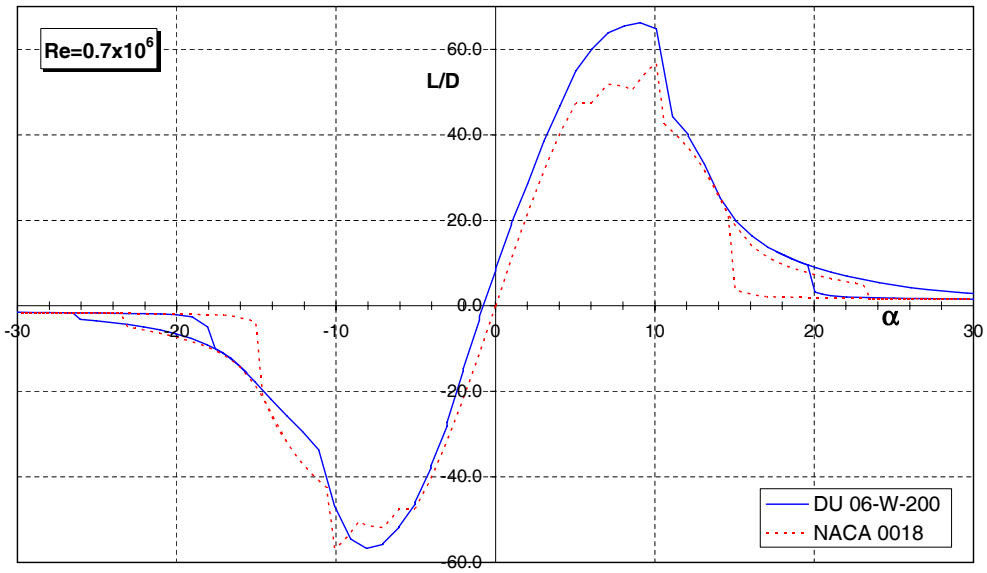

Figure 6.17: Comparison clean lift over drag data for Re=700,000

6.6.2 Fixed transition

The fixed transition characteristics of both the NACA 0018 and Du 06-W-200 were not correctly predicted by RFOIL. In this section the measured characteristics of both airfoils are compared, see figures 6.18 and 6.19. The DU 06-W-200 is an airfoil which is based on a large laminar region. If the airfoil is dirty, the flow over the complete airfoil is turbulent. The "laminar" DU 06-W-200 is expected to have a larger decrease in performance than the "turbulent" NACA 0018.

The zero lift drag of the Du 06-W-200 is higher than for the for the NACA 0018, which is expected for the thicker DU 06-W-200. The DU 06-W-200 has a much higher $C_{L,max}$ for both negative and positive angles of attack. As a results the drag bucket is much wider. For Re=300,000 the deep stall angle is the same for both airfoils for positive angles, but for Re=700,000 the deep stall angles are much higher than for the NACA 0018.

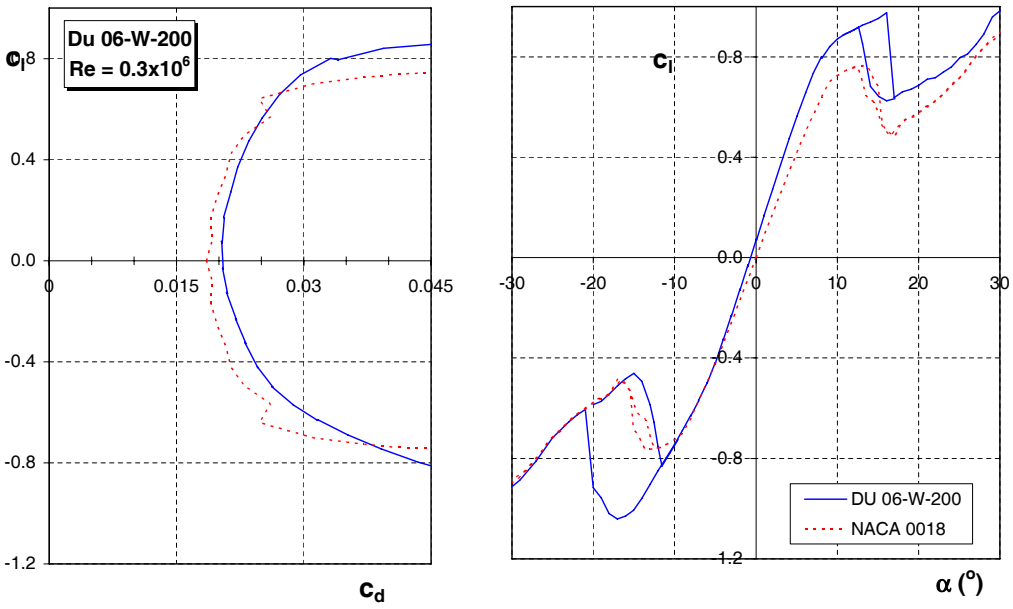

Figure 6.18: Comparison dirty wind tunnel data for Re=300,000

The decrease in performance for the DU 06-W-200 in comparison to the clean airfoil is less than for the NACA 0018. The new design, although it is a laminar profile, performs good in dirty configuration as well.

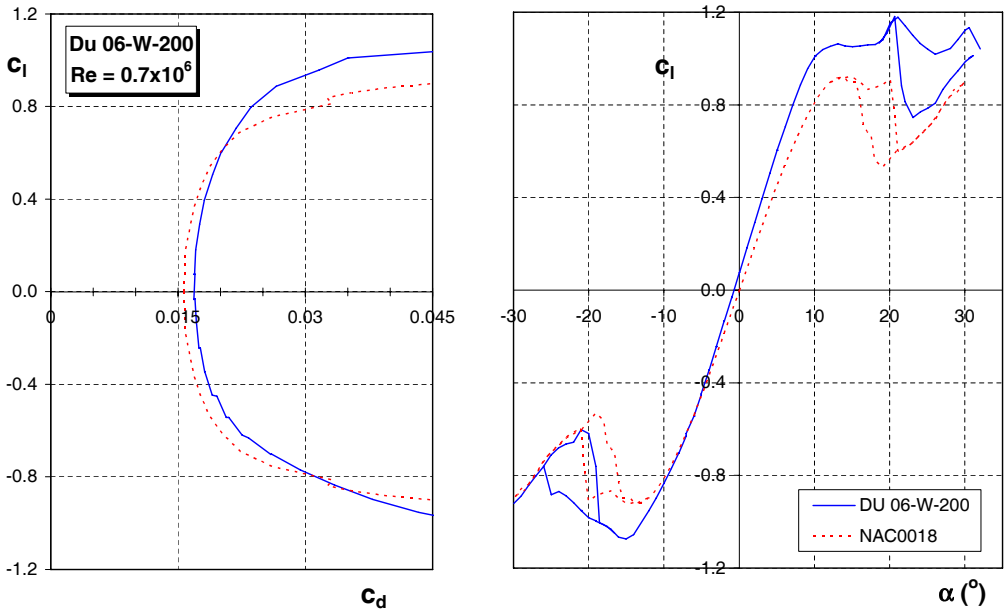

Figure 6.19: Comparison dirty wind tunnel data for Re=700,000

6.7 Simulation results

The measured data for the NACA 0018 and the DU 06-W-200 was implemented into the simulation program. The calculated performance difference between both airfoils is visualized for free transition (figure 6.20) and for fixed transition (figure 6.21). The shaded regions indicate where the DU 06-W-200 outperforms the NACA 0018 profile.

For the clean blades the increase in C_P starts much earlier, resulting in more power output at lower tip speed ratios. The $C_{P,max}$ is increased with 5% to 0.48. This value of $C_{P,max}$ lies for the DU 06-W-200 exactly at $\lambda = 3$, the operating tip speed ratio. If this value is compared to the C_P value for NACA 0018 at $\lambda = 3$, the increase is even 8%.

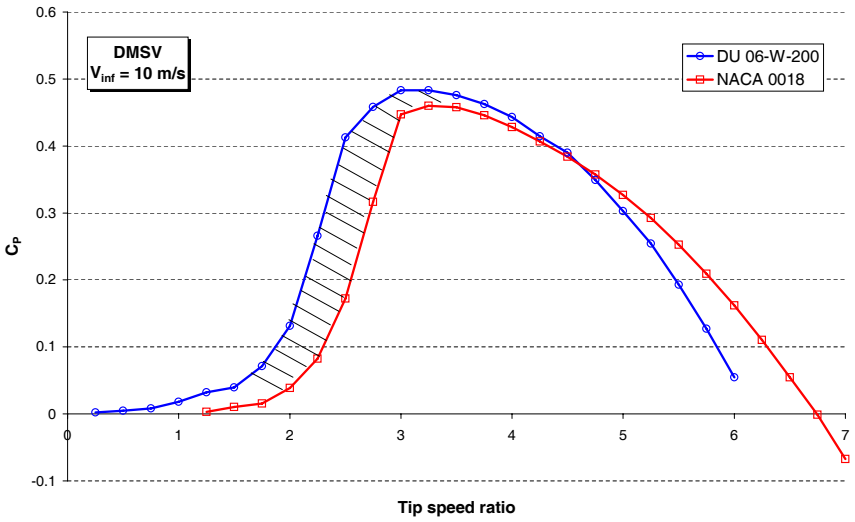

Figure 6.20: Turbine simulation results with the clean DU 06-W-200

If the blades are dirty, the performance of both airfoils decreases. The NACA 0018 has a large region with negative C_P, where during the start-up phase extra energy is needed to let the turbine rotate. This problem is not present at the DU 06-W-200 airfoil. Furthermore the $C_{P,max}$ is increased with 4% to 0.33. If the values of both the airfoils at $\lambda = 3$ are compared, it increases even 108% to 0.28.

The DU 06-W-200 is clearly an improvement with respect to the NACA 0018. The original turbine had to stop at $V_{inf} = 14\frac{m}{s}$ to prevent the blades from failing. The new profile is 2% thicker, resulting in a higher structural strength. This ensures that the turbine can operate at higher wind speeds. Also the maximum power coefficient is increased and the performance is better at lower tip speed ratios. This offers the possibility of operating at lower rotational speeds at high wind speeds while still producing adequate power. With lower rotational speeds the forces on the blades will be lower as well, eliminating the dangers of failure.

The NACA 0018 airfoil has a problem with laminar separation bubbles that extend

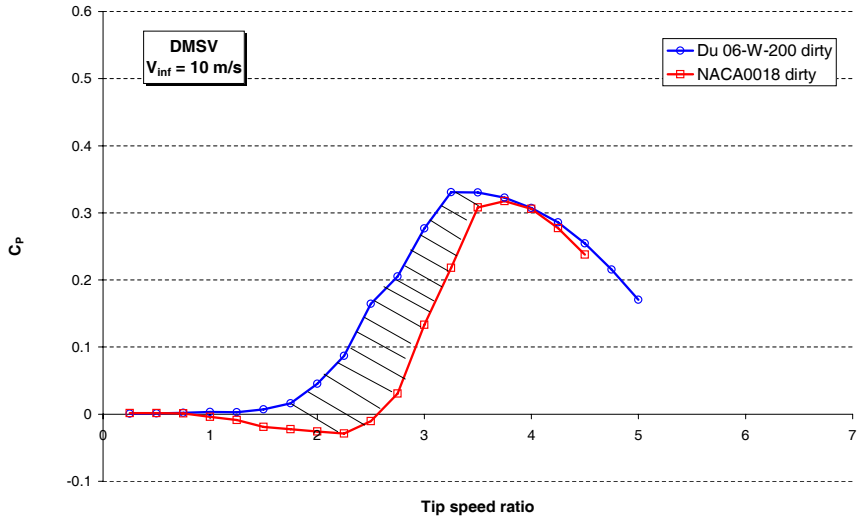

Figure 6.21: Turbine simulation results with the dirty DU 06-W-200

over the trailing edge of the airfoil. The bubbles cause the blades to vibrate and are a source of loud noise. As the turbines are destined to operate in urban environments, noise emission should be kept as low as possible. The laminar separation bubbles can be eliminated using a trip on the blades, only this was not economically feasible for the manufacturer to implement on the Turby VAWT. The DU 06-W-200 does not have this problem, resulting in a noise reduction without the need of applying a trip on the blades.

Chapter 7

Conclusions and recommendations

This report covers the design process of an airfoil dedicated to VAWT applications. In most VAWT produced today standard NACA symmetric airfoils are used. These airfoils were developed in the 1930's and for many of them usable measurement data is not available. During this project the current NACA 0018 is measured and a new design, the DU 06-W-200, is developed to improve the turbines performance. The conclusions are given in section 7.1. Recommendations for further research are given in section 7.2.

7.1 Conclusions

Design goals The NACA 0018 airfoil which is currently used in the Turby VAWT is taken as reference point for the new design. After reviewing the available literate on VAWT aerodynamics the following design goals were set:

- Operate at Reynolds numbers between 150,000 and 700,000 over a wide range of angles α
- Large width of the low drag bucket
- Cambered airfoil to improve the performance of the turbine
- A larger thickness than 18% to increase structural strength
- Start of deep stall at a large angle of attack with the minimum amount of drop in lift coefficient
- No laminar separation bubbles which extend past the trailing edge, which results in noise reduction

RFOIL program RFOIL is a computational program based on the panel method combined with boundary layer equations. This method is capable to predict 2D airfoil characteristics accurately for higher Reynolds numbers until the airfoil enters stall. The RFOIL code has more problems to accurately predict the the airfoil characteristics at Reynolds numbers between 300,000 and 700,000. The airfoil design process for this project lies in this Reynolds number range. However RFOIL gives accurate enough results to be a powerful design tool in this range. The calculated characteristics for a dirty airfoil shows no real similarity with available wind tunnel data, therefore the RFOIL program should be used for clean airfoil design only.

Simulation program The developed simulation program is based on the momentum theory. To enable velocity variation perpendicular to the free stream flow and between the upwind and downwind side, the Double Multiple Streamtube model with variable interference factors is implemented. The final Matlab program allows to adjust the turbines geometry, to choose from multiple airfoils and to implement a dynamic stall model or not. As such 2D airfoil characteristic from RFOIL can be inserted to view the turbines performance with this airfoil.

Design process These design tools together enable to design a new airfoil. The design process consisted of an iteration process of adjusting the airfoils shape, calculating the characteristics using RFOIL and calculating the performance results using the simulation program. The calculated RFOIL characteristics and the simulated performance results are then compared to the original NACA 0018 profile and previous designs in the design process. By adjusting the type of airfoil (laminar or turbulent), the thickness and camber an optimum design is found in the laminar NLF series. Using the NLF 0018 as starting point, this design is optimized by again adjusting the camber and thickness, but also by fine-tuning the geometry and the pressure distribution. This finally resulted in the final design:

DU 06-W-200

Validation The Du 06-W-200 airfoil is a laminar, 20% thick airfoil with 0.8% camber. The original NACA 0018 airfoil is a turbulent, symmetric airfoil with 18% thickness. To be able to compare both airfoils wind tunnel measurements were performed in the LTT wind tunnel at the Delft University of Technology. This measured 2D data is also used in the simulation program. From this data the following conclusions can be drawn:

- The added thickness of 2% will add to the blade strength and this is reached without decreasing the performance
- The added camber of 0.8% increases the performance with respect to a symmetric airfoil

- The DU 06-W-200 performs equal to the NACA 0018 for negative angles of attack
- The DU 06-W-200 has a much higher $C_{L,max}$ for positive angles of attack, resulting in a wider drag bucket
- Deep stall occurs at higher angles of attack with a lower drop in lift coefficient
- In contrast with the NACA 0018 the DU 06-W-200 does not have laminar separation bubbles which extend over the trailing edge
- The increase in turbine performance at operating tip speed ratio is 8% in clean conditions and 108% when dirty

7.2 Recommendations

Within the time frame of this project and within the facilities available certain issues are not covered in this project. Below the recommendations for future research in this subject are listed. These recommendations are mainly focused on improving the modeling methods for VAWT.

CFD modeling Performing CFD simulations of a complete 3D VAWT. This gives the possibility to visualize the flow phenomena and to get more detailed quantitative data of the flow through the turbine. The influence of the blades at the upwind side on the flow at the downwind side and the influence of the rotation axis can be quantified. Optimization of the geometry at the tips of the blades is also possible using CFD.

VAWT wind tunnel testing Wind tunnel test on VAWT to get more exact data to validate the simulations. In literature little applicable data on these turbines is available. Testing the turbine under controlled conditions offer the possibility to measure the power curve of the turbine without drive train influences and free stream airflow variations. This data can be used to validate and improve the momentum based simulation model and the CFD simulations.

Chapter 8

Bibliography

[Abbott and Doenhoff, 1949] Abbott, I. and Doenhoff, A. V. (1949). *Theory of Wing Sections*. Dover Publications, Inc., New York. [40]

[Althaus, 1980] Althaus, D. (1980). *Profilpolaren fur den Modellflug: Windkanalmessungen an Profiles im Kritischen Reynoldszahlbereich*. Neckar Verlag. [47]

[Berg, 1985] Berg, D. (1985). Structural design of the sanidia 34-meter vertical axis wind turbine. Technical Report SAND84-1287, Sandia National Laboratories. [65, 66]

[Brochier et al., 1986] Brochier, G., Fraunié, P., Beguiér, C., and Paraschivoiu, I. (1986). Water channel experiments of dynamic stall on darrieus wind turbine blades. *Journal of Propulsion*, 2(5):445–449. [11, 12]

[Claessens, 2006a] Claessens, M. (2006a). Du 06-w-200 measurement report. Technical report, TU Delft. [109]

[Claessens, 2006b] Claessens, M. (2006b). Naca 0018 measurement report. Technical report, TU Delft. [97]

[Fujisawa and Shibuya, 2001] Fujisawa, N. and Shibuya, S. (2001). Observations of dynamic stall on darrieus wind turbine blades. *Journal of Wind Engineering and Industrial Aerodynamics*, 89:201–214. [12, 13]

[Gopalarathnam et al., 2001] Gopalarathnam, A., Broughton, B., McGranaham, B., and Selig, M. (2001). Design of low reynolds number airfoils with trip. 19^{th} *AIAA Applied Aerodynamics Conference*. [50, 51]

[Gormont, 1973] Gormont, R. (1973). A mathematical model of unsteady aerodynamics and radial flow for application to helicopter rotors. Technical report, Boeing Co. Vertol Div. [28]

[Iida et al., 2004] Iida, A., Mizun, A., and Fukudome, K. (2004). Numerical simulation of aerodynamic noise radiated from vertical axis wind turbines. Technical report, Kogakuin University Department of Mechanical Engineering. [52]

[Jacobs and Sherman, 1937] Jacobs, E. and Sherman, A. (1937). Airfoil characteristics as affected by variations of the reynolds number. Technical report, N.A.C.A. [15, 47, 50]

[Kirke and Lazauskas, 1991] Kirke, B. and Lazauskas, L. (1991). Enhancing the performance if a vertical axis wind turbine using a simple variable pitch system. *Wind Engineering*, 15(4):187–195. [53, 54]

[Leclerce, 1997] Leclerce, C. (1997). Why use natural laminar airfoil profiles in vertical axis wind turbine applications? *AIAA Meeting Papers on Disc*, -(AIAA 97-0005). [64, 66]

[Loth and McCoy, 1983] Loth, J. and McCoy, H. (1983). Optimization of darrieus turbines with an upwind and downwind momentun model. *Journal of Energy*, 7(4):313–318. [24]

[Maughmer, 1999] Maughmer, M. (1999). Wind-tunnel test of the s824 airfoil. Technical report, Pennsylvania State University. [39]

[Migliore et al., 1980] Migliore, P., Wofle, P., and Fanucci, J. (1980). Flow curvature effect on darrieus tubrine blade aerodynamics. *Journal of Energy*, 4(2):49–55. [18]

[Paraschivoiu, 2002] Paraschivoiu, I. (2002). *Wind Turbine Design*. Polytechnic International Press. [16, 31]

[Paraschivoiu and Delclaux, 1983] Paraschivoiu, I. and Delclaux, F. (1983). Double multiple streamtube model with recent improvements. *Journal of Energy*, 7(3):250–255. [24]

[Sheldahl et al., 1980] Sheldahl, R., Klimas, P., and Feltz, L. (1980). Aerodynamic performance of a 5-meter-diameter darrieus turbine with extruded aluminum naca-0015 blades. Technical Report SAND80-0179, Sandia National Laboratories. [14, 16, 48]

[Strickland, 1975] Strickland, J. (1975). The darrieus turbine: A performance prediction model using multiple streamtubes. Technical Report SAND75-0431, Sandia Laboratories. [23, 29, 31, 32]

[Templin, 1974] Templin, R. (1974). *The Elements of Airfoil and Airscrew Theory*. Cambridge University Press, second edition. [22]

[W.A. Timmer, 2003] W.A. Timmer, R. v. R. (2003). Summary of the delft university wund turbine dedicated airfoils. *41st AIAA Aerospace Sciences Meeting and Exhibit*, pages 11–21. [10]

Appendix A

Airfoil coordinates

In this appendix the coordinates of the NACA 0018 (section A.1) and Du 06-W-200 (section A.2) profiles are given. These are the coordinates used for the wind tunnel models and for the program RFOIL.

A.1 NACA 0018

x/c	y/c	x/c	y/c	x/c	y/c	x/c	y/c
1	0.0019	0.2333	0.0884	0	-0.001	0.2469	-0.089
0.9938	0.0032	0.2201	0.0876	0.0001	-0.0029	0.2608	-0.0895
0.9837	0.0053	0.2073	0.0867	0.0003	-0.0048	0.275	-0.0898
0.9728	0.0075	0.1949	0.0856	0.0007	-0.0068	0.2894	-0.09
0.961	0.0099	0.1829	0.0844	0.0011	-0.0088	0.3041	-0.09
0.9484	0.0124	0.1714	0.0831	0.0017	-0.0108	0.3189	-0.0899
0.9349	0.0151	0.1604	0.0817	0.0024	-0.0128	0.334	-0.0896
0.9207	0.0178	0.15	0.0802	0.0032	-0.0149	0.3493	-0.0893
0.9059	0.0206	0.14	0.0786	0.0042	-0.0169	0.3647	-0.0887
0.8906	0.0235	0.1306	0.0769	0.0053	-0.0189	0.3802	-0.0881
0.8749	0.0263	0.1218	0.0752	0.0065	-0.0208	0.3959	-0.0873
0.8588	0.0292	0.1134	0.0734	0.0079	-0.0228	0.4117	-0.0864
0.8426	0.0321	0.1056	0.0716	0.0094	-0.0248	0.4277	-0.0853
0.8261	0.0349	0.0982	0.0698	0.011	-0.0267	0.4437	-0.0842
0.8095	0.0378	0.0913	0.0679	0.0127	-0.0287	0.4598	-0.0829
0.7929	0.0405	0.0848	0.0661	0.0146	-0.0306	0.476	-0.0816
0.7761	0.0433	0.0787	0.0642	0.0166	-0.0325	0.4923	-0.0801
0.7594	0.0459	0.073	0.0623	0.0188	-0.0344	0.5087	-0.0786
0.7426	0.0486	0.0677	0.0605	0.0211	-0.0363	0.5251	-0.0769
0.7257	0.0511	0.0627	0.0586	0.0235	-0.0382	0.5416	-0.0752
0.7089	0.0537	0.0579	0.0567	0.0261	-0.04	0.5582	-0.0734
0.6921	0.0561	0.0535	0.0549	0.0289	-0.0419	0.5748	-0.0715
0.6752	0.0585	0.0493	0.053	0.0318	-0.0437	0.5914	-0.0695
0.6584	0.0608	0.0454	0.0512	0.0349	-0.0456	0.6081	-0.0674
0.6416	0.0631	0.0417	0.0493	0.0382	-0.0475	0.6249	-0.0653
0.6249	0.0653	0.0382	0.0475	0.0417	-0.0493	0.6416	-0.0631
0.6081	0.0674	0.0349	0.0456	0.0454	-0.0512	0.6584	-0.0608
0.5914	0.0695	0.0318	0.0437	0.0493	-0.053	0.6752	-0.0585
0.5748	0.0715	0.0289	0.0419	0.0535	-0.0549	0.6921	-0.0561
0.5582	0.0734	0.0261	0.04	0.0579	-0.0567	0.7089	-0.0537
0.5416	0.0752	0.0235	0.0382	0.0627	-0.0586	0.7257	-0.0511
0.5251	0.0769	0.0211	0.0363	0.0677	-0.0605	0.7426	-0.0486
0.5087	0.0786	0.0188	0.0344	0.073	-0.0623	0.7594	-0.0459
0.4923	0.0801	0.0166	0.0325	0.0787	-0.0642	0.7761	-0.0433
0.476	0.0816	0.0146	0.0306	0.0848	-0.0661	0.7929	-0.0405
0.4598	0.0829	0.0127	0.0287	0.0913	-0.0679	0.8095	-0.0378
0.4437	0.0842	0.011	0.0267	0.0982	-0.0698	0.8261	-0.0349
0.4277	0.0853	0.0094	0.0248	0.1056	-0.0716	0.8426	-0.0321
0.4117	0.0864	0.0079	0.0228	0.1134	-0.0734	0.8588	-0.0292
0.3959	0.0873	0.0065	0.0208	0.1218	-0.0752	0.8749	-0.0263
0.3802	0.0881	0.0053	0.0189	0.1306	-0.0769	0.8906	-0.0235
0.3647	0.0887	0.0042	0.0169	0.14	-0.0786	0.9059	-0.0206
0.3493	0.0893	0.0032	0.0149	0.15	-0.0802	0.9207	-0.0178
0.334	0.0896	0.0024	0.0128	0.1604	-0.0817	0.9349	-0.0151
0.3189	0.0899	0.0017	0.0108	0.1714	-0.0831	0.9484	-0.0124
0.3041	0.09	0.0011	0.0088	0.1829	-0.0844	0.961	-0.0099
0.2894	0.09	0.0007	0.0068	0.1949	-0.0856	0.9728	-0.0075
0.275	0.0898	0.0003	0.0048	0.2073	-0.0867	0.9837	-0.0053
0.2608	0.0895	0.0001	0.0029	0.2201	-0.0876	0.9938	-0.0032
0.2469	0.089	0	0.001	0.2333	-0.0884	1	-0.0019

Table A.1: NACA 0018 coordinates

A.2 DU 06-W-200

x/c	y/c	x/c	y/c	x/c	y/c	x/c	y/c
1.00003	0.00033	0.424787	0.095466	0.99997	-0.001169	0.440534	-0.089484
0.995071	0.000991	0.413003	0.096877	0.994978	-0.001364	0.428714	-0.090318
0.988745	0.00179	0.40129	0.098182	0.988627	-0.001544	0.416892	-0.091073
0.980844	0.002821	0.389595	0.099392	0.980723	-0.001708	0.405087	-0.091739
0.971354	0.004134	0.377963	0.100483	0.971321	-0.001989	0.393277	-0.092315
0.960703	0.005676	0.366361	0.101453	0.960662	-0.002393	0.381483	-0.092805
0.949361	0.00738	0.354814	0.102282	0.949424	-0.002872	0.369702	-0.093194
0.937673	0.009188	0.343266	0.102969	0.93803	-0.00347	0.357917	-0.093494
0.925781	0.011064	0.331726	0.103514	0.926586	-0.004214	0.346164	-0.093688
0.913799	0.012967	0.320178	0.103912	0.91515	-0.005108	0.334386	-0.093785
0.901782	0.014892	0.308593	0.10418	0.903719	-0.00616	0.322646	-0.093783
0.889754	0.016828	0.297054	0.104309	0.892291	-0.007367	0.310901	-0.093673
0.877727	0.018779	0.285489	0.10429	0.88086	-0.008731	0.299179	-0.093459
0.865704	0.020741	0.273928	0.104142	0.869394	-0.010249	0.287455	-0.093136
0.853697	0.022719	0.262419	0.103851	0.857897	-0.011903	0.275771	-0.092709
0.841679	0.024714	0.25092	0.103406	0.846387	-0.013685	0.264104	-0.09216
0.829686	0.026717	0.239441	0.102815	0.83486	-0.015593	0.252445	-0.091498
0.81774	0.028741	0.228016	0.102074	0.823301	-0.017617	0.240824	-0.090722
0.805771	0.030796	0.216637	0.101172	0.811752	-0.019742	0.229267	-0.089822
0.793799	0.032857	0.205318	0.100103	0.800182	-0.021981	0.217718	-0.088783
0.781854	0.034939	0.194052	0.098861	0.788585	-0.024315	0.206246	-0.087627
0.769889	0.037053	0.182866	0.097447	0.77696	-0.02674	0.194835	-0.08631
0.757924	0.03918	0.171792	0.095845	0.765344	-0.029234	0.183459	-0.084857
0.746007	0.041327	0.160792	0.094042	0.753726	-0.031815	0.172199	-0.083251
0.734077	0.043511	0.149938	0.092038	0.742078	-0.034463	0.161017	-0.081472
0.722128	0.045716	0.13917	0.089806	0.730458	-0.03718	0.149918	-0.07952
0.710225	0.047936	0.128563	0.087366	0.718795	-0.039964	0.138941	-0.077391
0.698325	0.050176	0.118128	0.084689	0.707153	-0.042807	0.128085	-0.075067
0.686453	0.052417	0.107876	0.081772	0.69543	-0.045719	0.117402	-0.072555
0.674589	0.054685	0.097863	0.07861	0.683701	-0.048657	0.106888	-0.069816
0.662687	0.056949	0.088085	0.075175	0.671981	-0.051627	0.096591	-0.066865
0.650773	0.059221	0.078586	0.071484	0.660268	-0.05461	0.08651	-0.063669
0.638859	0.06148	0.069402	0.067515	0.648597	-0.057558	0.076717	-0.060244
0.626934	0.063716	0.060586	0.063284	0.63703	-0.060434	0.067244	-0.056572
0.615006	0.065934	0.052175	0.058794	0.625585	-0.063191	0.058159	-0.052655
0.603147	0.068109	0.044254	0.054063	0.614212	-0.065812	0.049507	-0.048508
0.591292	0.070229	0.036871	0.049124	0.60288	-0.068293	0.041417	-0.044177
0.57943	0.072307	0.030107	0.044037	0.591592	-0.07062	0.03397	-0.039704
0.567547	0.074343	0.024057	0.038898	0.58032	-0.072781	0.027288	-0.035182
0.555676	0.076339	0.018781	0.033816	0.569025	-0.074781	0.021456	-0.03074
0.543792	0.078282	0.014332	0.02893	0.557686	-0.07662	0.016534	-0.026484
0.531879	0.080195	0.010681	0.024359	0.546245	-0.078317	0.012477	-0.022518
0.519984	0.08206	0.007756	0.020195	0.534692	-0.079904	0.009224	-0.018871
0.508056	0.083885	0.00546	0.016479	0.523068	-0.081386	0.006653	-0.015533
0.496115	0.085679	0.00372	0.013151	0.511354	-0.08278	0.00463	-0.012507
0.484187	0.087431	0.002419	0.010168	0.499605	-0.084091	0.003065	-0.009755
0.472242	0.089147	0.001446	0.007489	0.487811	-0.085322	0.001862	-0.007256
0.460354	0.090814	0.000702	0.005102	0.475993	-0.08648	0.00098	-0.004968
0.448446	0.092426	0.000259	0.002932	0.464176	-0.087561	0.000385	-0.002855
0.436599	0.09399	0.000038	0.000944	0.452348	-0.088562	0.000046	-0.000911

Table A.2: DU 06-W-200 coordinates

Appendix B

NACA 0018 wind tunnel results

In this appendix a summary of the results of the wind tunnel tests on the NACA 0018 profile is given. First the test setup is discussed in section B.1. A more thorough report is available, [Claessens, 2006b]. In section B.3 the results for the airfoil in clean configuration are given. The laminar separation bubbles present in clean configuration were eliminated using zigzag tape. The results of this configuration can be found in section B.4. The results for the airfoil with fixed transition, with zigzag tape applied at 5% chord, are given in section B.5. Finally an overview of the measurements performed at angles of attack to 180° angle of attack cna be found in section B.6. As it is a symmetrical airfoil, this results in the data for the complete rotation of the airfoil.

B.1 Test setup

The tunnel used is the Low Turbulence Tunnel (LTT) at the Technical University of Delft. This wind tunnel is build in 1954 and has very little turbulence. This makes it especially suited for making research at low Reynolds numbers on the NACA 0018 profile. The turbulence level is 0.02% at low speeds and 0.20% at maximum speed.

Test section: 1.25 m high, 1.8 m wide
Maximum airspeed: 120 m/s

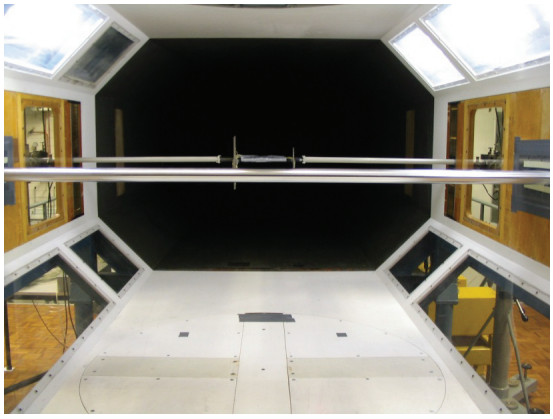

Figure B.1: The model placed inside the octagonal wind tunnel

B.2 Model

The NACA 0018 model used is made of solid aluminum. The full length is 2.8 m, the wing section itself is 1.8 m wide.

NACA 0018 profile
Length: 1.8 m
Chord: 0.25 m

B.2.1 Wake rake

The small wake rake is used for measurements in the wake of the model. It consists of 50 total pressure measurement tubes and 12 static pressure measurement tubes.

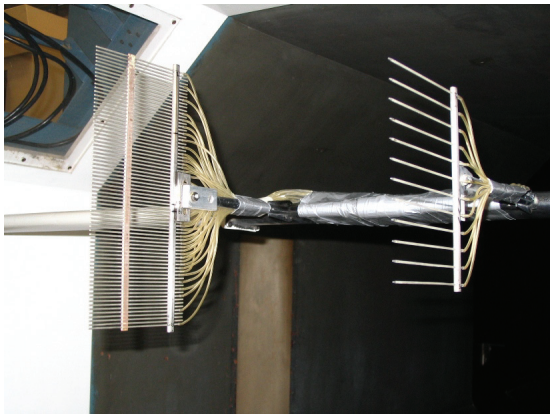

Figure B.2: The wake rake with the total and static pressure tubes

For the final measurements the manometer using fluids is used, see figures B.3 and B.4. It uses lasers to read the height of the different tubes of which each one is connected to one tube of the wake rake. This method is highly accurate; it has an error of 0.1 Pa. But before the measurements begin a zero run has to be made, which can also have an error of 0.1 Pa.

Figure B.3: The manometer

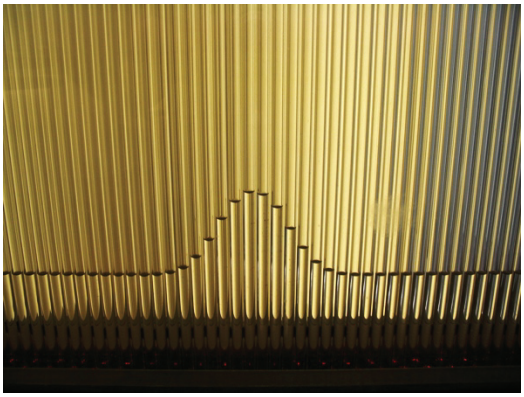

Figure B.4: Manometer detail of the total pressures in the wake

B.2.2 Balance system

The model is attached on both sides to a yoke, see figure B.5. This yoke is a new system which allows the angle of attack to be accurately controlled and ensures improved balance measurement results. The previous system had to be controlled manually, the new system is computer controlled. The balance can measure the forces in three directions and the moments around the three axis. For this experiment only the forces in two directions and the moments around one axes are used.

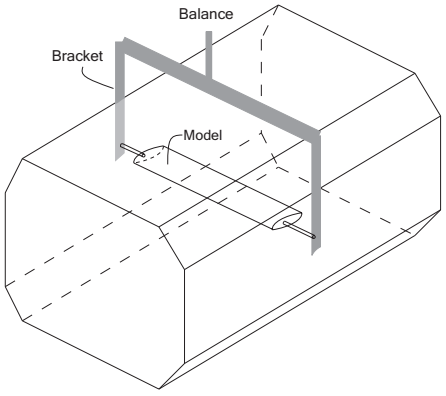

Figure B.5: Schematic of the test section

B.3 Free transition

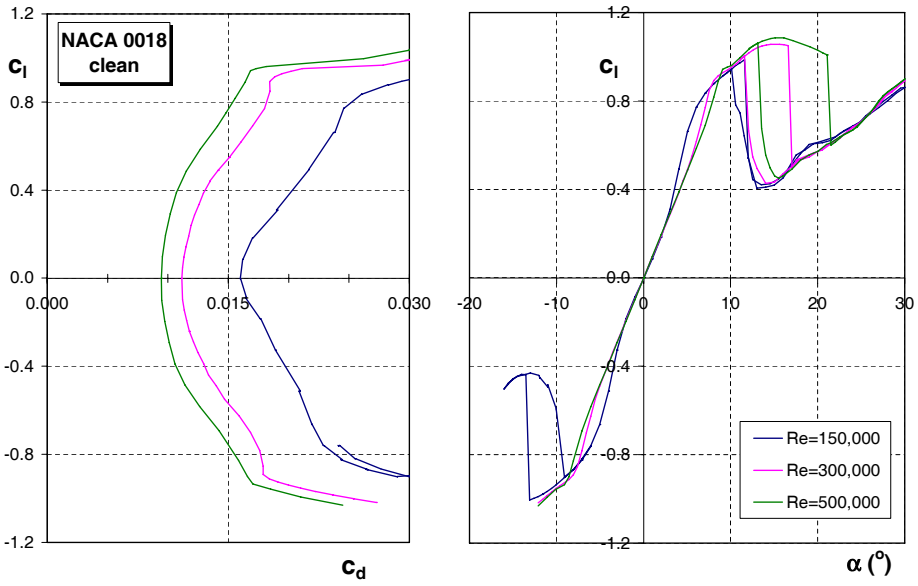

Figure B.6: Wind tunnel data for Re=150,000 - 500,000

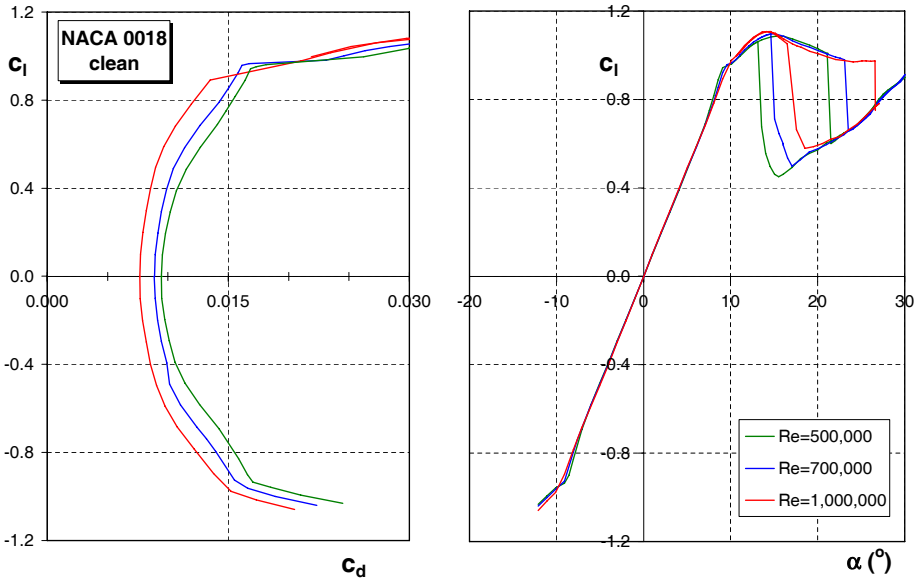

Figure B.7: Wind tunnel data for Re=500,000 - 1,000,000

B.4 With trip applied

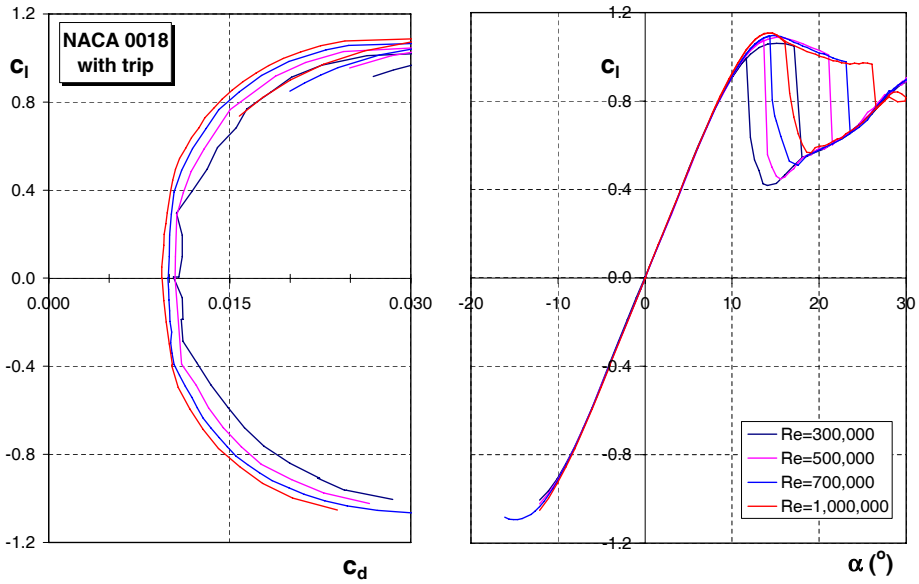

Figure B.8: Wind tunnel data for Re=300,000 - 1,000,000 with trip at 80%

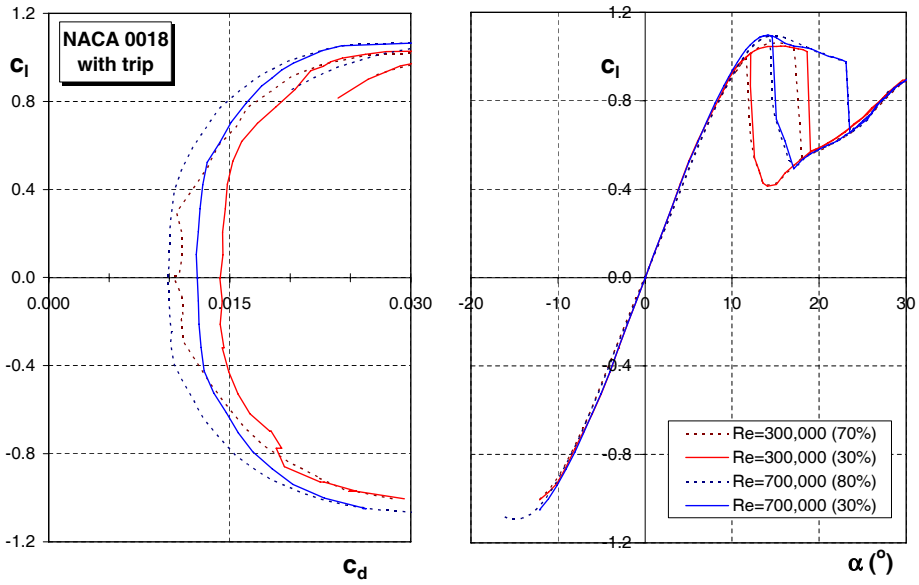

Figure B.9: Wind tunnel data for Re=300,000 and 700,000 with trip at 30%

B.5 Fixed transition at 5% chord

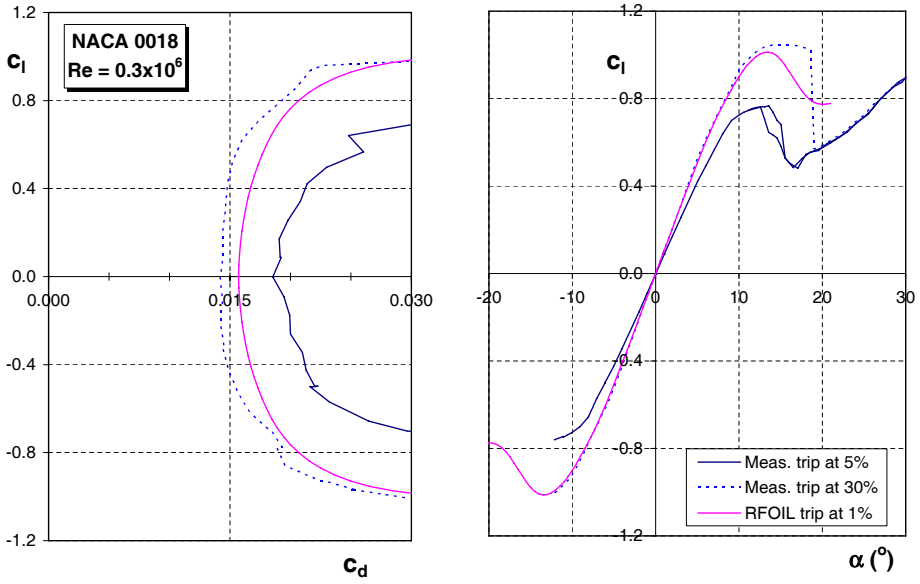

Figure B.10: Wind tunnel data for the fixed transition NACA 0018 at Re=300,000

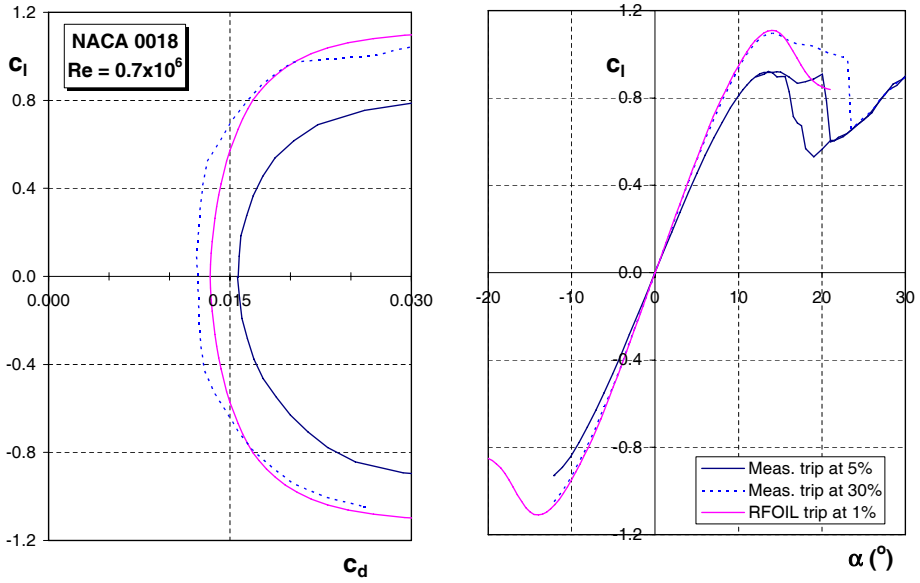

Figure B.11: Wind tunnel data for the fixed transition NACA 0018 at Re=700,000

B.6 Large angles

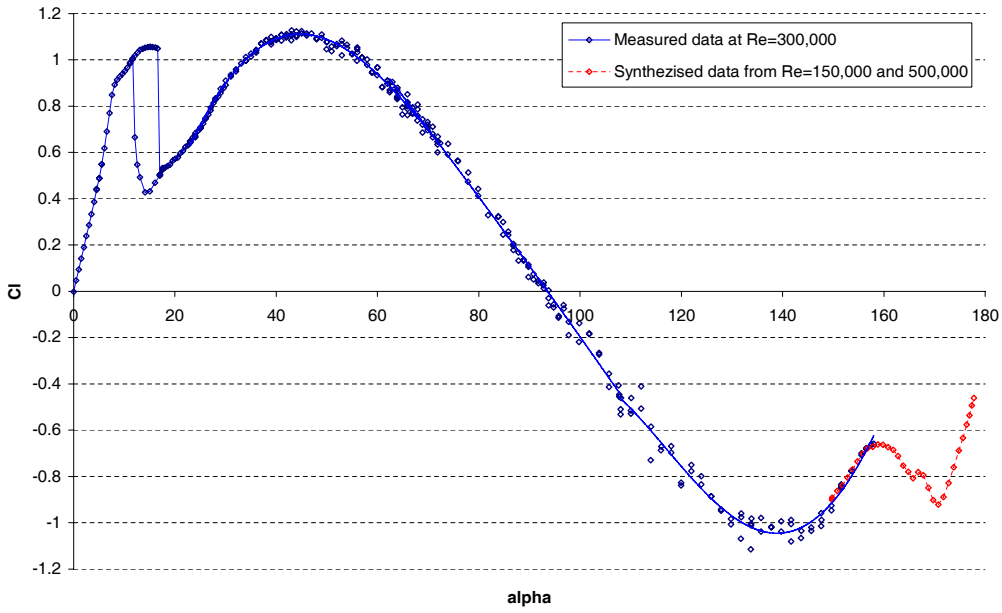

Figure B.12: NACA 0018 lift data for large angles at Re=300,000

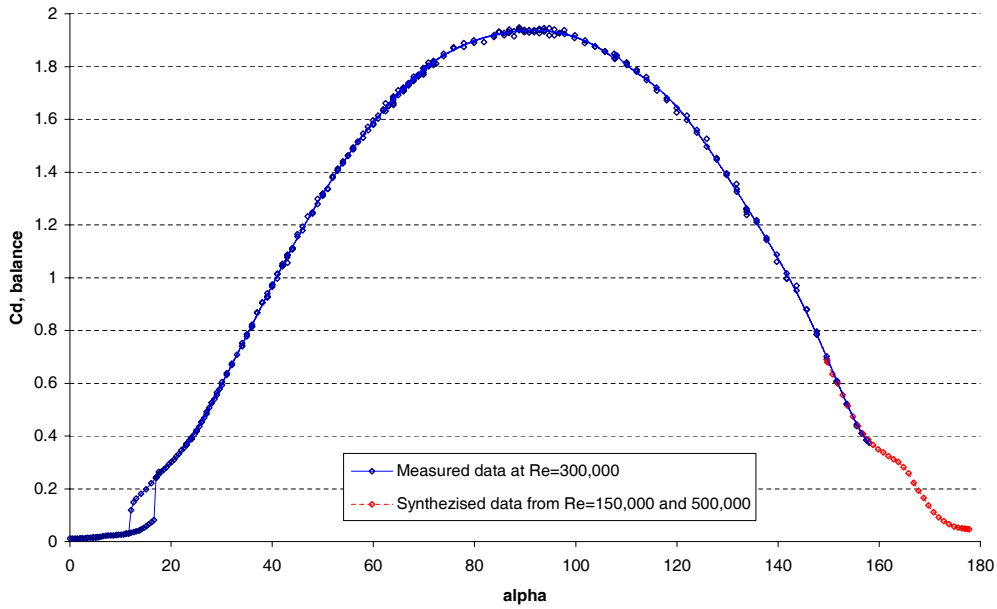

Figure B.13: NACA 0018 drag data for large angles at Re=300,000

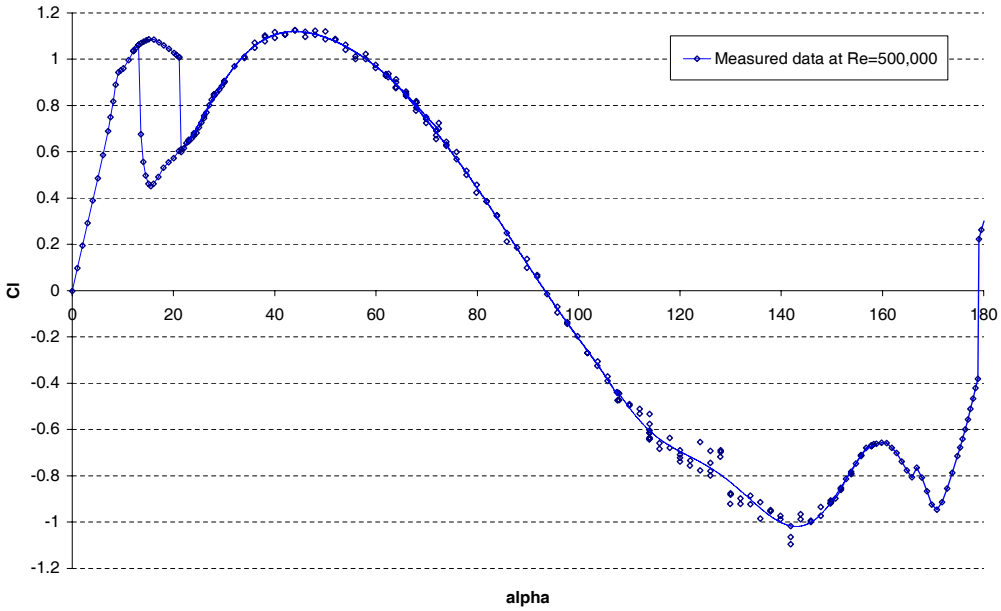

Figure B.14: NACA 0018 lift data for large angles at Re=500,000

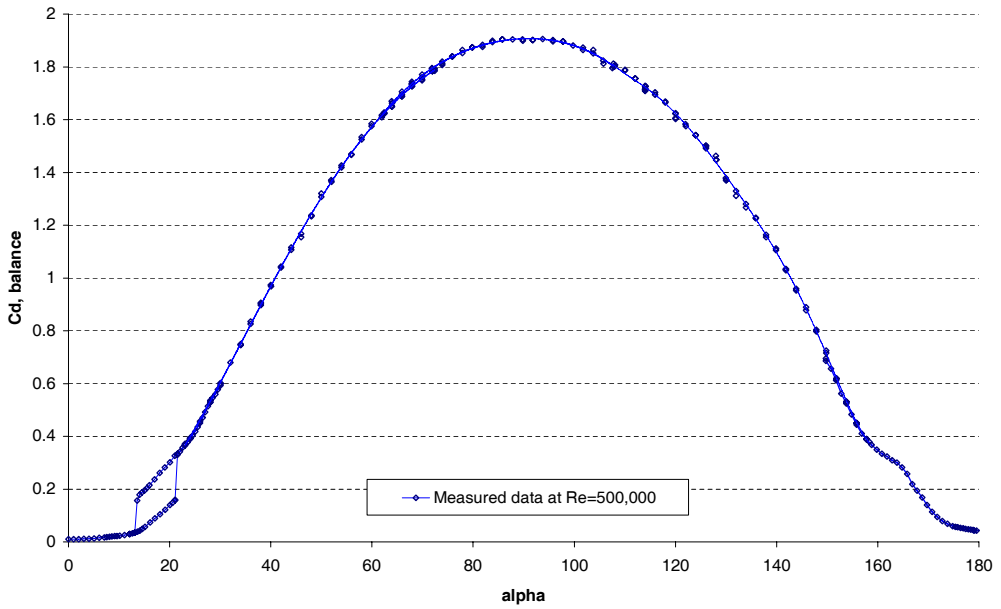

Figure B.15: NACA 0018 drag data for large angles at Re=500,000

Appendix C

DU 06-W-200 RFOIL data

In this appendix the calculated data using the RFOIL program is given. In section C.1 the RFOIL characteristics of the Du 06-W-200 are given for Re=300,000, 500,000 and 700,000. In section C.2 some detailed pressure distribution information is given for three angles of attack; α = -5, 0 and 5.

C.1 RFOIL characteristics

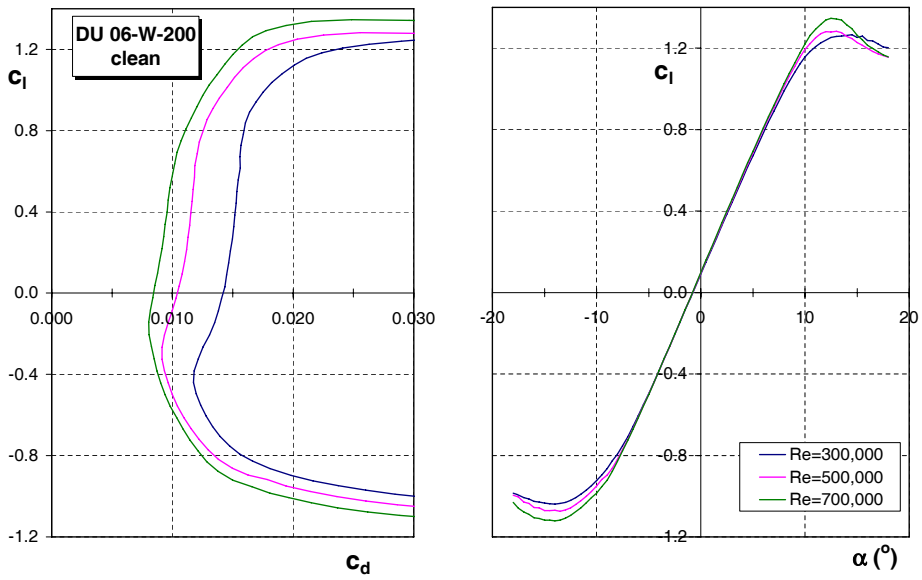

Figure C.1: RFOIL data for the DU 06-W-200 with free transition

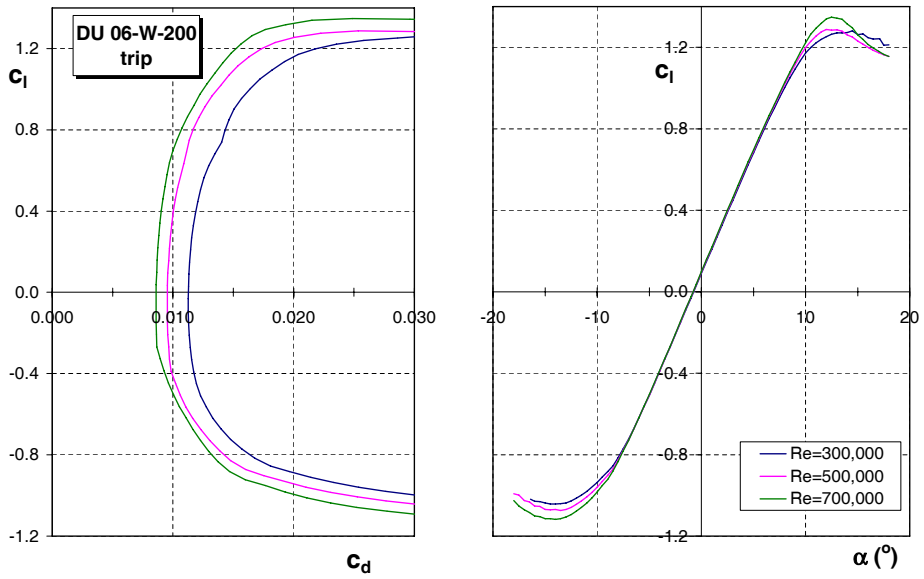

Figure C.2: RFOIL data for the DU 06-W-200 with trip at 40% up and 50% low

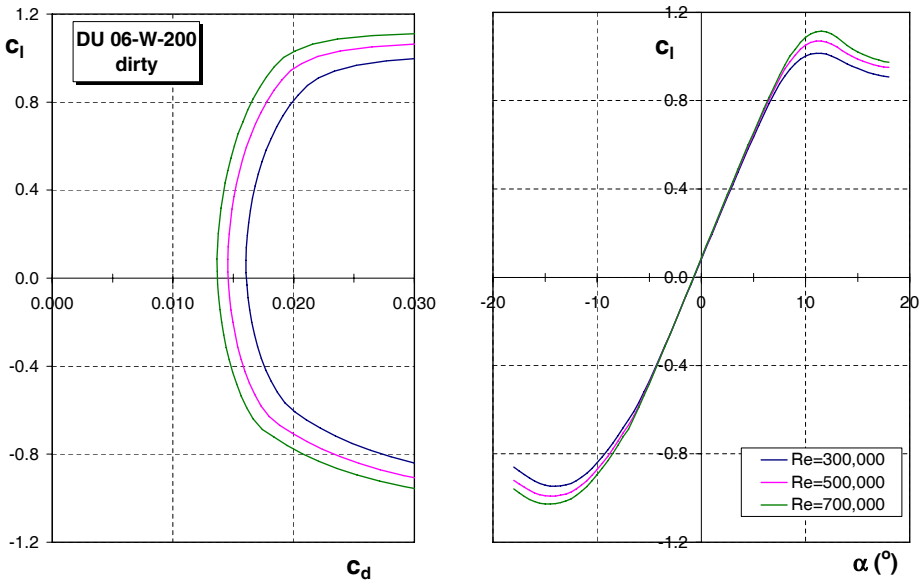

Figure C.3: RFOIL data for the DU 06-W-200 with trip at 5%

C.2 Pressure distributions

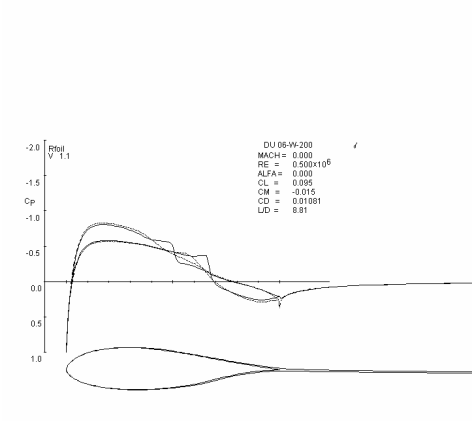

(a) C_p

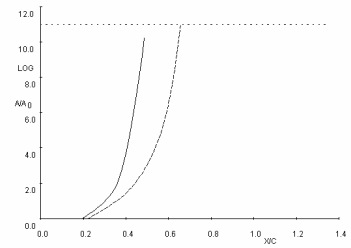

(b) Amplification factor

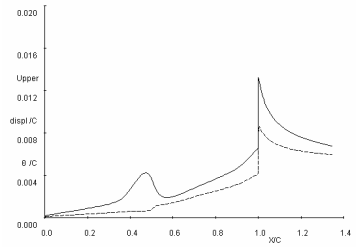

(c) DS

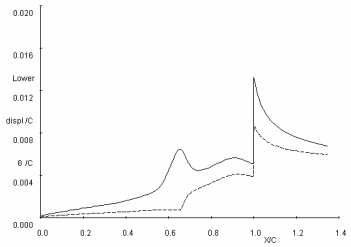

(d) DP

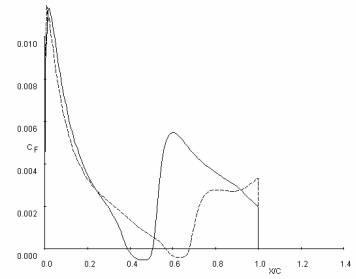

(e) C_f

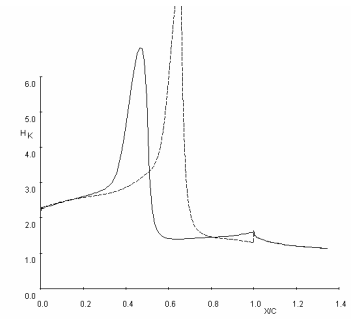

(f) H

Figure C.4: RFOIL data for the clean airfoil at α=0

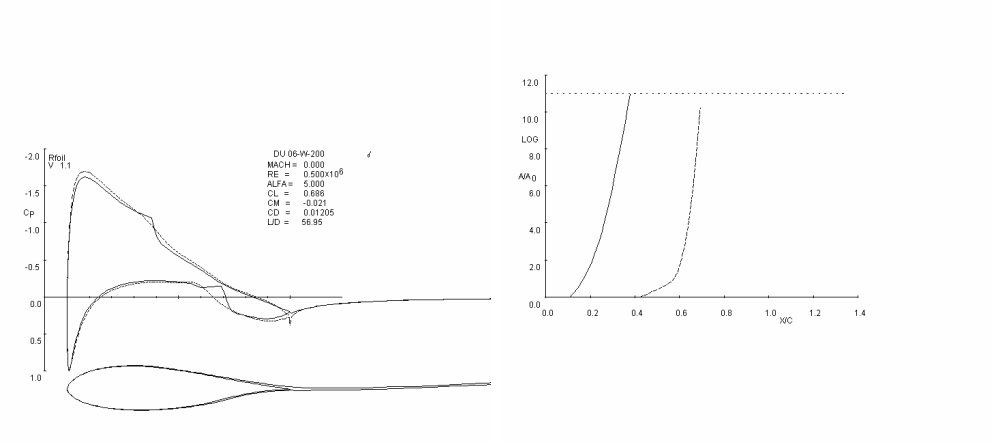

(a) C_p **(b)** Amplification factor

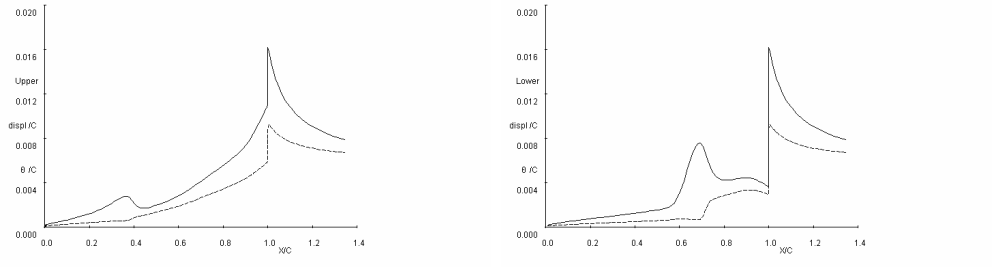

(c) DS **(d)** DP

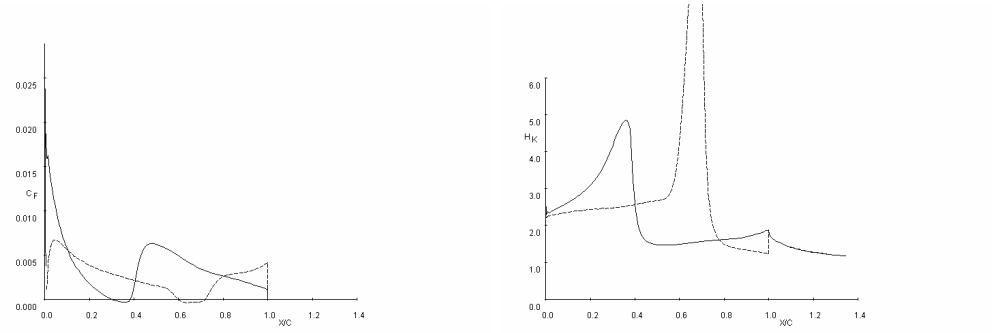

(e) C_f **(f)** H

Figure C.5: RFOIL data for the clean airfoil at α=5

Appendix D

Du 06-W-200 wind tunnel results

In this appendix an abstract of the measured wind tunnel data is given. The test setup is the same as used for the NACA 0018 wind tunnel tests, see section B.1. For more information the reader is referred to measurement report [Claessens, 2006a]. In section D.1 the results for the airfoil in clean configuration are given. The results for the airfoil with fixed transition, with zigzag tape applied at 5% chord, are given in section D.2. Finally an overview of the measurements performed at angles of attack to 78° angle of attack can be found in section D.3.

D.1 Free transition

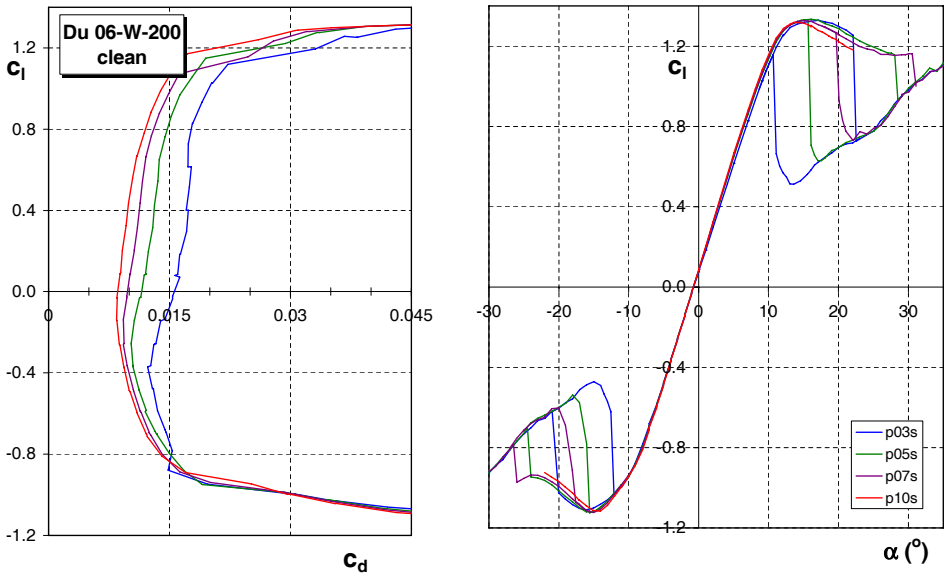

Figure D.1: Characteristics of the clean DU 06-W-200 profile

D.2 Transition fixed at 5% chord

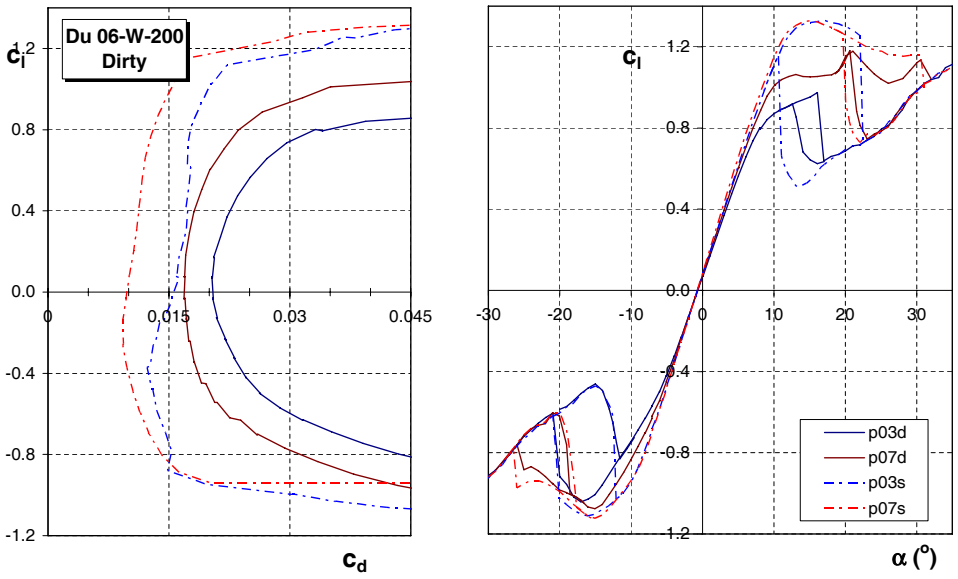

Figure D.2: Characteristics of the DU 06-W-200 profile with trip at 5%

D.3 Large angles

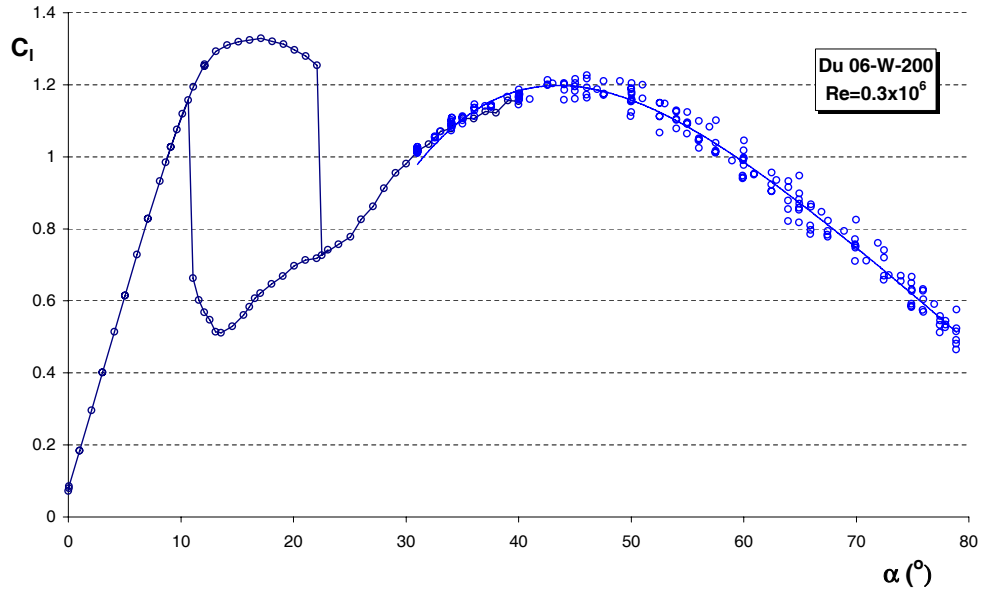

Figure D.3: DU 06-W-200 lift data for large angles at Re=300,000

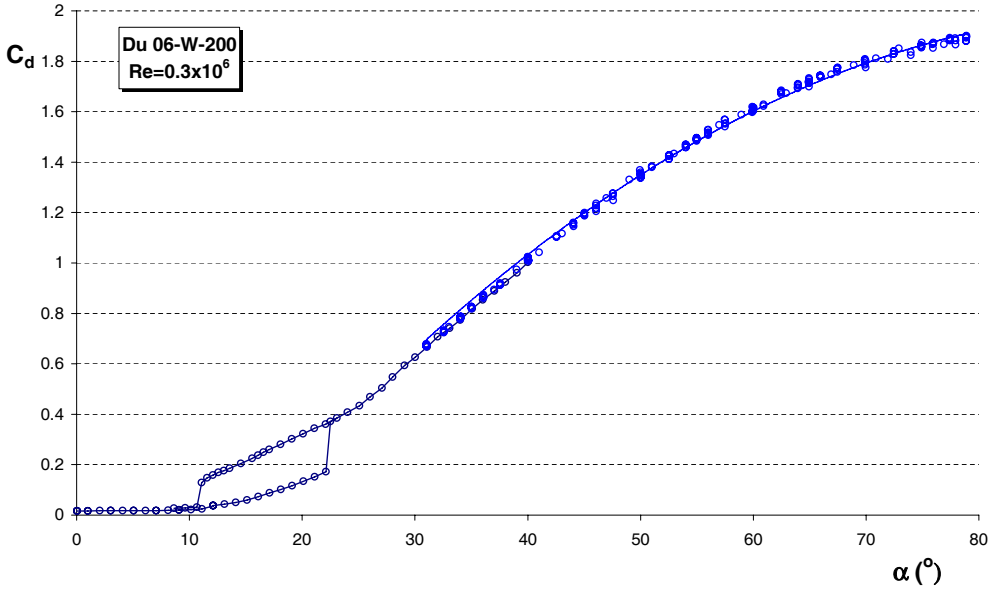

Figure D.4: DU 06-W-200 drag data for large angles at Re=300,000

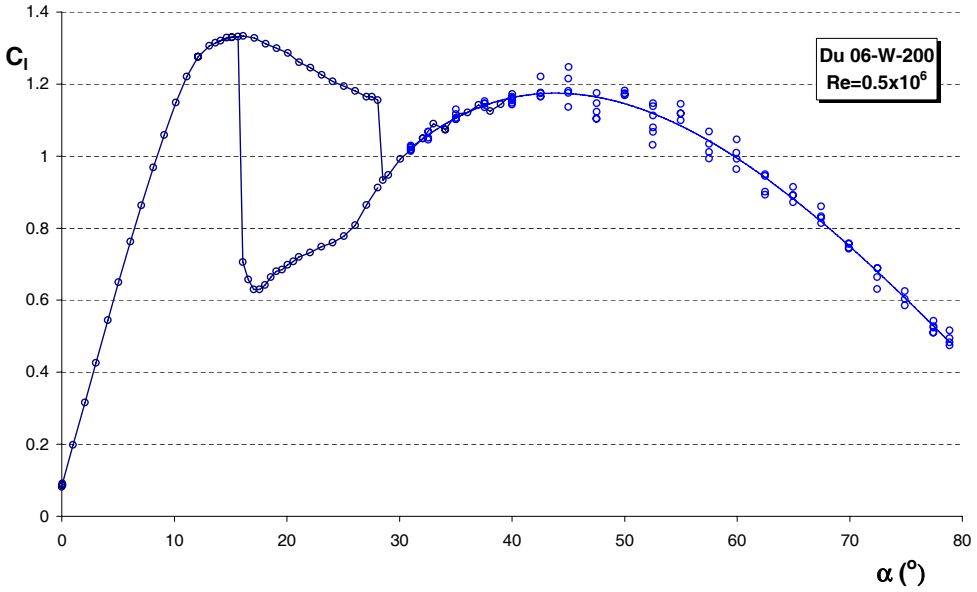

Figure D.5: DU 06-W-200 lift data for large angles at Re=500,000

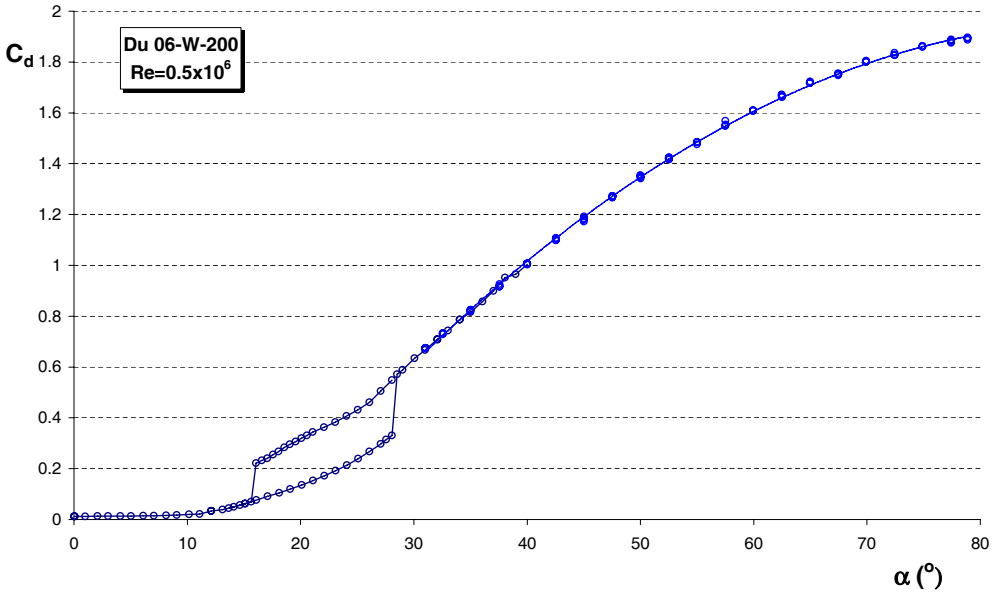

Figure D.6: DU 06-W-200 drag data for large angles at Re=500,000